2013

# DRUG DELIVERY MICRODEVICE: DESIGN, SIMULATION, AND EXPERIMENTS

Jae Hwan Lee
*Virginia Commonwealth University*

School of Engineering
Virginia Commonwealth University

This is to certify that the dissertation prepared by JAE HWAN LEE entitled DRUG
DELIVERY MICRODEVICE: DESIGN, SIMULATION, AND EXPERIMENTS
has been approved by his committee as satisfactory completion of the dissertation
requirement for the degree of Doctor of Philosophy in Engineering

Ramana M. Pidaparti, Ph.D., Dissertation Director, School of Engineering

Karla M. Mossi, Ph.D., Committee Member, School of Engineering

Manu Mital, Ph.D., Committee Member, School of Engineering

Gary M. Atkinson, Ph.D., Committee Member, School of Engineering

Hu Yang, Ph.D., Committee Member, School of Engineering

Gary C. Tepper, Ph.D., Department Chair, School of Engineering

Rosalyn Hobson, Ph.D., Associate Dean for Graduate Studies, School of Engineering

Barbara D. Boyan, Ph.D., Dean, School of Engineering

F. Douglas Boudinot, Ph.D., Dean, School of Graduate Studies

Date

DRUG DELIVERY MICRODEVICE: DESIGN, SIMULATION, AND EXPERIMENTS

A Dissertation submitted in partial fulfillment of the requirements for the degree of
Doctor of Philosophy in Engineering at Virginia Commonwealth University.

by

JAE HWAN LEE

M.B.A., Virginia Commonwealth University, Richmond, 2008
B.S.M.E., Myong-Ji University, Korea, 1988

Director: Ramana M. Pidaparti, Ph.D.
Professor, Department of Mechanical and Nuclear Engineering

Virginia Commonwealth University
Richmond, Virginia
April 2013

# Acknowledgement

I would like to thank Dr. Ramana Pidaparti, my advisor for his tremendous guidance, support, and mentorship he has been giving me since I started my PhD study for the last four years. With his knowledge and guidance, I have benefited a lot from him both professionally and personally. He also gave me an opportunity to work on many projects, which helped me develop my modeling, simulation, fabrication and testing skills. During my graduate study, I have benefited from him greatly in many aspects of academic research, theoretical, and experimental knowledge. His encouragement and feedback on presentations and journal publications have helped me enormously improve my communication skills, making me well prepared for my PhD research.

I am also grateful to other committee members: Dr. Karla M. Mossi, Dr. Manu Mital, Dr. Gary M. Atkinson, and Dr. Hu Yang, for their contributions and helpful advices about my dissertation. In addition, I would like to thank the faculty members and staffs of the Department of Mechanical and Nuclear Engineering for facilitating the excellent academic experience I have had here at Virginia Commonwealth University. I also wish to express gratitude to other graduate students in the Computational Intelligence & Simulation Lab for many years of fruitful interactions: Charles Cartin, PhD, Babak S. Aghazadeh, PhD, and Ronak Patel for discussion on microfabrication, oxygen plasma, and FEM simulations.

Finally, I would like to dedicate this thesis and a very special thank you to my parent, my wife, and two kids support, and bring me enjoyment during my graduate school life. Thank you so much!

## Table of Contents

# List of Tables

## List of Figures

<u>Abstract</u>

DRUG DELIVERY MICRODEVICE: DESIGN, SIMULATION, AND EXPERIMENTS

By JAE HWAN LEE

A Dissertation submitted in partial fulfillment of the requirements for the degree of
Doctor of Philosophy in Engineering at Virginia Commonwealth University.

Virginia Commonwealth University, 2013

Major Director: Ramana M. Pidaparti, Ph.D.
Professor, Department of Mechanical Engineering

Ocular diseases such as glaucoma, age-related macular degeneration (AMD), diabetic retinopathy, and retinitis pigmentosa require drug management in order to prevent blindness and affecting millions of adults in US and worldwide. There is an increasing need to develop devices for drug delivery to address ocular diseases. This research focused on an implantable ocular drug delivery device design, simulation and experiments with design requirements including constant diffusion rate, extended period of time operation, the smallest possible volume of device and reservoir. The drug delivery device concept uses micro-/nano-channels module embedded between top and bottom covers with a drug reservoir. Several microchannel design configurations were developed and simulated using commercial finite element software (ANSYS and

1

COMSOL), with a goal to investigate how the microchannel dimensions affect the diffusion characteristics. In addition to design simulations, various microchannel configurations were fabricated on silicon wafer using photolithography techniques as well as 3D printing. Also, the top and bottom covers of the device were fabricated from PDMS through replica molding techniques. These fabricated microchannel design configurations along with top and bottom covers were all integrated into the device. Both single straight microchannels (nine different sizes of width and depth) as well as four micro-channel configurations were tested using citric acid (pH changes) and Brimonidine drug (concentration changes using the Ultra-Violet Visible Spectrophotometer) for their diffusion characteristics. Experiments were conducted to obtain the diffusion rates through various single micro-channels as well as micro-channel configurations using the change in pH neutral solution to verify the functionality and normalized diffusion rate of microchannels and configurations. The results of experimental data of diffusion rate were compared with those obtained from simulations, and a good agreement was found. The results showed the diffusion rate and the optimum size of microchannel in conjunction with the required drug release time. The results obtained also indicate that even though specific diffusion rates can be obtained but delivering the drug with constant amount needs a mechanism at the device outlet with some control mechanism. For future studies, this result may be used as a baseline for developing a microfabricated device that allows for accurate drug diffusion in many drug delivery applications.

# CHAPTER 1 Introduction

## 1.1 Motivation

The human eye has a very exclusive and complicated function for visualization while magnifying and transferring its image data through the optic nerve in cooperation with various compartments of particularly special structures.  As shown in Figure 1.1, normal human eye can be divided into two main groups as the anterior segment includes the cornea, lens, iris, and ciliary body. And the posterior body contains the sclera, choroid, optic nerve, retina, macula, and vitreous body. There are many eye diseases which can affect to eye and led to vision loss. These diseases are correlated to the function of relevant anatomy and physiology of the eye. Typically, common eye disorder symptoms can be represented as redness (blood shot), itching, tearing, swelling, burning, trauma, pain or discomfort, blur (decrease in vision), and spots. The eye diseases in terms of treatments can be described as Cytomegalovirus Retinitis (CMV, is mostly affected to people with poor immune systems), Conjunctivitis (pink eye), Diabetic Retinopathy, Eye Herpes, Glaucoma, Age-related Macular Degeneration (AMD), Ocular Hypertension, Stargardt's Disease (STGD), and Retinitis Pigmentosa [1].

Most of ocular disease is treated by the topical application of solutions to the surface of the eye as drops because of relatively less expensive and of easy to use by patients. However, it has been estimated that typically less than 5% (or only 1 – 10%) of a topically applied drug absorbs the cornea and reaches intraocular tissues insufficiently [2, 3, 4, 5]. The relatively small proportion of a topically applied drug dose reaches at the back of the eye where the posterior segment as well as ocular tissues, and macula.
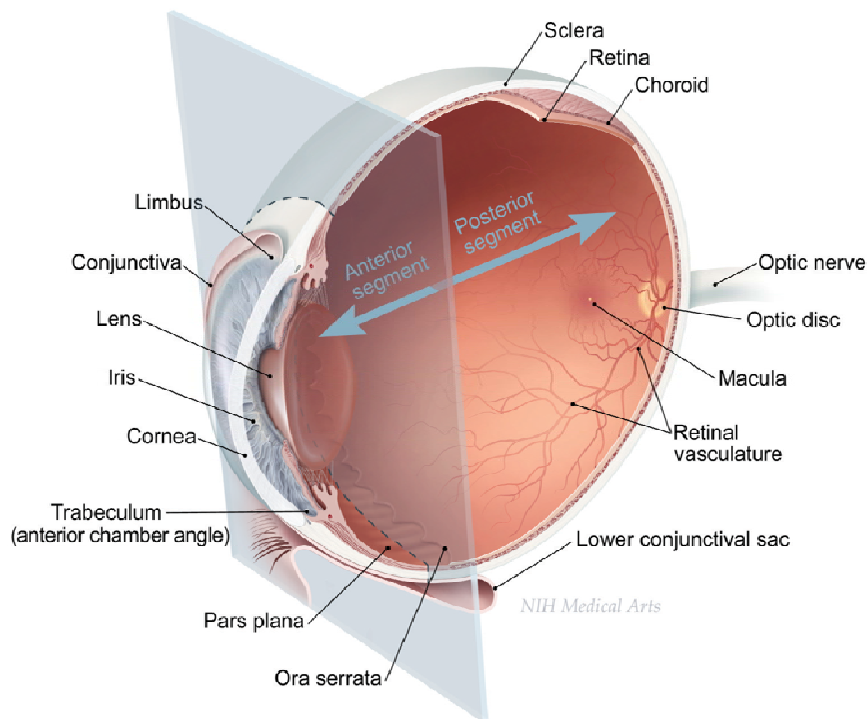
Figure 1. 1 Anatomy of the human eye, figure courtesy of NIH Medical Arts.

The conventional topical drop also can cause severe side effects of visual interferences in accordance with frequent dosing and amount of dosage. The drug using a needle with syringe can be injected, but it barely provides the right amount of dose and over doses may cause more severe problems such as swelling, fatigue, and damage photoreceptor molecules. Furthermore, most drugs run out in a month and repeated injections become necessary [2]. Developing an implantable drug delivery device will help reduce the costs and risks associated with frequent injections and facilitate delivering the drug in a controlled manner and in the required amounts and improve

therapeutic efficacy and safety of drugs. An accurately controlled release with biocompatible and especially refillable drug delivery device for a long time operation is necessary to improve for sufficient drug transport with high efficiency at the right time and right place and to provide better therapeutic performance of drug while avoiding an interruption of vision.

## 1.2 Approaches

Ocular diseases, such as, glaucoma, age-related macular degeneration (AMD), diabetic retinopathy, and retinitis pigmentosa require drug management in order to prevent blindness [6]. These incurable diseases require lifelong treatment through orally administered medications, intraocular injections, and biodegradable implants. Drug delivery to ocular tissue is very difficult due to area and size limitations in the eye. There are currently at least three major categories of ocular drug delivery systems as discussed in [7]: biodegradable or nonbiodegradable, atypical implantable pump systems, and implantable pump systems. Implantable pump systems dispense drugs from an internal reservoir and have the advantage of providing control over drug delivery rate and volume. Several types of implantable pumps, such as, infusion pumps, osmotic pumps, and peristaltic pumps have been developed and used successfully for applications, such as, insulin delivery but have been found to be unsuitable for ocular drug delivery due to space limitations. Typical implantable pump systems (hydrogel systems infused with drug swell via intake of biological fluids for example) minimize the drug volume

required for treatment and provide targeted delivery at a constant rate. However surgical procedures are required to implant and replace these devices, which may in turn contribute to additional side effects. Vitrasert and Retisert distributed by Bausch and Lomb are commercially available examples of nonbiodegradable systems. In these systems, the drug is released as a polymer matrix infused with drug dissolves or the drug is distributed from a nonbiodegradable reservoir. The disadvantages with these systems include in vivo polymer degradation (and the drug cannot be refilled) and the fact that drug delivery is dependent upon a limited volume available within the polymer.

Several Micro Electro-Mechanical System (MEMS) devices, such as microreservoirs and micropumps have been fabricated to address the spatial constraints posed by ocular drug delivery [7, 6]. Microreservoirs offer maximum control of drug delivery but cannot be refilled or reused, thereby ruling out suitability for treating chronic eye conditions. Peristaltic micropumps provide targeted drug delivery through active pumping but require considerable space to achieve a desired volume of flow per minute. To overcome these limitations, Lo et al. [8] recently developed a first generation prototype polymer MEMS delivery device with a refillable drug reservoir for treating ocular diseases. In addition to the refillable drug reservoir, the device consists of a transcleral cannula, check valve, and suture tabs. The device requires surgical implantation underneath the conjunctiva and the specified dose of medication is dispensed from the device when the reservoir is mechanically activated by the patient's finger. This device has several advantages when compared to existing systems including the following: the device is refillable, requires only a single surgical intervention, and is

suitable for treating chronic ocular conditions; it is compact and fits within the dimensions imposed by the ocular orbit (<2mm thick). However, the device requires patient's intervention in dispersion of the drug.

In order to cater to multiple scenarios in terms of amount of drug delivery and constraints, alternate MEMS devices might be of interest for treating ocular diseases. Nano-/microchannel-based drug delivery technologies represent an unprecedented opportunity to realize radically new devices that would exploit the novel features of the nanochannels, in which chip contains that drug reservoir with dose, provide unique performance in terms of diffusion and kinetics over existing technologies for drug delivery applications [9].

Age-related Macular Degeneration (AMD) is a common eye condition among people age 50 and older, and gradually destroys the macula. ADM disease causes the vision loss that makes it difficult to recognize faces, drive a car, read, print, or do close work. AMD does not advance vision loss in a short period of time. Therefore the constant long term drug application is desirable for patients suffering with chronic conditions as well as AMD. Many variables control availability that is dependent on composition. For drugs or compositions of solution, chemical reactivity, total drug concentration and kinetics of transport mechanism engage a significant part in controlling total mass diffusion rate/ flux. The chemical and physical properties of the drug itself are mostly influence to final drug diffusion and availability in ocular tissue [10]. The Fick's second law of diffusion model can predict the diffusion time of the local tissue concentration in the eye following a variety of microchannel geometries for ocular

implantable delivery. The diffusion coefficient of drugs may vary based on the chemical properties and internal structure as well as the molecular weight of the drug.

In this study, the design, simulations, fabrications, experiments, and evaluation are conducted to ensure that the diffusion occurs through a micro-scale channel and the effect of microchannel size. A novel approach to the fabrication of a diffusion-type microdevice and its PDMS, the various geometries using the microfabrication technology is conducted. The microchannel can be operated as the dynamic filter and controlled easily by the dimension of channel without any additional features for the fabrication of the microvalves.

## 1.3 Background and Significance

### 1.3.1 Impacts of AMD on Vision loss

New drugs for treating eye diseases have been developing over the past decade and are very unique for each eye diseases such as glaucoma, cataracts, and age-related macular degeneration (AMD). It is estimated that 1.6 million adults in the US over the age of 50 and above suffer from age-related macular degeneration and about 200,000 cases are diagnosed annually. Worldwide, about 500,000 cases are diagnosed annually [7]. AMD disease is the most cause of severe central vision loss in older people. It is a very critical disease that may advance rapidly and destroy central vision from Figure 1.2, it is shown that central vision is blurred after retina or macula damages with AMD diagnosed eye.

Drugs currently utilized for AMD are delivered via repeated intravitreal injections of the drug into the eye. Risks of repeated intravitreal injections can include intraocular infections (endophthalmitis), intraocular hemorrhage, and retinal detachment. Also, reducing the frequency of dosing will clearly benefit the patient by reducing the need for risky intravitreal injections and improving the pharmacokinetics of the drug in the eye. Eye disease in the posterior segment includes two different forms of AMD such as Dry and Wet. Approximately 90% of patients with AMD have the Dry form shown in small yellow and white deposits form made of proteins and waste products. Wet AMD is caused by abnormal blood vessels grow out of the retina followed by rapid vision loss. However these AMD diseases limit drug delivery in the retina region driven by eye drops [14, 15]. The treatment of vitreous body segment disease still has a significant limitation and difficulty in delivering effective doses of drugs to targeted area in the vitreous body of the eye [16, 17, 18].



a)

b)

c)
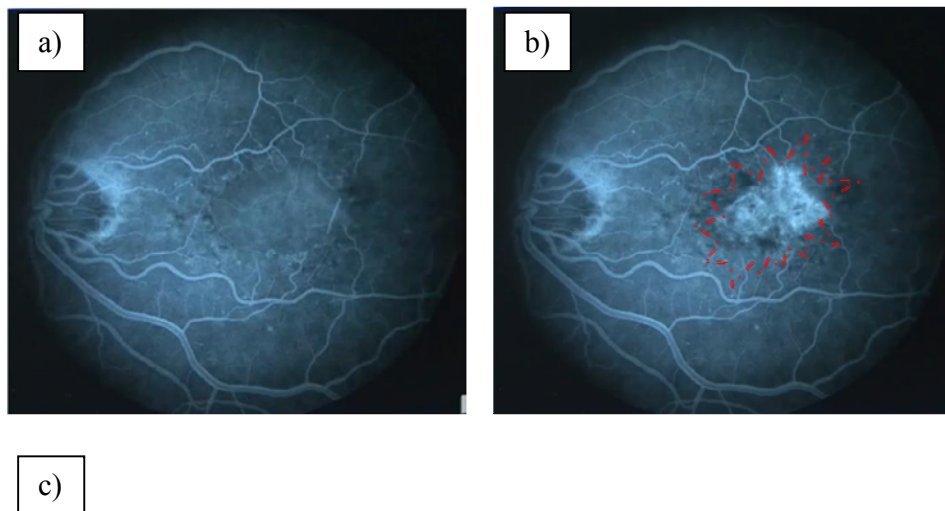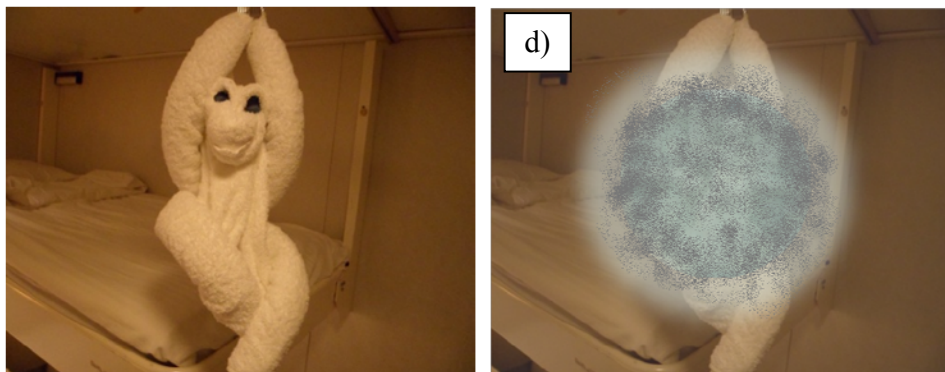
Figure 1. 2 Comparisons between normal and AMD diagnosed human eye; a) left, CT scan of normal and b) AMD diagnosed, c) people clearly perceive an object with normal vision, d) AMD patient has a difficulty to see center area of vision. A computed tomography (CT) scan captured from the www.FightBlindness.org, "Treatment & Therapy for AMD."

### 1.3.2    Drug Administration for Human Eye Diseases

Many ophthalmic drug delivery systems were developed and available to overcome specific problems. In the past decades, significant advances have been made to develop the drug delivery devices for the eye disease and to maintain effective drug doses methods such as in situ gel (hydrogels), ocular insert, nano/micro particle, nano/micro suspension and micro-emulsion has been developed [2, 19-24].

It can be seen in Figure 1.3 a), b) that high peak levels or less effective drug levels of dug amount can cause severe side effects. The controlled release and implant release concept (Figure 1.3 c), d)) are appropriate for drugs with a longer period of time to maintain therapeutic plasma concentrations. The administration intervals can be increased in accordance with elimination rate of drugs in the eye. Moreover, high plasma peak levels which can cause side effects can be reduced.

Figure 1. 3 Four different types of drug release; a) frequently dose every 1 or 2 weeks, b) rarely dose every 10 or 20 months, c) one time dose with controlled release, d) implant dose with diffusion release.

It is shown in Figure 1.4 that nonbiodegradable and biodegradable drug delivery methods in the eye region in accordance with the function of time and derivatives of fluid sources (drugs) are discussed [25]. The Vitrasert implant contains a ganciclovir tablet coated with polyvinylalcohol (PVA) and ethylene vinyl acetate (EVA) polymers. Research is continuing on biodegradable implants to determine their clinical application. Right side view shows biodegradable release systems include Lacrisert®, scleral plug, Episcleral implant, and Injectable rod. Figure obtained and modified from Tsutomu et al [25]. Left side view shows nonbiodegradable release systems include Prosert® (IOL Tech), Lacrisert®(hydroxypropyl cellulose-ocular system; Merck), Vitrasert®(sterile

intravitreal implant with ganciclovir; Bausch &Lomb), and Retisert® (fluocinolone-intravitreal implant;Bausch & Lomb) [25].
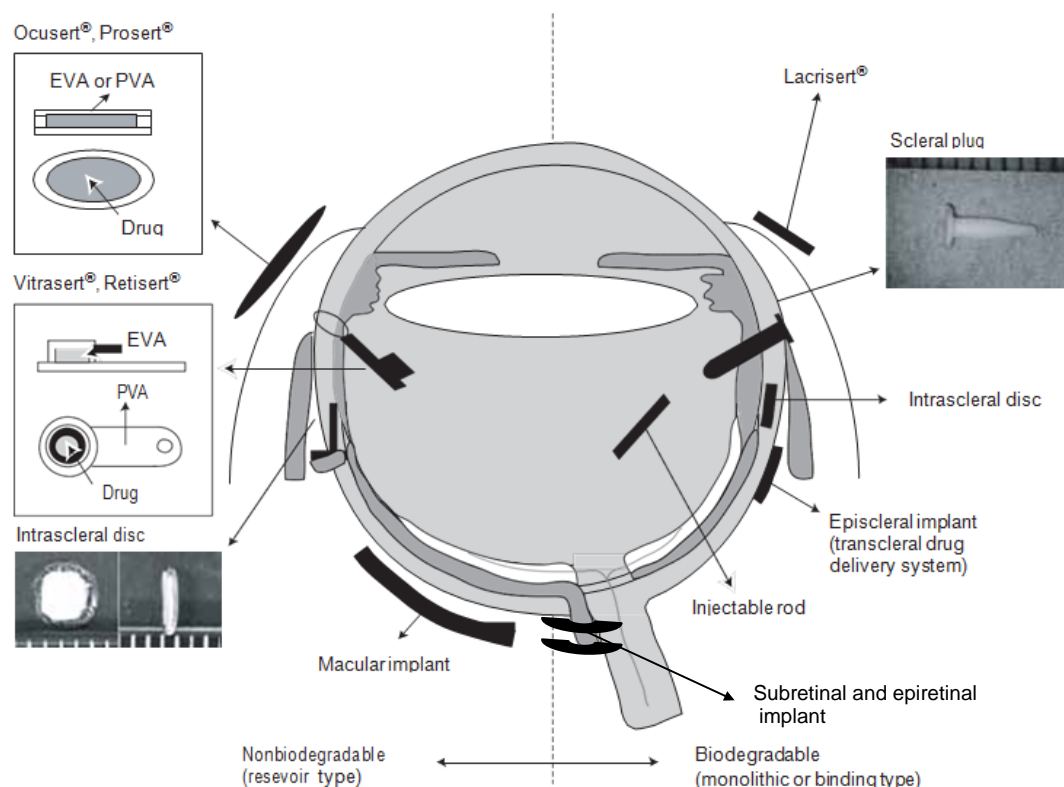


Figure 1. 4 Schematics of ocular controlled release systems; a left-side view shows nonbiodegradable release systems (reservoir type) include Ocusert®, Prosert®, Vitrasert®, Retisert®, Intrascleral disc, and Macular implant. A right side view shows biodegradable release systems include Lacrisert®, scleral plug, Episcleral implant, and Injectable rod. Figure obtained and modified from Tsutomu et al [25].

### 1.3.3  Features of Vitreous Body

The vitreous body is supported by a network of collagen and contains a transparent gel between the lens and the retina. It is about 80% of the volume of the eyeball and delivers an object image to the optic nerve. About 2% of salts, sugars and

collagen fibers make up the vitreous body. 98 % of the body is hyaluronic acid that a substance is an excellent eye lubricant and a stronger bonder with water. Viscosity of vitreous is about 2 to 4 times higher than pure water. There are no blood vessels. Vitreous keeps contact with the retina and helps it keep immobile by pressing against the choroid. Vitreous contents are not continually replenished like those of aqueous humor. The contents are static, meaning that if anything gets into it, it will remain there unless surgically removed [26].

### 1.3.4   Types of Controlled Drug Release System

Typical oral administrations are essentially inefficient and often require repeated dosing to maintain the amount of drug within the therapeutic range. It sometimes requires increased dosages to ensure release of a sufficient amount of drug to the target site. Moreover, specific methods of injection administration can be painful based on the cyclic dose and the amount of injection. The controlled drug release system of therapeutics offers significant advantages over conventional delivery methods of drug administration. Controlled release devices can provide drugs at a steady-state, and constant rate for over long periods of time while minimizing deviations from the therapeutic range. Such advantages of controlled-release devices increase a patient convenience and reduce a waste of drug.

### 1.3.4.1 Dissolution controlled systems

There are two main types of dissolution controlled system; the encapsulation and matrix dissolution controlled system. Micro-encapsulation of drug particles is a common method that is used to develop reservoir type of devices including drug cores. Typical drug particles are coated by microencapsulation form which can be added into the drug device. The drug encapsulation is influenced by certain characteristics of the particle such as properties of drugs, biodegradable polymer, and organic solvent; and operating conditions including drug concentration, diffusion coefficient, solubility, temperature, pressure, and the level of mixing. Therefore, optimization of these conditions is very important to produce the appropriate particle size with narrow distribution [27, 28, 29].

Matrix dissolution controlled system is related to the fraction of drug loaded into the matrix that will eventually be released. The volume fraction dissolubility is importance of matrix dissolution controlled system as a release rate of drug from polymeric matrices. These applications have enabled new insights about the design and characterization of dosage forms and drug release properties. In this system the drugs in surface layer exposed to the solution are dissolved and then diffused out of the matrix. This process continues within the boundary between solution and the solid drug moving controlled. The rate of dissolution of drug particles within the matrix must be faster that the diffusion rate of dissolved drug leaving matrix. Some researchers were studied basic percolation concepts to modify and evaluate the pseudo-steady models in pore diffusion problems as matrix release systems [30, 31, 32].

### 1.3.4.2 Diffusion (reservoir) controlled systems

The drug release rate of diffusion controlled systems is dependent on its diffusion coefficient through membrane barrier. A core of the drug is surrounded by polymeric membrane. The nature of this membrane determines the release rate of drug from system. According to the Fick's law, the amount of drug passing across a unit area in the process of diffusion is proportional to the concentration difference across the area [33].

### 1.3.4.3 Water penetration controlled systems

The release rate in water penetration controlled delivery systems is determined by the penetration of water into the system. Two general types of these systems include, swelling controlled release systems and osmotically controlled delivery systems. Swelling controlled release systems are initially dry, when first placed into the body. The system will absorb water or other biological fluids and swells. Swelling increases the aqueous solvent content within the formulation as well as the polymer mesh size, enabling the drug to diffuse through the swollen network into the external environment. However most of the materials used in swelling controlled release systems will swell without dissolving when exposed to water or other biological fluids [34]. The drug release from the osmotic system is largely independent of the pH reaction. The membrane in the osmotic system is selectively a water permeable membrane and an effective isolation of dissolution process of drug core from the surrounding environment. The cellulose polymer acetate membrane is commonly used because of its high water permeability characteristics and it can be adjusted for various degrees of acetylation of the polymer. The permeability of this

membrane can be increased further by adding plasticizer to the polymer. This increases the water diffusion coefficient or hydrophilic flux enhancer which increases the water sorption of the membrane [35, 36, 37].

### 1.3.4.4 Hydrogels

Hydrogels are a special type of mesh like hydrophilic polymer that has the ability to absorb large amounts of fluid. It can absorb typically 60-90% fluid at complete swell and only 10-40% polymer remains as its fibroin structure. In case of polymer hydrogel, initially the diffusion coefficient of agent in the dehydrated hydrogel is very low. However once the gel absorbs water, a significant increase of the diffusion coefficient is occurred. The degree of cross-linking, linear molecules bonded to each other, is partly determined by the concentration of the polymer. The polymer will be a weak mesh at low concentration. Cross-linking will become the tighter when concentration is increased. The most well known hydrogel is gelatin which is a processed version of collagen that accounts for one thirds of the protein in the body [38]. Wang et al [38] have studied the nonlinear mechanical coupling between pH-responsive polymers and ion-exchange reactions for periodically releasing enclosed particles without external resources.

### 1.3.5  Refillable Drug Release System

In a recent study, Ellis Meng et al (2012) [39] have investigated the implantable delivery device as a micro-electromechanical system (MEMS) for the treatment of chronic and

refractory ocular diseases [8, 40, 41]. It can be seen in Figure 1.5 that their device can be refilled with drug solution to provide long-term drug therapy while avoiding repeated surgeries. The first generation of MEMS is a manually controlled system limited by variations in the drug-release duration and force applied for depressing of the reservoir. To resolve this problem, the next generation device consists of an electrolysis chamber with electrolysis actuation to precise delivery of the desired dosage volume, a drug reservoir with refill port, battery and electronics. Biocompatible and flexible parylene is used to construct the MEMS. Battery and wireless inductive power transfer can be used to drive electrolysis.
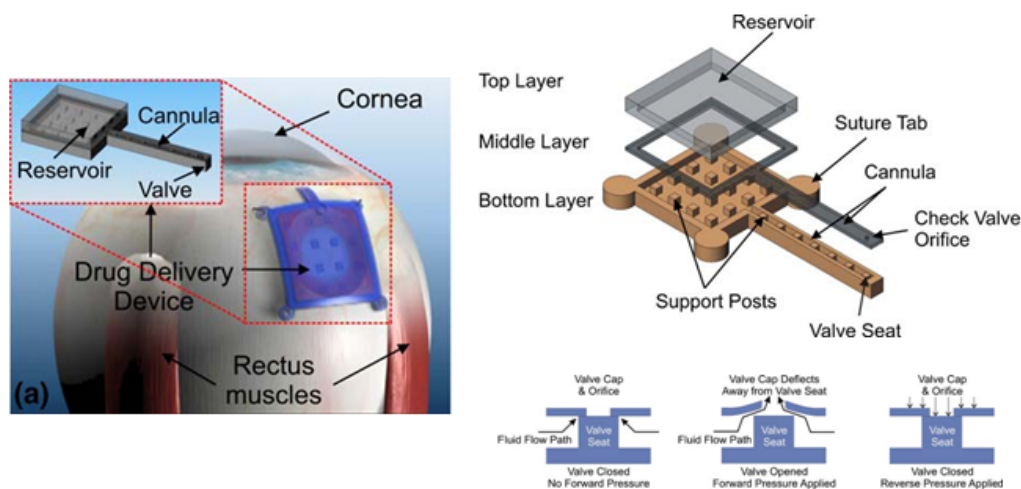


Figure 1. 5 Illustration of the implantable ocular drug delivery device concept with a refillable port, reprinted from Lo, R. et al, 2009 [8]

Electrolysis is a low power process in which the phase change of water to hydrogen and oxygen gas is induced electrochemically. The change generates pressure in the reservoir forcing the drug through the cannula [8]. The reservoir is implanted in the subconjunctival space, and the flexible cannula is inserted through an incision into the

anterior or posterior segment. Gonzalez-Soto et al [42] have demonstrated that a slower prolonged infusion of the same volume and concentration of intravitreal ranibizumab is equivalent to a bolus intravitreal injection of ranibizumab in a human VEGF-induced retinal hyperpermeability model in rabbits.

In 2009, Replenish Inc. have started clinical trials for F.D.A. approval for a refillable and programmable pump that would be implanted into the eye to feed medicine for glaucoma or AMD. They focused on the controlled release, which would last for more than 5 years before replacement is required. This is much longer than current treatments [43].

Genentech developed a refillable port drug delivery system (PDS) that was designed to release ranibizumab over a period of months in collaboration with ForSight Vision 4 Inc. [44]. To develop the PDS, a safety and preliminary efficacy study have been conducted in patients with neovascular AMD [45].

### 1.3.6  Computational Models for Investigating Ocular Drug Delivery

A simplified cylindrical vitreous body model had been developed by Ohtori et al [46] for the pharmacokinetic model of intravitreal drug injection. Their cylindrical vitreous body model had well presented the elimination profile of ocular drugs in the rabbit eye. The model parameters, such as the diffusion coefficient, the partition coefficient, the metabolic reaction rate constant were studied. The vitreous concentration is basically very low and decreases extremely close the posterior segment based on the boundary barrier and elimination factors, which are related to complicate

distribution and consumption. The retina membrane could be considered as an elimination component of drug molecules while analyzing a cylindrical vitreous model. They also investigated the parameters of binding in the vitreous body from the in-vitro experiment [46, 47].

Drug diffusion in the vitreous body of the three dimensional eye model have been performed by Friedrich et al [48] and Park et al [49]. The combined effects of diffusivities were simulated to evaluate the influence of vitreous outflow on drug distribution while keeping the retinal permeability constant. The effect of the high ($D_h$; $1 \times 10^5$ cm$^2$/s) and low ($D_l$; $1 \times 10^7$ cm$^2$/s) diffusivity of drug in vitreous humor was investigated while comparing an intravitreal injection and implant using a finite element model. They suggested that the implantable drug delivery device could be advantageous to reduce the risks of instantaneous high concentration from an injection and to sustain the releasing of the drug for a long period of time.

### 1.3.7   Drugs and Diffusion Coefficient for AMD

Several models have been used to study the drug delivery mechanisms [50, 51]. Recently, a review of barriers to posterior eye drug delivery and the challenges and opportunities were discussed by Thrimawithana et al. [52]. Table 1 summarizes various drugs, their diffusion coefficients, the average dosage, and the frequency to treat AMD diseases. Fick's second law of diffusion can be used to describe the transport of drug into the eye using microchannels. As the drug delivery device is implanted in the vitreous

body of the eye, usually the diffusion rate depends on the local concentration between the

drug reservoir and the vitreous humor.

Table 1 Diffusion coefficient of drugs for the AMD disease

| Drug | Drug name (type) | Diffusion Coefficient ($cm^2/s$) | Average Dosage (nl/min) | Injection amount/periods | References |
|---|---|---|---|---|---|
| Anti-angiogenic | Macugen (Pegaptanib sodium) | $3 \times 10^{-7}$ | 0.2083 | 3mg/10days | Swanson S. D. (2006) [53] |
| | Lucentis (Ranibizumab) | $2.08 \times 10^{-7}$ | 0.0124 | 0.5mg/month | Molokhia et al. (2010)[54] |
| | Intravitreal Avastin (Bevacizumab) | $1.25 \times 10^{-7}$ | 0.0289 | 1.25mg/month | |
| Synthetic corticosteroid | Fluocinolone Acetonide, | $2.3 \times 10^{-7}$ | 0.0744 | 15mg/20weeks | Li T.et al. (1997) Jaffe G. J. (2000) [55, 56] |

### 1.3.8 <u>Drug Therapy for Ocular Glaucoma Disease</u>

Treatment in glaucoma disease is mainly to lower intraocular pressure (IOP) in

order to decrease the risk of severe progress and vision loss. The brimonidine is one of

the appropriate drugs to effectively lower IOP [82, 83]. Due to the similar diffusion

boundary conditions with AMD, the Brimonidine is applied to characterize the diffusion

rate and is well tolerated. In this study, the Brimonidine for the treatment of glaucoma is

investigated for the possible drug for diffusion.

## 1.4 Specific Objectives

The overall goal of this research is to develop the optimized drug delivery system

while studying the role played by various geometrical components of fluidic

microchannels. And then develop the microchannel fluid model to study velocity and

pressure distributions in the eye. After understanding fluid characteristics of the microchannel, diffusion with hydrophilic surface for drug delivery application is developed. The various microchannels in a drug delivery device are investigated to achieve a constant diffusion rate for its application in the AMD disease.

This study focuses on the design, simulation, and development of an implantable ocular drug delivery device. A novel design concept consisting of micro/nanochannels embedded between top and bottom covers with a drug reservoir made from PDMS material was developed. Several simulations were carried out with different microchannel configurations in order to see the feasibility for ocular drug delivery applications. Finally, the drug release time from the drug delivery device in accordance with a size of microchannel and diffusion coefficient can be predicted from the diffusion rate profile by the present model.

 The procedure consists of four main steps:

Step 1: Design

In step 1, simple idealized microchannels with five different sizes of width and depth are developed. The straight microchannel A (100μm - 1000μm) is designed 10 mm long that can be inserted into the device and tested with same amount of the vitreous liquid of eye.   The straight microchannel B (200μm - 1000μm) is designed 20mm long that is considered to obtain the diffusion rate and particle image velocimetry. The eyeball with device implants is developed based on the possible application and surgery easiness. The alignment of the device is optimized when the results of simulation are obtained. The four different microchannel configurations are developed to be performed as a filter for

drugs and to avoid the back flow from the vitreous segment of eye. The generic drug delivery system based on PDMS (Polydimethylsiloxane) is designed.

Step 2: Simulation

In order to understand the design characteristics of the channel, a micro-device for drug/fluidic transport mimicking the coarse-grained representation of the microchannel geometry through computational fluid dynamic analysis and optimization is developed. Specifically, the role of the channel configurations in active fluidic transport and passive transport is investigated. Results of flow rate, pressure and velocity profiles obtained from the models indicate that the microchannel plays a major role in transport through this entire device. The results of this investigation show that fluidic transport and flow passages are important factors in designing microchannel based devices for drug delivery.

The present approach can be extended along with multi-scale microchannels to further understand the diffusion characteristics of microchannel geometry.

In practical applications of microchannel flow, we assume that the majority of micro-system flows are laminar due to the high pressure drop in microchannels caused by relatively small channel dimensions. A combination of dimensionless Reynolds numbers indicates the importance of inertial to viscous forces, energies and time scales present at the microscale [11, 12, 13]. Within a certain low range of Reynolds numbers (Re< 1), laminar incompressible viscous flow may dominate the flow field over the entire microchannel length. The design concept of microchannels within the drug delivery device has been investigated to develop constant diffusion rate and low pressure operations if it is applicable.

Using ANSYS thermal transient analysis, the several design concepts for drug delivery channel within a device are investigated and simulated to obtain an optimum and constant diffusion rate for the drug concentration. ANSYS Fluent and Post-CFD is performed to optimize diffusion flow of a micro fluidic device in which is implanted into the barrier of vitreous body of the human eye. COMSOL Multiphysics® is performed to compare diffusion rate of the Brimonidine (drug therapy for an ocular glaucoma disease) with experiments.

Step 3: Fabrication

In the following, five straight microchannels are fabricated on the Lexan® glass to obtain diffusion performance. And then the fabrication of PDMS and microchips, which allows inexpensive, durable, and biocompatible devices, is processed. Microchannels are fabricated by micro-electronic technologies onto the substrate followed by bonding a PDMS of reservoir. A bonding process is conducted by oxygen plasma treatment. PDMS and Si substrate have typically hydrophobic surface that affects diffusion coefficient. Thus the surface treatment using optimized oxygen plasma process is conducted to form a silanol group. A solvent assisted system is considered to soften less than 50 nm of the surface of microchannel during bonding while maintaining microchannel integrity.

Step 4: Test

After completion of prototype samples, the change in pH neutral solution is measured to verify the functionality and diffusivity of the single microchannels and entire device including various microchannel configurations. Both design simulations and experiments are carried out to evaluate the drug delivery device for its functionality and diffusion characteristics. The evaluation test in comparison with the analytical solution is completed using micro-PIV (particle image velocimetry). The micro particle image velocimetry (μPIV), an optical method, is performed to visualize and analyze the flow rate and flow characteristics in the microfluidic channels using MATLAB PIVlab 1.31, which is one of the latest user defined computational code. The diffusion rate of polystyrene with standard 3.0μm diameter (National Institute of Standards and Technology (NIST), traceable particle size standard) is measured as a similar to drug concentration.

## 1.5 Organization of the Dissertation

The rest of the dissertation is structured as the followings. Chapter 2 discusses the details used to develop the model design. The concepts of the drug delivery model are also provided. Chapter 3 describes the procedures and the boundary conditions of the model to perform the simulation of single microchannels and the entire device model. The results from the microchannel and entire device model are also discussed. Chapter 4 provides all details of the fabrication of PDMS and Microchannels include curing process,

Si substrate oxidation, KOH etching and oxygen plasma. This chapter illustrates the

experiment techniques that are used to conduct the diffusion test using present models.

Finally, scientific contributions of the research and recommendations for other

researchers are presented in the Chapter 5.

## CHAPTER 2 Model Designs for Device and Experiment

### 2.1 Introduction

Controlled release drug delivery is a challenging way to treat illnesses. The term

controlled release refers to the ability of a drug delivery system to release a drug over an

extended period of time at a controlled rate. Over the last 20 years, it has become more

popular for treatments of chronic diseases. It generally involves implanting a biocompatible polymer directly into the diagnosed region of the body that is affected by a disease. Since the polymer is implanted directly into the tissues affected by disease, the side effects are often small compared to conventional drug delivery (i.e. eye drop or injection). A controlled release system can increase accuracy of the dosing to overcome the side effects of pulsed dosing produced by conventional systems. It is possible to provide comfort, better compliance to the patient and to improve the therapeutic performance of drug. Diffusion represents a highly efficient means for the generation of concentration gradients for a long time operation. Drug concentration in DI water can be generated with relative concentration of the vitreous cavity along the gradients. Therefore, microfluidic channels are used. As a first step, diffusion of drug in single straight microfluidic channels is investigated.

### 2.2 Theoritical Background

The movement of drug across a microchannel in a manner driven solely by the concentration gradient is a passive diffusion. In passive diffusion, drug moves from a region of greater concentration to a region of lesser concentration. When the dose of a compound that is released by passive diffusion is increased, the percent of the dose that is eliminated remains the same. In contrast, there is a decrease in the percent of the dose that is eliminated when increasing the dose of a drug released by a concentration process. We can illustrate the power of this approach by deriving Fick's law of diffusion in one dimensional model [57].

### 2.2.1      Diffusion by Fick's Law

The principle mechanics in physics depict that a particle in a mechanical or gravitational field always moves from a point of high potential energy to one of lower potential energy. Another way of stating this fact is that there is a force on the particle given by

$$F_r = -\nabla V(r) \tag{1}$$

or in one dimension

$$F_x = -\frac{dV}{dx} \ \ or \ -\frac{\partial V}{\partial x} \tag{2}$$

However, in contrast to motion in free space, motion of molecules in liquid involves frictional forces. A particle moving in such a medium must cause displacement and separation of these interacting molecules. Force is required and the net result is an expenditure of energy. When the path of a particle involves the separation of two or more molecules, work is done by the particle on these two or more molecules. This work or energy expenditure is not recovered by the particle when the two or more molecules again return to their average intermolecular distances. Instead, this work of separation is dissipated as heat characteristic of irreversible processes. In fact, the rate of energy dissipation by the moving particle is proportional to its velocity. This rate of energy dissipation is known as a frictional force. This frictional force is not only a property of the particular medium through which the particle is moving, but is also dependent on the particle size and shape. The larger the size, the greater the resistance encountered. The inherent property of the medium which determines the friction force is called viscosity $\eta$,

and is related, in part, to the degree of molecular interaction and molecular size and shape. Thus, the diffusion coefficient also depends on size and shape of molecule, interaction with solvent and viscosity of solvent. The diffusion coefficient equation is given as

$$D = \frac{k_b T}{f} \tag{3}$$

Where $f$ is a friction coefficient, it can be expressed by

$$f = 6\,\pi\eta r \tag{4}$$

By substituting equation (4) into equation (3), we get

$$D = \frac{k_b T}{6\pi\eta r} \tag{5}$$

in which $k_b$ is the Boltzmann-constant, T the absolute temperature, $\eta$ the viscosity of the medium, and $r$ the radius of a sphere diffusing in the liquid, the diameter of a sphere diffusing in water.

### 2.2.2 New Fick's Law with Navier-Stokes Equation

Mass transfer by viscous flow is much faster than that by diffusion under all the simple channel flows. If the simple channel flows are due to biased random motions of atoms, the same driving force such as a pressure gradient should produce similar rates. However it is proven to differ by many orders of velocity and pressure magnitude. Whether these are entirely different processes or same processes remains a question. In a liquid, all atoms are moving in random motions which produce both diffusion and viscous flow when influenced by a driving force. It is difficult to see how they can proceed by exclusive singular motion mechanisms. The solid states in a liquid are

different because self-diffusion takes place by atom-vacancy exchanges and such diffusion may produce shape changes or particle flow of solids. If all the contiguous atoms are moving in one direction, the central atom can be moved in the same direction without any effort of its own. In other words, it moves with its adjacent without any chemical potential gradient at all in the moving direction. In addition, if an atom has a chemical potential gradient, it moves forward to adjacent atoms in accordance with the novel idea of Fick's first law [58].

Once we set the velocity $u_x$ of a molecule in the $x$ direction in a flow field, it can be relative to some fixed frame. Then the velocity of the molecule ahead of it is

$$u_x + a \frac{\partial u_x}{\partial x} + \frac{a^2}{2} \frac{\partial^2 u_x}{\partial x^2} \qquad (6)$$

In which a is the distance at which the first peak of the radial distribution function appears. Usually the first nearest neighbor is located there. Similarly the velocity of the nearest neighbor at the back of it is

$$u_x - a \frac{\partial u_x}{\partial x} + \frac{a^2}{2} \frac{\partial^2 u_x}{\partial x^2} \qquad (7)$$

Since the velocity difference between front and back neighbors such as $\frac{\partial \mu_x}{\partial x}$, $- a \frac{\partial \mu_x}{\partial x}$, the average velocity of the two neighbors is expressed by

$$u_x + \frac{a^2}{2} \frac{\partial^2 u_x}{\partial x^2} \qquad (8)$$

Hence the velocity of this atom relative to its neighbors in the x direction is

$$u_x - \left(u_x + \frac{a^2}{2} \frac{\partial^2 u_x}{\partial x^2}\right) \qquad (9)$$

If there is a driving force for diffusion such as a gradient of chemical potential$\frac{\partial \mu}{\partial x}$, this atom should have a velocity relative to its neighbors based on Fick's law:

$$\frac{a^2}{2} \frac{\partial^2 u_x}{\partial x^2} = \frac{D}{RT} \frac{\partial \mu}{\partial x} \qquad (10)$$

For all three components of 3D coordinates of velocity, it can be expressed

$$\nabla^2 u_x = \frac{6D}{a^2 RT} \nabla \mu \qquad (11)$$

Since the velocity u is the flux J divided by the concentration c, this equation can also be written as

$$u_x = \frac{J}{c} \qquad (12)$$

$$\nabla^2 J = \frac{6cD}{a^2 RT} \nabla \mu \qquad (13)$$

where c is number of moles per unit volume or the reciprocal of molar volume. This is the new Fick's law for self diffusion in liquids [58].

### 2.2.3     Mass Transfer Coefficient in Molecular Diffusion

Mass transfer through diffusion occurs whenever fluid has different concentration of the physical properties so that some mass is diffused from one place through another. This research is not focused on mass transported by this volume fluid motion, but rather on the transport of one chemical species within a mixture of chemical species that occurs as a direct result of a concentration gradient and is independent of a pressure gradient. Many of the solution techniques for conduction heat transfer can be applied directly to mass transfer and diffusion problems. Mass diffusion refers to the diffusive transport of a

species due to concentration gradients in a mixture. Mass transport by diffusion is analogous to conduction, which is the diffusive transport of energy due to temperature gradients. Therefore, the molecular description of diffusion is similar to the molecular description of conduction.

The flux of molecules of all species that are passing through a horizontal plane at position $x$ is proportional to the molar density of the mixture $N$ and the mean velocity of the molecules $v_m$ at that location. These molecules practice their last molecular interaction at $x–L_m$, where $L_m$ is the average distance between molecular interactions.

Therefore, the number of these molecules that are of species $i$ is proportional to the mole fraction of species $i$ at position $x-L_m$. The molar flux of species $i$ passing through a plane located at position $x$ in the positive $x$-direction due to diffusion ($\partial N_{i,x}^{''}$) is given approximately by

$$\partial N_{i,x}^{''} \approx N v_m y_{i,x-L_m} \tag{14}$$

The length between molecular interactions is much smaller than the length scale that characterizes the problem, Equation14 can be written in terms of the gradient in the mole fraction of species $i$

$$\partial N_i^{''} \approx -2N v_m L_m \frac{\partial y_i}{\partial x} \tag{15}$$

Equation 15 provides the motivation for Fick's law, which states that diffusive mass transfer is proportional to the gradient in the mole fraction of species $i$. The diffusion coefficient for species $i$ through the mixture ($D_{i,m}$) can be expressed by

$$\partial N_i^{''} = -N D_{i,m} \frac{\partial y_i}{\partial x} = -D_{i,m} \frac{\partial n_i}{\partial x} \tag{16}$$

On a mass basis, the gradient in the mass fraction or mass concentration of species is connected to the diffusive mass flux of species $i$ ($\partial m_i^{''}$), Fick's law can also be written by

$$\partial m_i^{''} = -\rho D_{i,m} \frac{\partial mf_i}{\partial x} = -D_{i,m} \frac{\partial c_i}{\partial x} \tag{17}$$

Equations 16 and 17 are statements of Fick's law of diffusion and define the diffusion coefficient for species $i$ in the mixture in the same way that the empirical observation that the flux is linear in the gradient is follow as Fourier's law of heat conduction.

$$q^{''} = -k \frac{\partial T}{\partial x} \tag{18}$$

The diffusion coefficient is related to the product of the mean velocity of the molecules and the average distance between molecular interactions. Notice that the diffusion coefficient has unit m²/s as does thermal diffusivity ($\alpha$) and kinematic viscosity ($\upsilon$). The diffusion coefficient plays the same role in diffusion mass transfer processes that $\alpha$ and $\upsilon$ play in heat transfer and momentum transfer processes, respectively [59].

### 2.2.4 Frequency Input Parameter to Eye for Passive Diffusion

Previous research (Nickerson et al, 1963) [60] in the testing of the resonant frequency of the human eye showed a little effect at frequencies greater than 50Hz. They suggest that a maximum of 40Hz as the resonant frequency of the eye is reasonable to avoid abnormal vision. Since distortion of the sinusoidal input at lower frequencies makes very low frequency analysis, the lower limit of 5 Hz is the constraint limit.

Incremental variations in frequency are enough to induce adequate diaphragm displacement while maintaining within safety limits for human subjects. Therefore if implant drug delivery device is not sufficient to provide the amount of therapeutic drug,

the structure of device including a membrane can be optimized to actuate from the external resonant vibration.

### 2.2.5    Small Deflection of PDMS Membrane

Since we consider the actuation manually at the beginning of the implant, a deflection of PDMS at the top of reservoir should be clarified to obtain the pressure and radius of forcing area. It is well known that solutions for small deflection of membrane theory. Small deflection in membrane theory is dominated by stresses in the plate [61]:

$$w(r) = \frac{Pr_d^2}{4\sigma_i h}\left[1 - (\frac{r}{r_d})^2\right] \qquad (19)$$

where w is the deflection of membrane, P is a uniform pressure on the surface of membrane, $\sigma_i$ is the intrinsic stress of a PDMS membrane, r, $r_d$, and h are the radial coordinate, diaphragm radius, and thickness.

The linear solution form for the deflection of a circular membrane under a uniform pressure and a pre-tension can be expressed by

$$w = w_0\left[1 - (\frac{r}{r_d})^2\right]^2 \qquad (20)$$

$$w_0 = \varepsilon\, r_d^3 \sqrt{\frac{qr_d}{Eh}} \qquad (21)$$

where $w_0$ is the maximum deflection at the center of the membrane, E, h, and ε are Young's modulus, plate thickness, and Poisson's ratio, respectively [61].

2.3 Design Concept

In order to determine the width and depth of channels that enable a robust, convection-free diffusion, two different microchannel A and B are firstly investigated. Mircochannel is expected to work as the medium of the reservoirs. Since microchannel is located between reservoir and the outlet, it may reduce the back flow of drug or make more slow diffusion to contribute the velocity magnitude. The active microchannel is useful to control the diffusion rate under the some concentration difference, but its measuring process is complicated. The microchannel acts as a filter for drug particles transport and has simple structures compared to typical micro pore filters. It is easier to control reverse diffusion than micro-pore filters under the concentration difference.

### 2.3.1     Single Straight Microchannel A

To understand the microchannel behaviors under diffusion, we have developed simple microchannel models with single straight channel that mimic the actual amount of drug and volume of vitreous cavity. One single reservoir was connected to microchannel that has an inlet and an outlet. The whole structure had a height of about 2.5mm. The widths of the channels ranged from 100 μm to 1000 μm and the depth of the channel was 65 μm. The channels acted as quasi-one-dimensional structures for diffusion. The schematic of single microchannel A is shown in Figure 2.1 that microchannel was 10mm long, and various widths (100, 250, 500, 750, and 1000 μm) are applied. The thickness of around 1.2 mm PDMS was covered on the top of the microchannel with a hole that was connected with a tube. The solution in reservoir could be exchanged via the microchannel with the outlet.
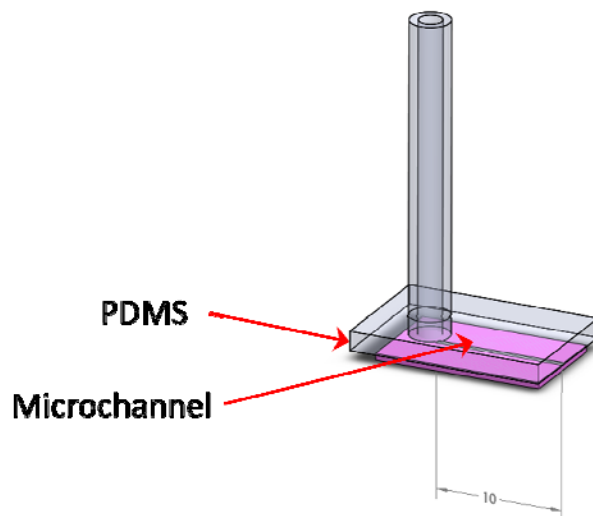
Figure 2.1 Design concept of single microchannel A being made of silicon wafer and covered with PDMS (Sylgard 184, Dow Corning) and tube (PTFE, PolyTetraFluoroEthylene, VICI AG International).

### 2.3.2    Single Straight Microchannel B

Two reservoirs were connected by channels of identical diameter. Each reservoir had an inlet and an outlet. The whole structure of reservoir had a height of 3mm and a diameter of 12mm. The widths of the channels ranged from a square of 200 μm to 1000 μm. The schematic of single microchannel B is shown in Figure 2.2 that microchannel was 20mm in length, and various widths (100, 250, 500, 750, and 1000 μm) were applied. The thickness of around 1.2 mm PDMS was covered on the top of the microchannel with holes on both reservoirs. The solution in each reservoir could be exchanged via the inlets and the outlet.
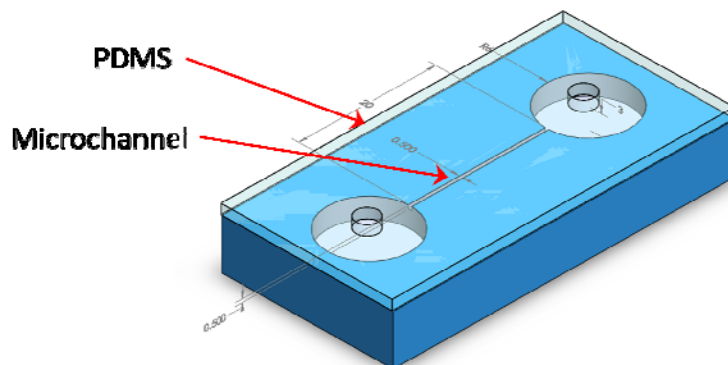
Figure 2.2 Schematic of single microchannel B being made of Lexan® glass with machining.

Table 2 Comparison of specifications between microchannel A and B

| Objects | Microchannel A | Microchannel B |
|---|---|---|
| Microchannel Length | 10 mm | 20 mm |
| Microchannel dimension | Depth of 65 $\mu$m, 100, 250, 500, 750, 1000 $\mu$m | Square of 200, 500, 750, 1000 $\mu$m |
| Amount of drugs | 5 $\mu\ell$ | 339.29 $\mu\ell$ |
| Solution | 50 % of citric acid in a drug of eye multi- purpose solution (10g of citric acid is dissolved in 20ml of drug until all anhydrous crystalline is invisible) | |
| Amount of DI water | 8580 $\mu\ell$ (same amount of human eye vitreous fluid) | 339.29 $\mu\ell$ |
| Initial value of pH | Drug solutions include citric acids – 0.3 pH / DI water – 6.7 pH | |

For measuring micro-particle image velocimetry, a test piece of microchannels including eight different sizes of channel was developed with one central located reservoir. The schematic of test piece of microchannels (Figure 2.3) shows that microchannel was 20mm long. Various two straight lined microchannels were a square of

250, 500, 750, and 1000 μm. The thickness of around 1.2 mm PDMS was covered on the

top of the microchannel without a hole. The solution in each reservoir could be

exchanged via the inlets and the outlet.
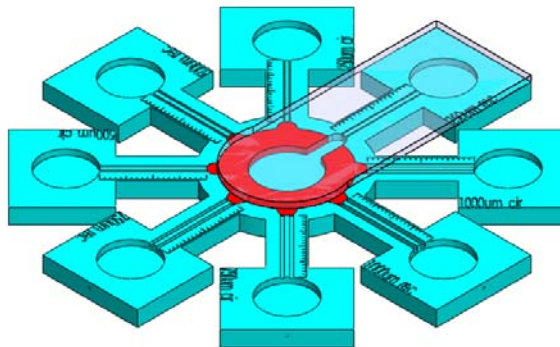


Figure 2. 3 Schematic of test piece of microchannels (250, 500, 750, and 1000 μm width
and depth) being made by Accura ®, Viper machine, 3D systems, for Particle Image
Velocimetry.

### 2.3.3    Various Geometry Microchannels

Various microchannel geometries are developed to simulate the thermal diffusivity as

shown in Figure 2.4. Four different micro-channels (type #1-4), which were straight,

meshed, tournament, and osmotic, were developed to maintain a constant flow rate.
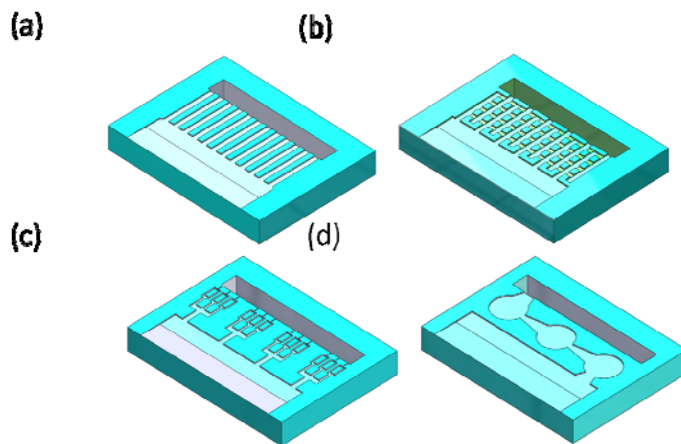
Figure 2.1 Various microchannels patterns considered for design analysis and simulation [62].

### 2.3.4      Device including Microchannels

A novel implantable device incorporating microchannels was proposed for ocular drug delivery. As shown in Figure 2.6, the drug was stored in a reservoir at one end of the device. Microchannels were coated with hydrophilic coatings so that the drug from the reservoir diffused through the channels at specified/designed rate into the eye eliminating the need for any controlled actuation.

In order to meet these characteristics, a unique design of an implantable micro-channel for medical drug delivery system should be proposed. The design concepts of drug delivery device will consist of two layers of PDMS and micro-channel. Both upper and lower PDMS will be bonded through oxygen plasma process and filled with Hydrogels. Overall dimensions can be 1.5mm×1.0mm×max.1.0mm as shown in Figure

2.5. A schematic of the implantable drug delivery device in the eye in which reservoir will be made by PDMS and polymer resin - Accura ® 50 (3D system corp.) is illustrated in Figure 2.6. In this study, the check valve was not applied in the drug delivery device; however, some micro-channels should be performed as its function of valve.
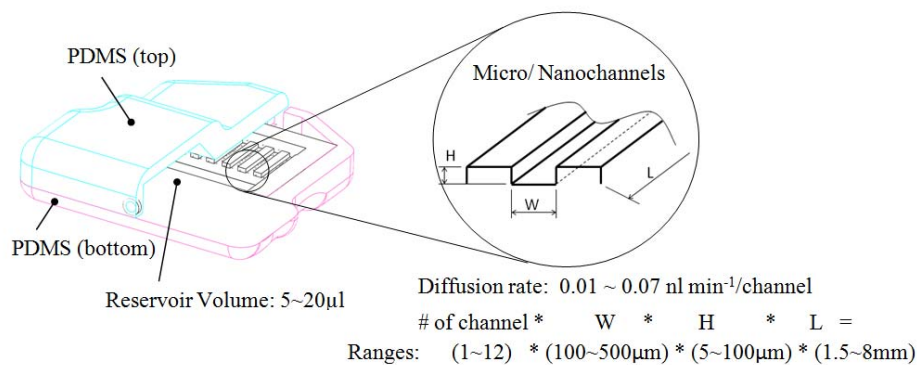


Figure 2.2 Overall dimensions of present device [62].
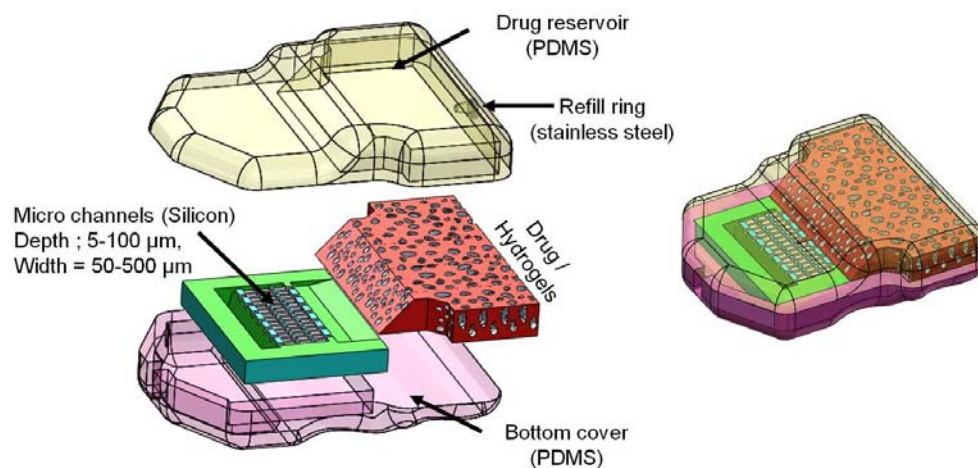


Figure 2.3 Present device design concept for ocular drug delivery [62].

Hydrogels (MIRAgel, MIRA Inc,Waltham,Mass), consisting of poly (methyl acrylate-Co-2-Hydroxyethyl acrylyte), are considered as means to passively induce the drug delivery into the microchannels so that the drug diffuses freely through the channels and reaches the outlet for delivery as a future work. The microchannel component with inlet/outlet reservoirs will be enclosed in a PDMS case whose base is rounded to match the curvature of the eye globe. The device is attached securely to the sclera of the eye with fine 10–0 or 9–0 nylon sutures. Ideally, the device would be surgically, transclerally implanted in the vitreous space with an external thin curved spherical surface flange that would be nearly flush with the sclera and sutured in place (see Figure 2.7).

Figure 2.4 Overview of the attachment of the implanted drug delivery device to the eye [62]

The design requirements for the proposed drug delivery device are as follows:

(i) target overall volume is less than 280mm$^3$;

(ii) diffusion rate is less than 0.07 nL/min;

(iii) target diffusion time period will be around 1 to 2 years;

(iv) kinetics: reliable diffusion coefficient of drugs through the microchannels;

(v) implantable: eliminate repeated injections for effective treatment;

(vi) actuation: sustained release drug delivery methods.

### 2.3.5      Eyeball including Implanted Drug Delivery Device

The diffusion model of drug movement in the eye can be depicted by Fick's second law.

$$\frac{\partial c}{\partial t} = \frac{\partial}{\partial x}\left(D\frac{\partial c}{\partial x}\right) + k_e c_0 \tag{22}$$

Where D is the diffusion coefficient or diffusivity in dimension of cm$^2$/s, c is the concentration of drugs in the reservoir, and $k_e$ is drug elimination constant.

In this study, we developed a diffusion model with a modified sphere eyeball for the pharmacokinetics of ocular drug delivery. The present model can predict the local velocity magnitude and pressure distribution as a function in time in the eye with

implantable delivery device. The diffusion coefficient of a drug across ocular tissues may depend on the chemical structure and the physicochemical properties as well as the molecular weight of the drug. The diffusion coefficient of a vitreous body ($2 \times 10^{-5}$ $cm^2$/sec) was observed by Tojo [50]. The diffusion coefficient in ocular tissues is mainly influenced by the molecular weight of the drug. The diffusion coefficient in the vitreous cavity is 10 times less than that in the aqueous humor.
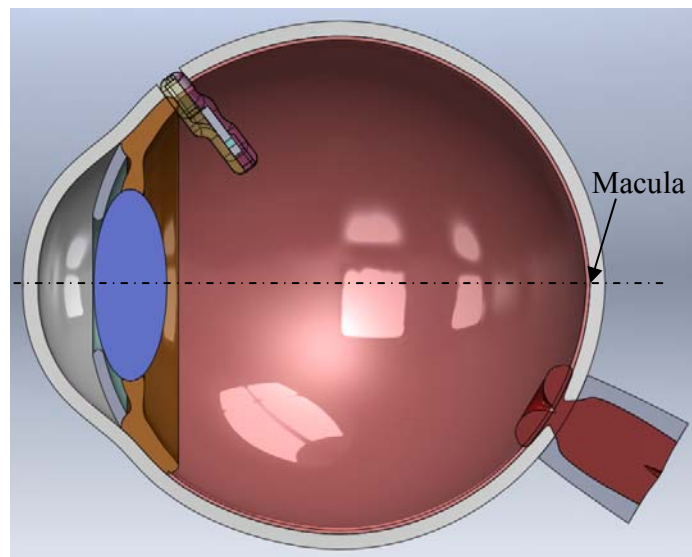


Figure 2.5 Schematic of a modified eyeball model with an implantable drug delivery device. The device is initially implanted as a perpendicular from a surface of eyeball.

The macula, which is related the AMD disease, is located at the back of the eye and is aligned with a center line of lens as shown in Figure 2.8. The present model is developed with actual size of eyeball to evaluate the concentration distribution in the macula region.

2.4 Design Calculations

To illustrate the targeted volume and rate of the drug delivery device, the following section provides the details of calculations. It has been assumed that drug-contained deionized water will be transported through the microchannel from a reservoir. The corticosteroid fluocinolone acetonide has low solubility, so that solution was made by dissolving 59 mg of $C_{24}H_{30}F_2O_6$ in deionized water of 50 μL (concentration in the device ≈ 1.18 mg/μL). We also assumed that the concentration of drugs in the water within the reservoir was around 1.18mg/cm$^3$ and concentration within the retina region of the eye was zero. Using this value of concentration, we could estimate the flux density of drug-contained water transport into the retina region by molecular diffusion. However, in this study, we assumed that the diffusion coefficient for typical eye drug, which is the corticosteroid fluocinolone acetonide in the deionized water, was equal to $2.5 \times 10^{-7}$ cm$^2$/s. The concentration of drug in the reservoir was very large in comparison to the concentration in the retina region. To calculate the flux density, we use Fick's Law (1), assuming that the gradient of concentration with length is linear over the microchannels path. The diffusive flux will be from the reservoir to the eye, from a high concentration to a lower concentration.

It is a natural phenomenon that a substance goes from high concentration regions to low concentration regions. The movement of *c(x, t)* is called the flux of the population density, which is a vector. This principle is called Fick's first law in one dimension, which relates the diffusive flux to the concentration and is given as,

$$J = -D* \, \partial c \, / \, \partial x \; + \; k_e \cdot c \tag{23}$$

where, $J$ is the diffusion flux (g/cm$^2$·s), $D$ is the diffusion coefficient or diffusivity in dimension of cm$^2$/s, $c$ is the concentration of drugs in the reservoir, and $k_e$ is a drug elimination constant. $k_e$ is not considered in this simulation because it may vary based on the property of drug and the absorption rate of drug in the human eye.

Using, the above values, we get

$$J = - 2.3 \times 10^{-7} \text{ cm}^2/\text{s} \cdot 1.18 \text{ g/cm}^3/0.8 \text{ cm}$$

$$= - 3.39 \times 10^{-7} \text{ g/cm}^2 \cdot \text{ s}. \tag{24}$$

Ignoring the diffusion direction, we calculate the flux density of $3.39 \times 10^{-7}$ g/cm$^2$ · s and it can be used to calculate the total mass flux of drug into the eye using (3) given below. For example, if the straight microchannel has an inlet area of 0.0005 cm$^2$ with 12 separate pathways, then the total flux into the eye is

$$M_{total} = J \times A, \tag{25}$$

where, $A$ is a section area at the inlet.

Using the above values, we get

$$M_{total} = 3.39 \times 10^{-7} \text{ g/cm}^2 \cdot \text{s} \times 0.0005 \text{cm}^2 \times 60 \text{ s/minute}$$

$$= 1.02 \times 10^{-8} \text{ g/ min}$$

$\approx 1.04 \times 10^{-4}$ μL/ min or 2.58mg/month (total 12 microchannels).          (26)

As per our specification, the drug delivery device contains drug of 6mg in the deionized water, it can be continuously used for around 11 to 12 months without refilling injection [62].

In molecular diffusion, a transport of molecules varies linearly with respect to time for Fickian diffusion and a diffusion rate can be explained by

Diffusion rate = J x A

Substitute by Diffusion rate = - $D_{diff} \times (C_{reservoir} - C_{outlet}) / L \times A$

Where, $D_{diff}$ = Drug diffusion coefficient ($cm^2$/s), $C_{reservoir}$ = Concentration of drug in a reservoir (mol/$cm^3$), $C_{outlet}$ = Concentration of drug at the outlet (mol/$cm^3$), L = Length of micro-channels (cm), and A is equal to area of micro-channel ($cm^2$).

Once we assumed that a diffusion coefficient of Brimonidine in water is 2.34 x $10^{-9}$ $cm^2$/s, drug concentration changes at the outlet of device is divided by length of microchannel. Therefore, for instance, diffusion rate of straight channel can be calculated by

2.34 x $10^{-9}$ x ((0.273879 – 0) /1) x 0.05 x 0.0065 = 2.082 x $10^{-13}$ (kmol/s).

2.5 Similarity with Scale Up Model

Even though the implantable device is at a micro-scale, a scaled up millimeter-device from micro-scale to millimeter scale model (from 10 μm to 1 mm) was developed in this investigation. This is due to our ultimate objective of developing a micro-fluidic drug delivery device (1 nL/s ~100 nL/s) mimicking the overall microchannel geometry configuration. Table 2.2 lists the various parameters (length, diameter, water density, and viscosity) of the nano-scale biological motor and the present microchannel B model. The similarities between the nano-scale biological device and the present micro-device are shown in Table 2.3. As can be seen from Table 2.3, we kept the geometric similarity to be 1 so that the continuum mechanics were held and the results of velocities and flow rate would be similar between the nano-scale and millimeter scale considered. In order to further illustrate this aspect, a nano-scale model was built and the results were compared to those obtained by the micro-scale model. In general, the results from the millimeter micro-device model were applicable to the nano-scale model with the scaled up ratio ($\lambda$) and the trends were also similar. In addition, surface area is another factor that becomes important at the micro-scale. As an example, a 35 mm diameter beaker half full of 2.5 mL water had a surface area to volume ratio of 4.2 $cm^{-1}$, whereas a microchannel 50 μm tall, 50 μm wide, and 30 mm long, a 75 nL volume, had a surface area to volume ratio of 800 $cm^{-1}$. When going from the macroscale to the microscale, an increase in the surface area to volume ratio by orders of magnitude is not uncommon. A very large surface area to volume ratio makes capillary effect more efficient in microchannels [63].

Table 3 Various parameters used in the present microchannel B model in comparison to nano-scale biological device [63].

| Variable | Nano-scale biological motor | Present micro-scale device | Ratio ($\lambda$) | Units |
|---|---|---|---|---|
| Length($L$) | $0.2 \times 10^{-3}$ | 20 | $10^5$ | mm |
| Diameter($D$) | $0.12 \times 10^{-3}$ | 12 | $10^5$ | mm |
| Density of water($\rho$) | 1000 | 1000 | 1 | $kg \cdot m^{-3}$ |
| Dynamic viscosity($\mu$) | $1.0 \times 10^{-3}$ | $1.0 \times 10^{-3}$ | 1 | Pa·s ($N \cdot s \cdot m^{-2}$) |

Table 4 Dimensionless similarities between nano-scale biological device and the present micro-scale model of microchannel B.

| Similarity | Variable | Scaled ratio ($\lambda$) |
|---|---|---|
| Geometric | Rate of diameter over length ($D/L$) | 1 |
| Kinematic | Velocity ($V$) | $10^5$ |
| | Flow rate ($Q$) | $10^{15}$ |
| Dynamic | Pressure ($P$) | $10^{10}$ |

## 2.6 Hydrophobic and Hydrophilic

Hydrophobic molecules tend to be non-polar and thus prefer other neutral molecules and non-polar solvents. Hydrophobic molecules in water often cluster together forming micelles. Water on hydrophobic surfaces will exhibit a high contact angle.

In general, a hydrophobic surface that has an original contact angle greater than 90° becomes more hydrophobic when microstructured – its new contact angle becomes

greater than the original. However, a hydrophilic surface that has an original contact angle less than 90° becomes more hydrophilic when microstructured – its new contact angle becomes less than the original.

A liquid droplet rests on a solid surface and is surrounded by air. From Figure 2.8, the contact angle, $\theta_C$, is the angle formed by a liquid at the three phase boundary where the liquid, air, and solid intersect.
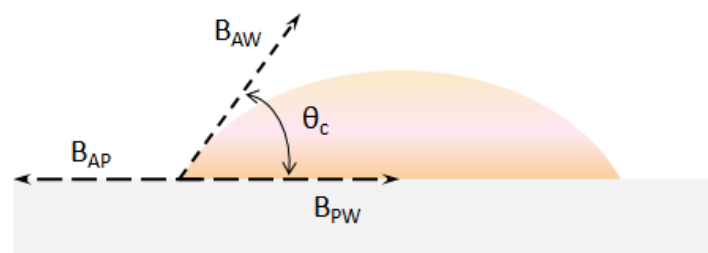


Figure 2.6 Schematic overview for the contact angle between water droplet and PDMS surface; $\theta_C$ is the contact angle, $B_{AW}$ is the boundary line between air and water following $B_{AP}$ - air and PDMS, $B_{PW}$- PDMS and water.

## 2.7 Discussion

In a liquid, every atom is in random motions and these random motions produce both diffusion and viscous flow when the motions are driven by a force. The Fick's law depicts that the diffusion occurs when molecular particle in high concentration moves forward to low concentration region.

The design of an implantable drug delivery device and experimental models should be comparable to verify the diffusion rate and drug releasing time. Although the diffusion coefficient of a drug may depend on the chemical structure and the physicochemical properties as well as the molecular weight of the drug, a consistent boundary condition and various size of microchannel are mainly focused to manipulate the diffusion rate and to obtain the best fit of microchannel geometry. Although the diffusion rate is calculated based on the diffusion coefficient of $2.5 \times 10^{-7}$ cm²/s and flux density of $3.39 \times 10^{-7}$ g/cm² · s, the rate of diffusion may change with respect to time. The single straight microchannel A and B have developed to investigate the diffusion characteristics in the microchannel. Both microchannel A and B have a different cross section area of microchannel and length to ensure that the diffusion rate are proportional to the size of microchannel and adversely proportional to the length of microchannel.

The similarities between the nano-scale biological device and the present micro-device are discussed to understand the continuum mechanics and the results of velocities. The molecular flow rate will be similar at the nano-scale and micrometer scale.

## 2.8 Summary

Based upon the theoretical background of the diffusion, several straight microchannels were developed to analyze the diffusion coefficient in associate with dimension of microchannel. Two different microchannels were firstly investigated such as microchannel A and B. Mircochannel was expected to work as a medium of reservoir. Since microchannel was located between reservoir and the outlet, it may reduce the back

flow of drug or make more slow diffusion to contribute the velocity magnitude. An implantable drug delivery device integrated microchannel may be suitable for a practical application with free diffusion.

# CHAPTER 3 Simulations for Microchannels and Devices

## 3.1 Introduction

To understand the characteristics of diffusive drug delivery through the proposed microchannel design, three-dimensional flow characterizations were conducted using combined computational fluid dynamics (CFD) analysis based on Eulerian-Lagrangian methods. Computational fluid dynamics is became a leading component in microfluidic device design by providing predictions of device performance for a variety of research focuses. With increases in computational resources and numerical techniques, the accuracy and scope of CFD applications are rising. For microfluidic devices such as micro-pump, micro-value, micro-dispensing, and micro-spotter, CFD could provide cost-effective insight into device performance compared with conventional prototyping, manufacturing and experiments. [64 - 69, 71]  Over the couple of decades, numerical analysis of the diffusion flow using CFD have been utilized for evaluating characteristics of microchannel designs such as diffusion coefficient, pharmacokinetics, and molecular particle transport properties [72, 73]. With adjustments in simulated boundary and diffusion conditions, parameters influencing diffusion coefficient are easily modified to obtain a device with desired properties. In this research, the finite element method was performed for the microchannel A, microchannel B, entire device, various geometry microchannel, and eyeball with implantable device using ANSYS V12 – Fluent and COMSOL multiphysics. COMSOL has a flexible platform that allows modeling all relevant physical aspects of model designs. It is useful to develop customized solutions,

applicable to unique circumstances. When starting a new project, using COMSOL Multiphysics helps to understand its several problem solving. User can perform to test out various geometrical and physical characteristics of diffusion model in order to obtain the important design challenges.

Currently the only approach available to users is a trial-and-error approach that requires large numbers of experimental tests or numerical simulations. The numerical simulations typically involve unacceptably long computation time and are limited by algorithmic stability. For example, accurate simulations of microchannel diffusion at the various geometry regions by finite volume approaches become very difficult due to errors associated with numerical diffusion, unless extremely fine meshes are used. To address these issues, several modified form models have been developed for diffusion coefficient.

## 3.2 Single Straight Microchannel A

### 3.2.1   Governing Equations and Computational Methods

The general form of the diffusive transport equation for additional variable is

$$\frac{\partial(\rho\emptyset)}{\partial t} = \nabla \cdot (\rho D_c \nabla \emptyset) + S_\emptyset \tag{27}$$

By substituting the conserved quantity, $\emptyset = \frac{c}{\rho}$, we get

$$\frac{\partial c}{\partial t} = \nabla \cdot (D_c \nabla c) + S_{c/\rho} \tag{28}$$

Where $\rho$ is the mixture density, mass per unit volume, c is the conserved quantity per unit volume, or concentration, $S_{c/\rho}$ is a volumetric source term, with units of

conserved quantity per unit volume per unit time, and $D_c$ is the kinetic diffusivity for the scalar.

### 3.2.2    Computational Models and Boundary Conditions

The first step to begin this analysis was to create a three-dimensional fluid model of the single straight microchannels using modeling software, which was the SolidWorks (Dassault Systèmes SolidWorks Corporation, Waltham, MA). Once a three dimensional fluid model of the single straight microchannels was completed, this fluid model may work to convert a solid model of structural compartments. (Figure 3.1).

ANSYS Workbench software was the unifying graphical user interface to the multitude of ANSYS simulations, which were predominantly based on implementations of the finite element method and computational fluid dynamics. This workbench had a Fluent analysis function includes a design modeler, meshing and defining a boundary surface, and CFD-post. These functions were used to develop the three-dimensional model of the microchannel and reservoir geometry. In this study, the three-dimensional fluid model then was imported into design modeler with a parasolid format and meshed (Figure 3.2). This software allowed the mesh to be generated and created, which was a standard preprocessor for ANSYS-Fluent software. Due to symmetry, only one half of the domains were constructed. A structural hexahedral mesh was employed to provide a high quality flow field solution.

The ANSYS Fluent utilized finite volume based methods to mathematical solve non-linear partial differential equations and simplified them into a system of algebraic equations which were solved numerically through various iterations. Values derived from

the fluent usually experienced discretization using central difference methods and in most instances were second-order accurate in diffusion terms.

The segregated solver was chosen and mainly utilized for flow that was incompressible where the resulting algebraic equations were solved sequentially as opposed to the couple solver which solved the algebraic equations simultaneously due to the inter-dependence of scalars associated with the flow field. The model was also laminar which results in no energy equation being solved. The fluid was set as water-liquid with the corresponding properties: Density, $\rho$: 998.2 kg/m$^3$ and Viscosity, $\mu$: 1x10$^{-3}$ kg/m-s, diffusion coefficient, D: 2.5 x 10$^{-7}$cm$^2$/s.

The inlet boundary condition at the top of the reservoir was a diffusion logarithmic form, which was produced by pH value with respect to time in the first diffusion experiments. The properties of drug are assumed to be those at 27 °C. No pressure outlet of the fluid domain was applied. A no-slip boundary condition was applied at the fluid-solid interface. Figure 3.1 shows the finite element model and all boundary conditions of the single straight microchannel A.

| Domain | Nodes | Elements |
| --- | --- | --- |
| 100 µm | 28326 | 124855 |
| 250 µm | 29106 | 132870 |
| 500 µm | 41257 | 190724 |
| 750 µm | 52574 | 245500 |
| 1000 µm | 66962 | 312552 |

Materials
water- liquid
Density: 998.2 kg/m³
Viscosity: 0.001003 kg/m·s

VELOCITY-INLET

Vitreous Body volume (8.58ml)

Drug volume (5µl)
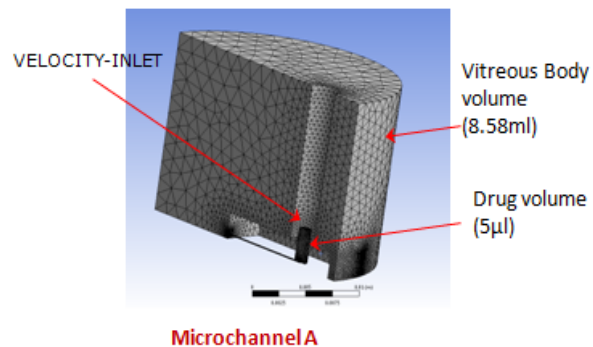
**Microchannel A**

Figure 3. 1 Finite element model and all boundary conditions of straight microchannel A, denotes the number of elements and nodes for each microchannel size.

The model solution methods were set as variables for pressure-velocity coupling schemes as well as the method of computing the gradient in Least Squares Cell Based Flow which contained the discretization schemes available for the pressure and momentum equations: first order upwind and second order upwind.

### 3.2.3  Diffusion Motion

A user-defined function written in the C programming language was used to manipulate the movement of the particle at the inlet which located on top of the reservoir. The uniform diffusion was set on top of the reservoir, which was governed with the following expression in order to create the periodic velocity changes associated with the diffusion coefficient and the logarithmic changes that we obtained from the first measurement:

```
c# program code
/* UDF for specifying a transient velocity profile boundary condition */
DEFINE_PROFILE(Diffusive_velocity, thread, position)
{
 face_t f;
 begin_f_loop(f, thread)
  {
   real t = RP_Get_Real("flow-time");
   if(t<=1.0)F_PROFILE(f, thread, position) = 0.0000000025;
   else if(t>1.0)F_PROFILE(f, thread, position) = 0.0000000025*(-0.028*log(t) + 0.8972);
   else {}
  }
 end_f_loop(f, thread)
```

This program was utilized and defined to the diffusive velocity at the inlet, which allowed one to determine the diffusion characteristics of the fluid. The expected operating method of the diffusion was to travel particles (or fluid) from inlet to outlet, which was studied for all the microchannel models.

### 3.2.4  Model Validation

Most CFD applications in microfluidic devices investigated steady-state and transient conditions such as pressure distribution and velocity fields. Pathlines and streamlines yield information as to how diffusion flowed through microchannels and variances in fluid velocities, particle residence time, and pressure contours have been used to assess global uniformity of the flow field.

It is well known that non-uniform diffusion characteristics were undesirable, and it is often believed that flow path heterogeneities could lead to inactive diffusion flow. Likewise, single straight microchannels were designed to achieve uniform flow

distribution in order to eliminate significant factors of pressure and concentration changes from the geometric configurations, and to optimize diffusion efficiency.

A mesh-independence study was performed on the solid and fluid domains to confirm that a fine enough element had been used to represent both solid and fluid domains. The mesh-independence study begun with a mesh discretization and recorded a solution. Then the finer elements were used to represented fluid domains. The results from the finer-element model were then compared with those from the first model. If the results were nearly similar, then the first mesh was probably good enough for that particular geometry, loading and constraints. If the results differed by a large amount, the process was repeated with the finer elements. Maximum pressure and velocity were used as convergence criteria for the fluid domain. A converged model was obtained when changes in those solutions were less than 5%. Having performed the mesh-independence study, the diffusion velocity from the finite element model for a single divergence was then compared to the experiment by single straight microchannel A.

### 3.2.5   Diffusion model in COMSOL

The transient analysis of diffusion in 2D was performed according to concentration changes while using COMSOL multiphysics. The diffusion coefficient D and concentration changes with respect to time were a variable for this analysis. The other boundary condition and temperature were a constant.

Boundary condition;   C0 = 1, at the reservoir

C0 = 0, at the microchannel and outlet

D = 2.34 x10$^{-9}$ cm$^2$/sec

C0,t = D*(-0.028*log(t[1/s]) + 0.8972
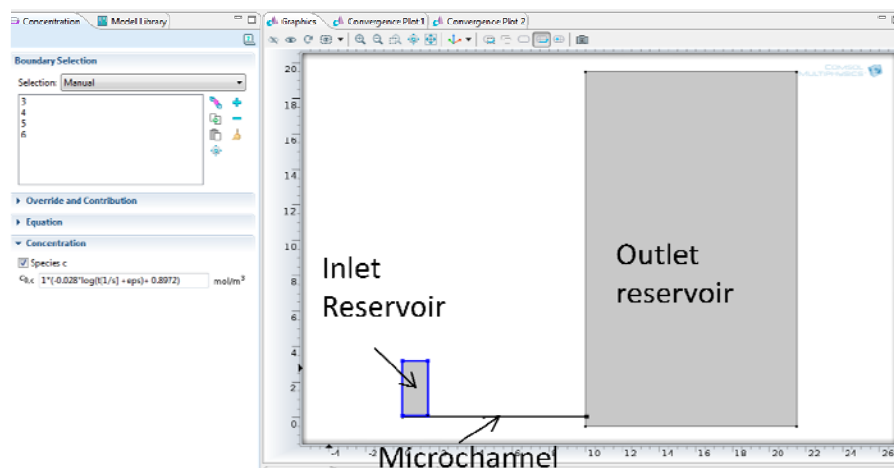


Figure 3. 2 Geometry and boundary conditions of microchannel A in COMSOL

3.3 Single Straight Microchannel B

3.3.1    Governing Equations and Computational Methods

The general form of the diffusive transport equation for additional variable was applied

same as governing equation of previous microchannel A.

$$\frac{\partial c}{\partial t} = \nabla \cdot (D_c \nabla c) + S_{c/\rho} \tag{29}$$

### 3.3.2    Computational Models and Boundary Conditions

Once a three dimensional fluid model of the single straight microchannel B was completed, this fluid model may work to convert a solid model of structural compartments. (Figure 3.2).

The segregated solver was chosen and mainly utilized for flow that was incompressible. The model was also laminar which results in no energy equation being solved. The fluid was set as water-liquid with the corresponding properties: Density, $\rho$: 998.2 kg/m3 and Viscosity, $\mu$: $1 \times 10^{-3}$ kg/m-s, diffusion coefficient, D: $2.5 \times 10^{-7}$ cm$^2$/s.

The inlet boundary condition of the fluid domain was a diffusion logarithmic form, which was produced by pH value with respect to time in the first diffusion experiments. A pressure accounting at the outlet of the fluid domain was applied as zero. A no-slip boundary condition was applied at the fluid-solid interface. Figure 3.2 shows the finite element model and all boundary conditions that were applied same as the single straight microchannel A.

| Domain | Nodes | Elements |
|---|---|---|
| 200 µm | 21970 | 92888 |
| 500 µm | 10296 | 44106 |
| 750 µm | 7352 | 31365 |
| 1000 µm | 5670 | 24005 |

**Materials**
water- liquid
 Density: 998.2 kg/m³
 Viscosity: 0.001003 kg/m·s



Figure 3. 3 Finite element model and all boundary conditions of straight microchannel B, denotes the number of elements and nodes for each microchannel size.

Again, same as like microchannel A, the model solution methods were set as variables for pressure-velocity coupling schemes as well as the method of computing the gradient in Least Squares Cell Based Flow which contained the discretization schemes available for the pressure and momentum equations: first order upwind and second order upwind.

### 3.4 Various Microchannel Configurations

### 3.4.1 <u>Governing Equations and Computational Methods</u>

The ANSYS Multiphysics product supported a transient thermal analysis. Transient thermal analysis determined temperatures and other thermal quantities that vary over time. We commonly used temperatures that a transient thermal analysis calculated as input to structural analyses for thermal stress evaluation or diffusion simulation because the preliminary equations were identical. A transient thermal analysis followed basically the same procedures as a steady-state thermal analysis. The main difference was that most applied loads in a transient analysis were functions of time. To specify time depend loads, we used the function tool as a boundary condition.

The first law of thermodynamics stated that thermal energy was converged. Specializing this to a differential control volume:

$$\rho h \left[ \frac{\partial T}{\partial t} + \{v\}^T \{L\} T \right] + \{L\}^T \{q\} = \ddot{q} \tag{30}$$

where ρ is density of the fluid, h is specific heat, T is temperature, and t is time.

{L} is a vector operator and $\{v\}$ is a velocity vector for mass transport of heat

$$v_x$$
$$v_y$$
$$v_z$$

$$\{L\} = \left\{ \begin{array}{c} \frac{\partial}{\partial x} \\ \frac{\partial}{\partial y} \\ \frac{\partial}{\partial z} \end{array} \right\} \qquad \{v\} = \left\{ \begin{array}{c} \\ \\ \end{array} \right\} \tag{31}$$

Where $\{q\}$ is heat flux vector, and $\ddot{q}$ is a heat generation rate per unit volume.

### 3.4.2        Computational Models and Boundary Conditions

Microchannel pattern was considered to be also provided by the recent reviews on the application of microfluidic lab-on-a-chip platforms [74, 75]. The first step to begin this analysis was to create a three-dimensional fluid model of four different microchannel configurations using modeling software, which was the SolidWorks. Once a three dimensional fluid model of different microchannel configurations was completed, this fluid model may work to convert a solid model of structural compartments (Figure 3.3). The overall dimensions of microchannels were within a range of 1.5 ~ 8.0mm in length, had a depth of 5 to 100 μm and a width may vary based on the geometry of microchannels (50 ~ 500 μm) as shown in Figure 3.3
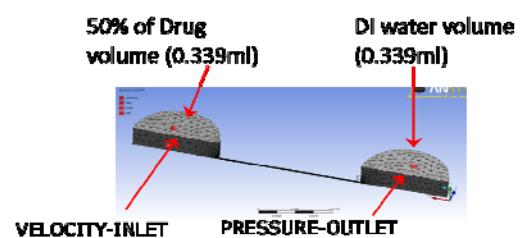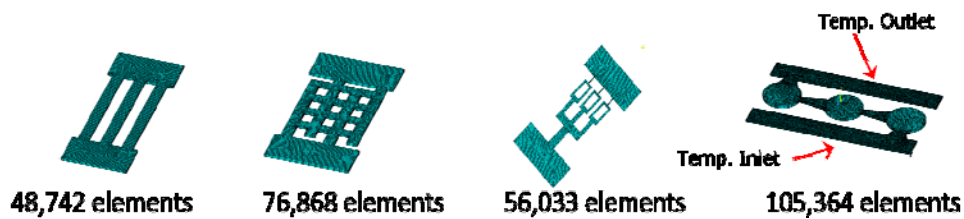
Figure 3. 4 Finite element model and all boundary conditions of various microchannel configurations, denotes the number of elements for each microchannels [62].

In order to understand the design characteristics of the microchannels, we developed a coarse-grained representation of the microchannel geometry through computational fluid dynamic analysis and optimization. Specifically, the role of the microchannel geometry in passive free diffusion that molecules could pass freely through the microchannel follow concentration gradients was investigated and discussed. Figure 3.6 shows the finite element model and all boundary conditions that were used for the various microchannel configurations. Finite element (FE) analysis using ANSYS-Multiphysics module was used to perform the design simulations. Four different microchannel geometries were developed to simulate the thermal diffusivity as shown in Figure 3.3. Drug concentration at the reservoir was assumed to be 1 kmol/m$^3$ and drug concentration at the outlet to be 0 kmol/m$^3$. This concentration represented drug concentration in the eye. Drug diffusivity was assumed to be the same as the synthetic corticosteroid Fluocinolone acetonide in deionized (DI) water ($2.3 \times 10^{-7}$ cm$^2$/s) [22].

The properties of fluid material;

Density:  $\rho$ = 998 kg/m$^3$

Viscosity: μ = 0.001

Conductivity: k = 0.6 W/m-K

Specific Heat: $h_p$ = 4181.3 J/kg-K

Element type:  Thermal -3D SOLID 90

Boundary conditions: 60°C at the inlet wall, 37.5°C at the outlet wall and other fluid walls

### 3.5 Drug Delivery Device include Microchannels

#### 3.5.1    Governing Equations and Computational Methods

The general form of the diffusive transport equation for additional variable is applied same as governing equation of previous microchannel A.

$$\frac{\partial c}{\partial t} = \nabla \cdot (D_c \nabla c) + S_{c/\rho} \tag{29}$$

#### 3.5.2    Computational Models and Boundary Conditions

Once a three dimensional fluid model of the microchannel configurations was completed, this fluid model may work to convert a solid model of structural compartments. (Figure 3.4).
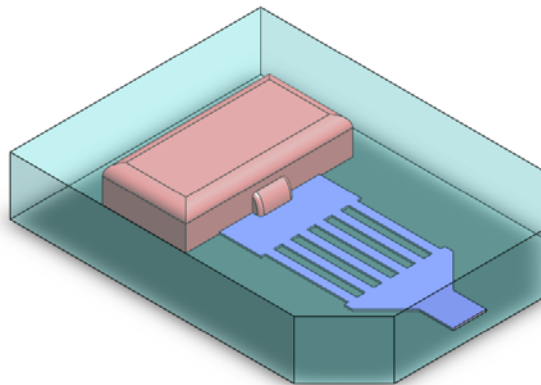
Figure 3. 5 Solid model of microchannel configuration within the device using Solidworks

The segregated solver was chosen and mainly utilized for flow that was incompressible. The model was also laminar which results in no energy equation being solved. The fluid was set as water-liquid with the corresponding properties: Density, $\rho$: 998.2 kg/m$^3$ and Viscosity, $\mu$: 1x10$^{-3}$ kg/m-s, diffusion coefficient, D: 2.5 x 10$^{-7}$cm$^2$/s.

The inlet boundary condition at the top of reservoir was a diffusion logarithmic form, which was produced by pH value with respect to time in the first diffusion experiments. A pressure accounting at the outlet of the fluid domain was applied as zero. A no-slip boundary condition was applied at the fluid-solid interface. Figure 3.5 shows the finite element model and all boundary conditions that were applied same as the single straight microchannel A.

$$D = 2.34 \text{ x}10^{-9} \text{ cm}^2/\text{sec}$$

$$C0,t = D*(-0.028*\log(t[1/s]) + 0.8972$$



Figure 3. 7 Geometry and boundary conditions of device in COMSOL

3.6 Results

3.7.1        Effect of Microchannel A



Figure 3. 8 Simulation results of maximum velocity magnitude for five different microchannels, data is observed at the outlet of microchannel A.

The results of maximum velocity magnitude for five different microchannels showed that a smaller cross section of microchannel had higher velocity magnitude than small one (Figure 3.9). The velocity magnitudes were adversely nonlinear to the size of microchannel. It can be assumed that a modeling the various size of microchannel properly played an important role in the prediction of microchannel efficiency.

Figure 3. 9 Simulation results of velocity profiles for four different microchannels, data is observed at the inlet, middle, and outlet of microchannel A.

The above Figure 3.10 shows the comparison of the simulation results of velocity profiles for each microchannel. The microchannel size influenced the diffusivity all through microchannel coordination.  However since there was no slip boundary condition, the wall slip velocity was about zero. The slip velocity at wall was much smaller then that at the channel center. The flow velocity profile along horizontal central line y (m) of channel section for all microchannel size was shown in Figure 3.10.

Figure 3. 10 Simulation results of diffusion rate at one second for five different microchannels.



Figure 3. 11 Simulation results of diffusion rate at ten seconds for five different microchannels.

The above Figure 3.11 and 3.12 show the comparison of the simulation results of diffusion rate at 1 and 10 seconds for each microchannel. The diffusion rate increase along

the microchannel size increase, as previously predicted by diffusion equation 28. The variations of diffusion rate showed linearly decreasing with respect to time for 10 seconds.



Figure 3. 12 Simulation results of velocity differences at one second for five different microchannels.

Figure 3. 13 Simulation results of velocity differences at ten seconds for five different microchannels.

Figure 3.13 and 14 show that the velocity differences between inlet and outlet at 1 and 10 seconds explained small microchannel size generated relatively high resistance for the diffusion. The diffusive velocity difference increased with decrease of the microchannel size. Similarly the change of velocity difference reduced along the time goes on.
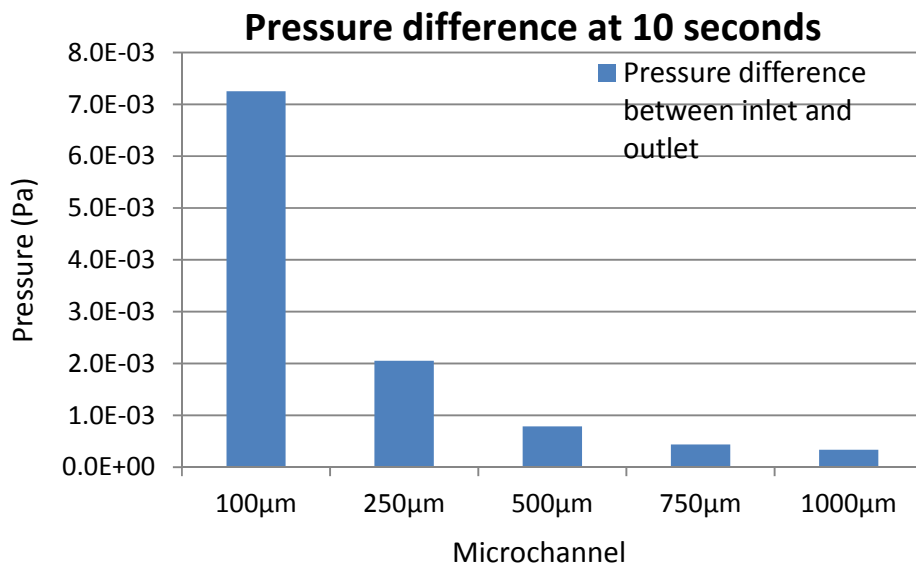
Figure 3. 14 Simulation results of pressure differences at ten seconds for five different microchannels.

The relationship of the pressure difference of the microchannel size is shown in Figure 3.15. The microchannel size increased with decrease of the pressure difference. Similar behaviors were found for diffusion rate. It indicated that the decreasing microchannel size enhanced the viscous effects on diffusion flow when pressure gradient was constant.

### 3.7.2     Effect of Microchannel B

The maximum velocity magnitude of microchannel is shown in Figure 3.16. The rest of parameters which were the relationship of the pressure, velocity difference with time variations against microchannel size were the same as the microchannel A.

From the velocity profile (Figure 3.17), we can be assumed that slowed diffusion also generate a parabolic curve along the channel length because it was similar as incompressible and laminar flow in the channel. Although diffusion was a molecular or viscous flow, velocity profiles and maximum velocity with microchannel size showed similar behaviors as small volume fluid flow.
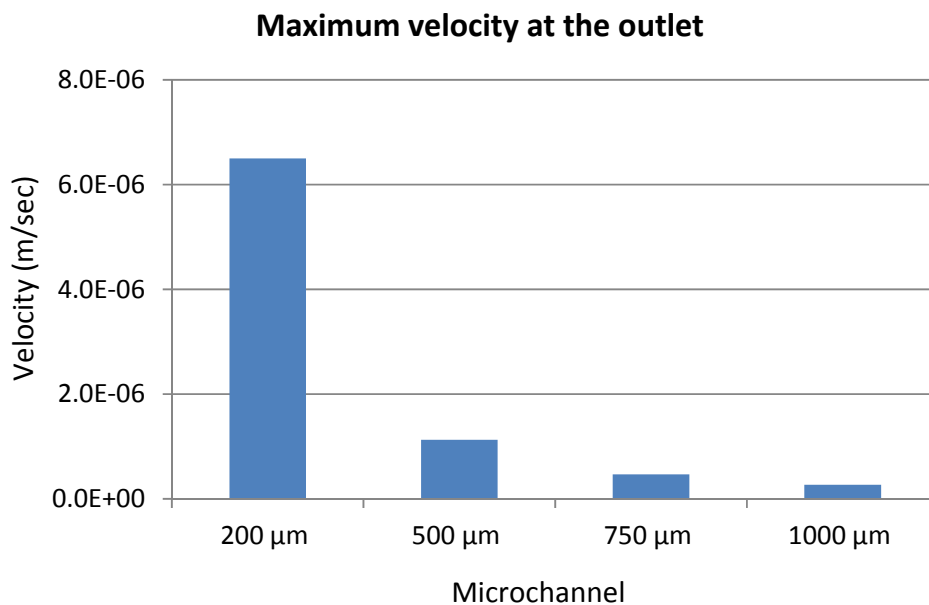


Figure 3. 15 Simulation results of maximum velocity magnitude for four different microchannels, data is observed at the outlet of microchannel B.
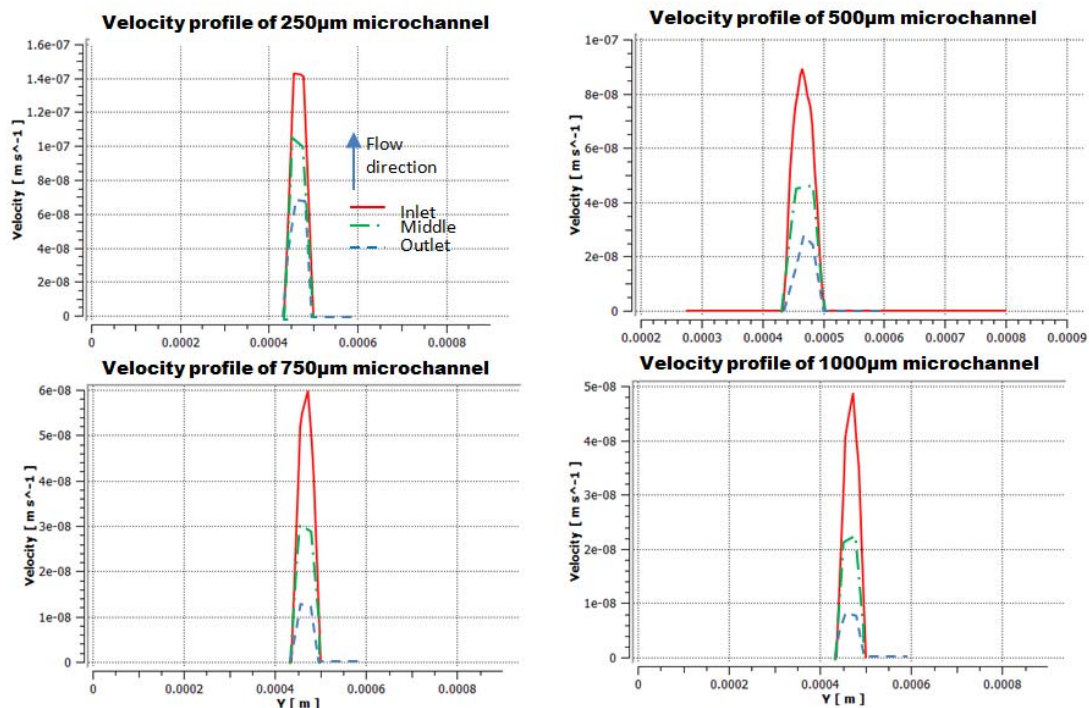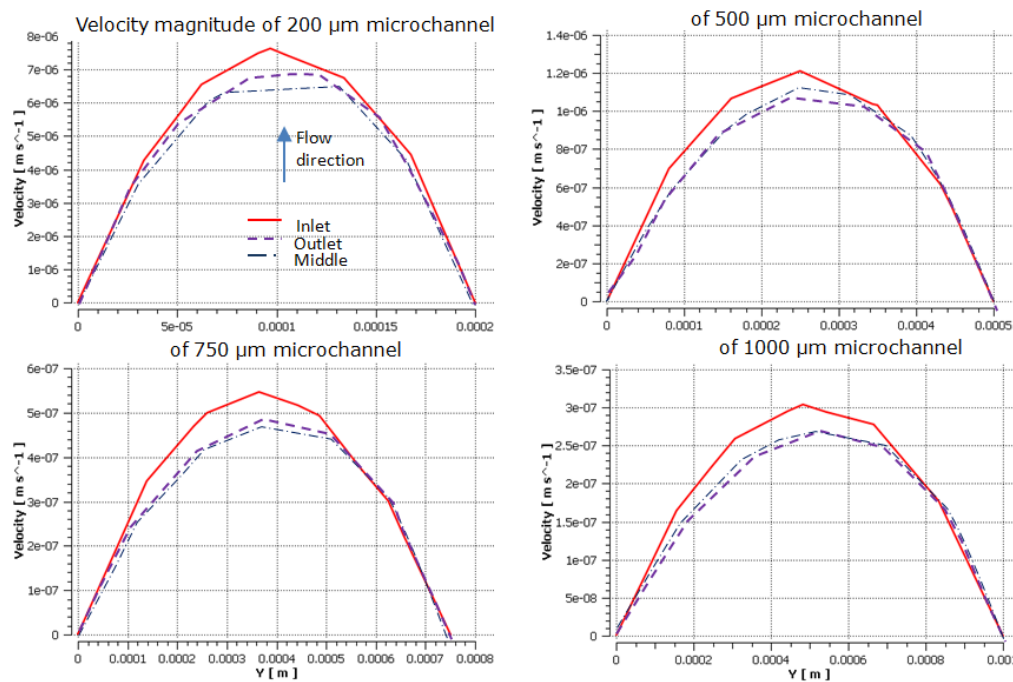
Figure 3. 16 Simulation results of velocity profiles for four different microchannels, data is observed at the inlet, middle, and outlet of microchannel B.

Again, the above Figure 3.17 shows the comparison of the simulation results of velocity profiles for each microchannel. The microchannel size influenced the diffusivity all through microchannel coordination. However since there was no slip boundary condition, the wall slip velocity was about zero. The slip velocity at wall was much smaller then that at the channel center. The flow velocity profile along horizontal central line y (m) of channel section for all microchannel size was shown in Figure 3.17.
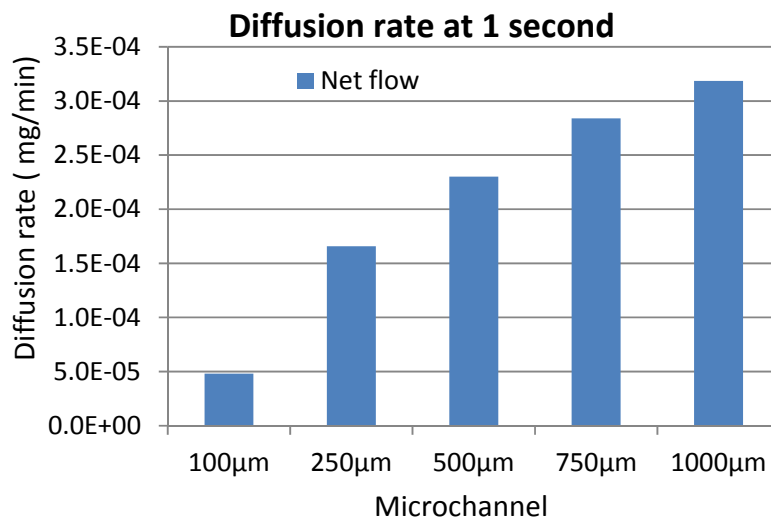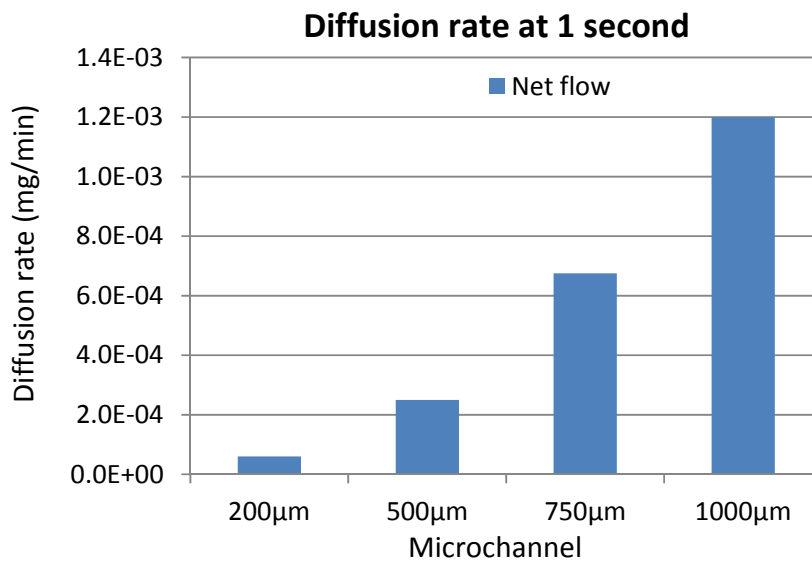
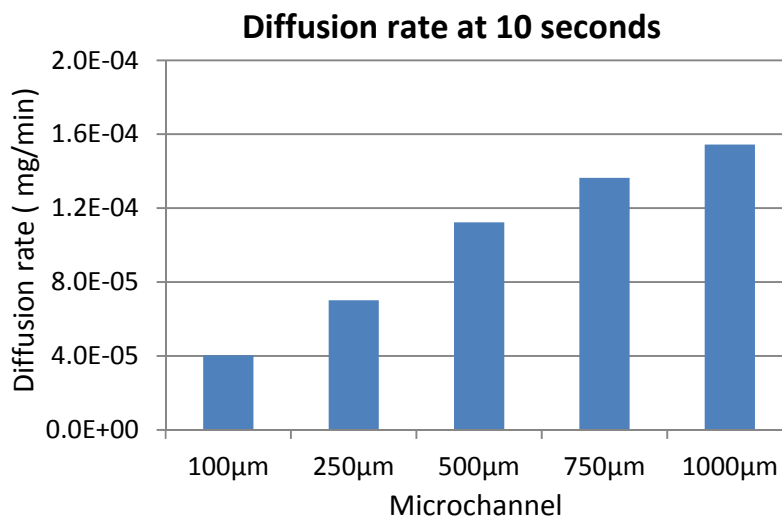Figure 3. 17 Simulation results of diffusion rate at one second for four different microchannel B.
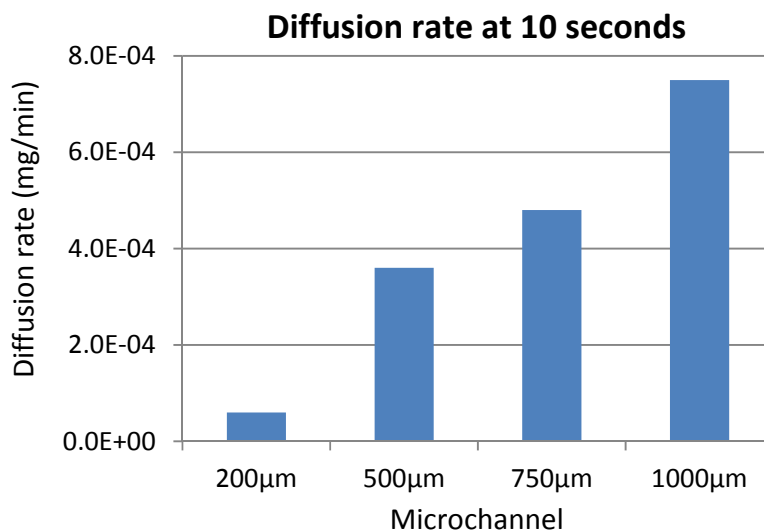


Figure 3. 18 Simulation results of diffusion rate at ten seconds for four different microchannel B.

Again, the above Figure 3.18 and 3.19 show the comparison of the simulation results of diffusion rate at 1 and 10 seconds for each microchannel. The diffusion rate increased

along the microchannel size increase, as previously predicted by diffusion equation 28. The variations of diffusion rate showed linearly decreasing with respect to time for 10 seconds.
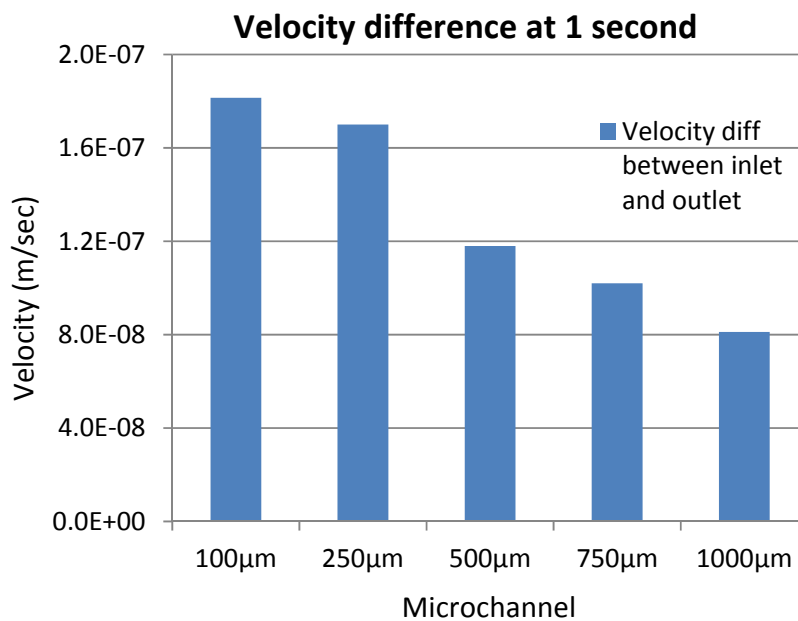


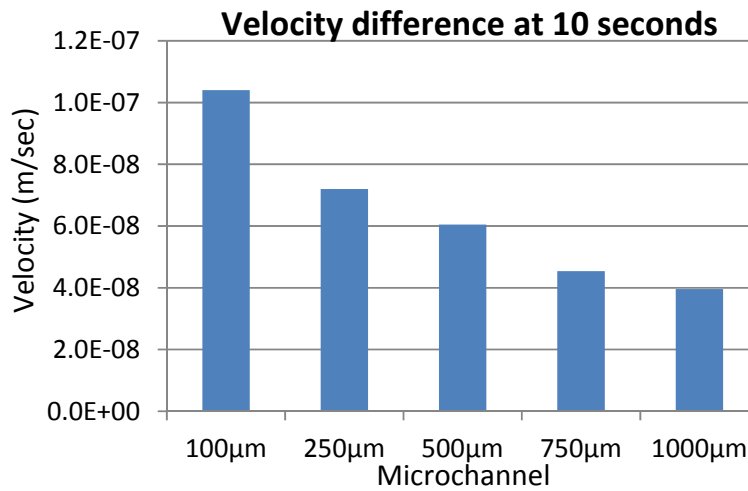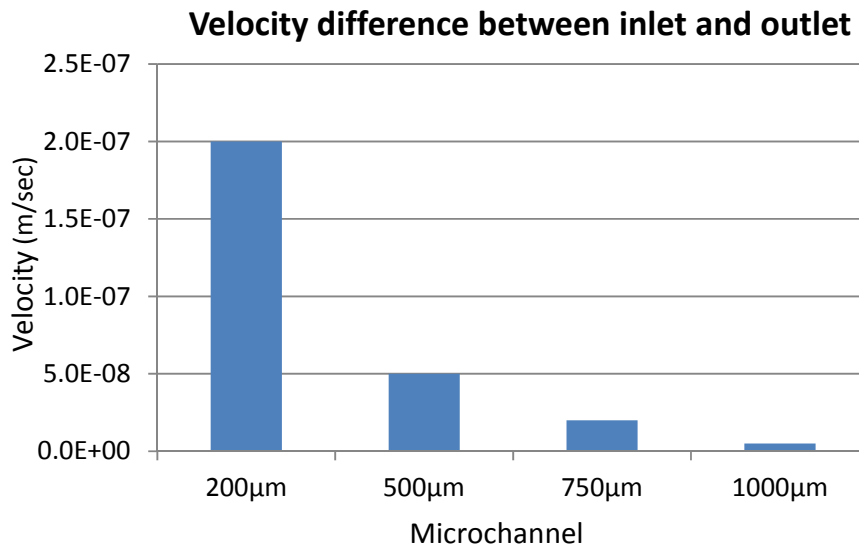Figure 3. 19 Simulation results of velocity differences at ten seconds for four different microchannel B.

**Pressure differences at 10 seconds**
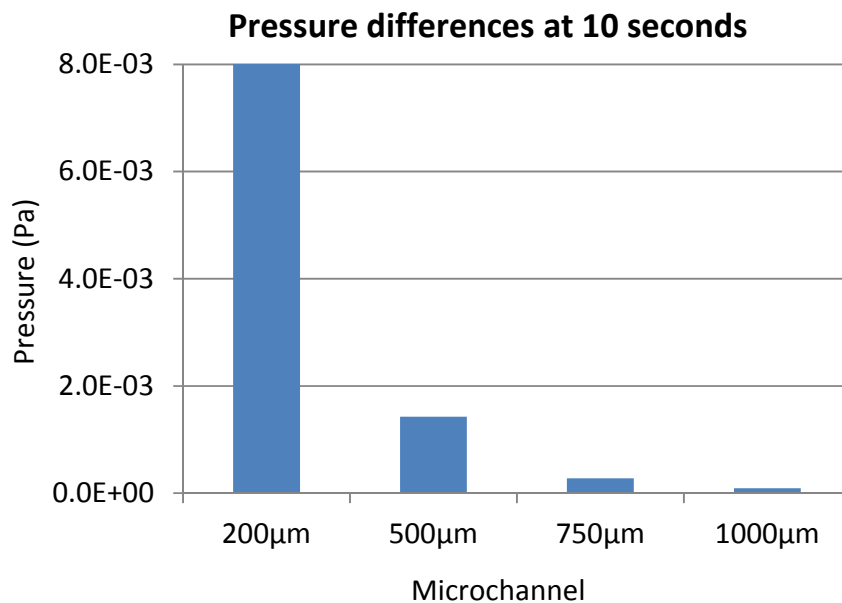
Figure 3. 20 Simulation results of pressure differences at ten seconds for four different microchannel B.

Due to high ratio of channel cross section area in comparison with microchannel A, the pressure difference and velocity difference were proportionally increase or decrease along the microchannel size as shown in Figure 3. 20 and 21. The results of diffusion rate with different size of microchannel showed a consistent agreement with the principle equation of diffusion.

### 3.7.3    Effect of Microchannel Configurations

The length of microchannels depended on the geometry of diffusion channels. Several simulations of drug diffusion rates from various microchannel configurations were carried out. The result of molecular diffusion rate through typical straight microchannels was shown in Figure 3.22. The length and width of the straight

microchannel for this simulation were 8mm and 500 μm. Initially, there was a drastic increase and after a certain time while the diffusion rate was almost constant.
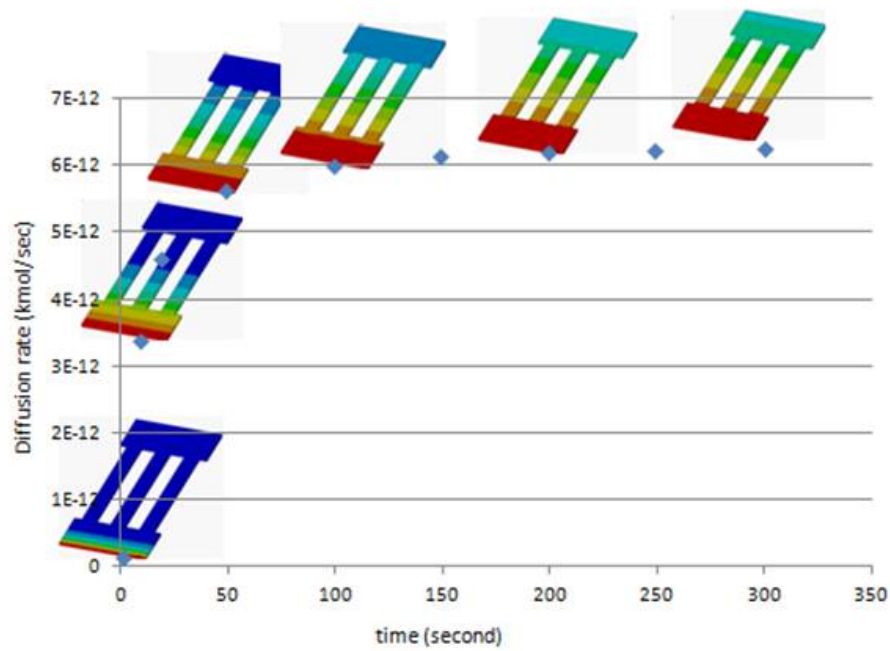


Figure 3. 21 Simulation results of drug diffusion through a straight type micro-channel configuration [62].
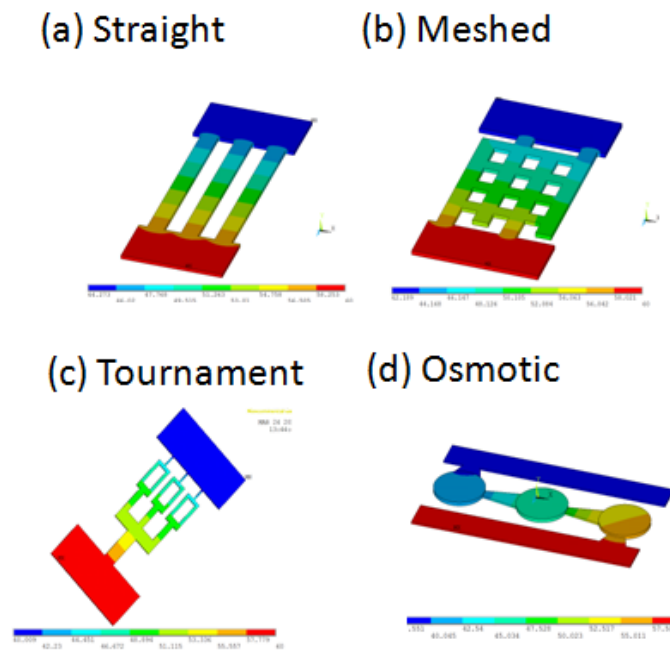
Figure 3. 22 Simulations of drug diffusion at 50 seconds through various microchannel configurations [62].

Flow field reached at the end of the channel within 38 seconds. Fully developed flow, with sustainable diffusion rates, occurred at approximately 150 seconds. The results of drug diffusion at 50 seconds through various microchannel configurations considered are shown in Figure 3.23. It was interesting to note that different microchannel configurations would give rise to different diffusion rates.
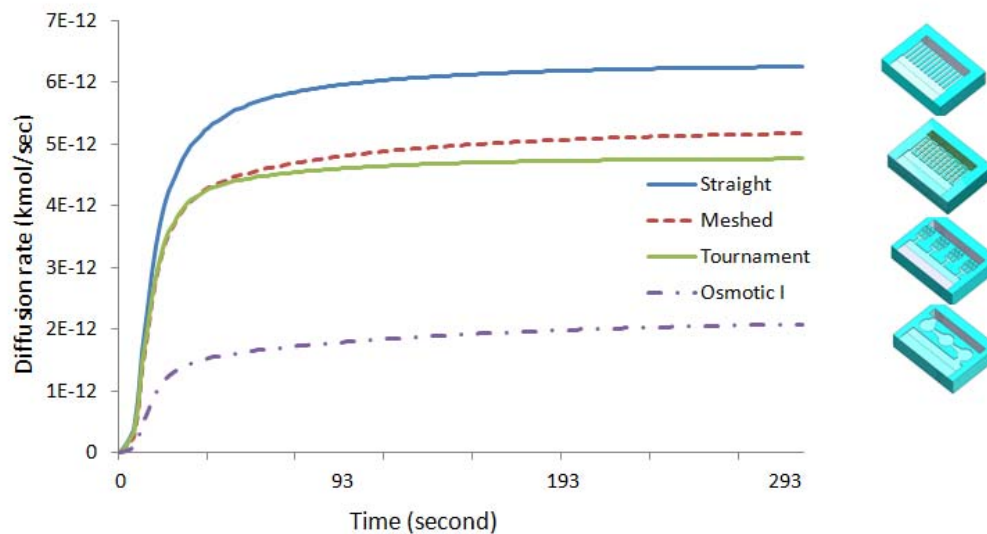
Figure 3. 23 Molecular diffusion rate for various microchannel configurations considered.

The drug diffusion rate as a function of time for various microchannel configurations was presented in Figure 3.24. It can be seen from Figure 3.24 that each of the microchannel configurations exhibited different diffusion characteristics in terms of drug diffusion rates. Initially, there was a drastic increase and after a certain time while the diffusion rate was almost constant. If the drug was to be delivered at a constant rate over a one-hour period then the inlet flux of straight microchannel would be $6.25 \times 10^{-12}$ kmol/s. Over the first second, there was a rapid increase of diffusion rates up to approximately $1.24 \times 10^{-13}$ kmol/s and then a more gradual increased to approximately $6 \times 10^{-12}$ kmol/s after 105 seconds. Overall, each of the microchannel configurations could deliver the drug at different diffusion rates.

### 3.7.4     Effect of Device with Microchannels

Simulation results of drug diffusion within the microchannels as a function of time and drug diffusion from the drug reservoir to opposite site revealed high-concentration area to zero drug concentration area. The diffusion coefficient was dependent on the time factor as well as microchannel size and drugs. Figure 3.25 showed that the simulation results of velocity vector for four different microchannel configurations were presented. All the microchannels generated the maximum velocity at the critical flow bending region or narrow region. However, a range of the velocity magnitude was relatively small (3.3 - 4.2 x $10^{-7}$ m/s) based on small variations of the cross section area of each microchannel.
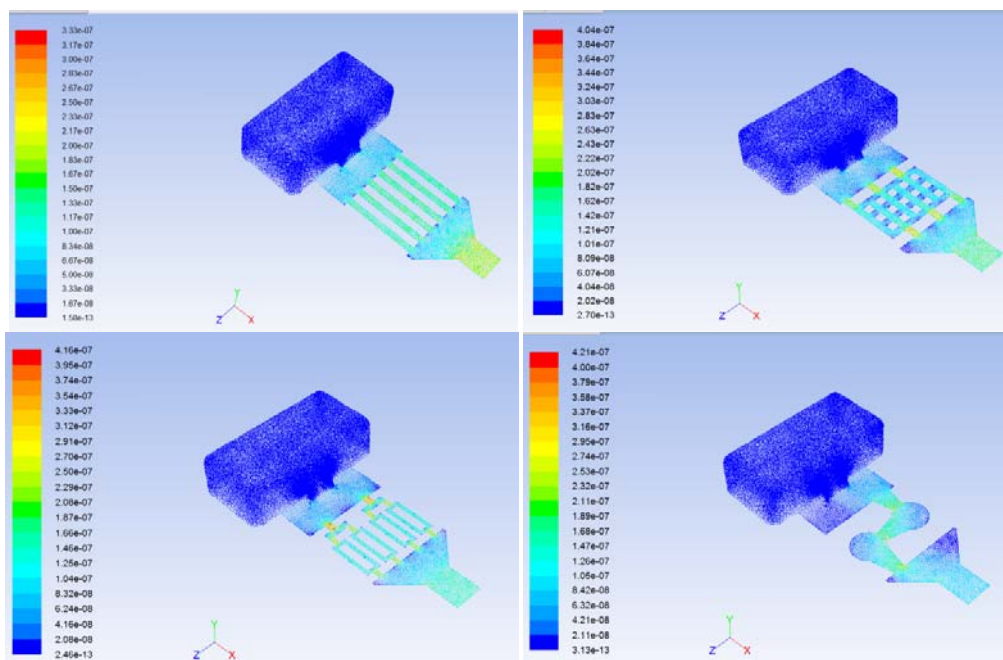


Figure 3. 24 Simulation results of velocity vector for various microchannel configurations.

Results of velocity magnitude as a function of time were performed for four microchannel configurations. It can be seen in Figure 3.26 that the velocity magnitude of osmotic microchannel was smaller than the other channel configurations. It was assumed that the diffusion length and resistance from two directional flow of osmotic channel may affect the velocity magnitude with respect to time.
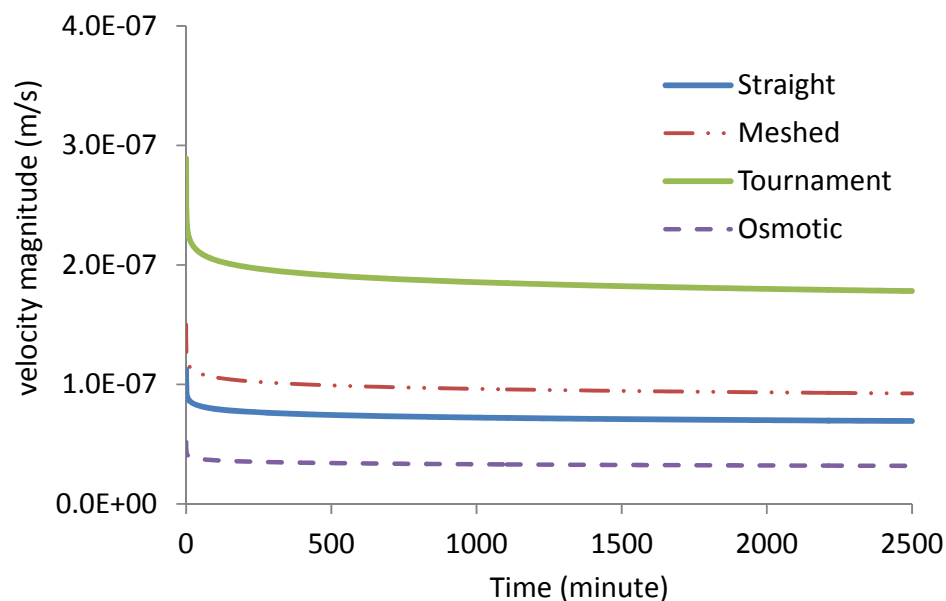


Figure 3. 25 Simulation results of velocity magnitude as a function of time for various microchannel configurations.

### 3.7.5    Effect of Microchannel A using COMSOL

The boundary condition of outlet reservoir was axial symmetry along the center axis of entire volume in 2D model. Values for diffusion coefficients and rate constants came from the literature, Heeren A. et al [72] and experiment results.

Figure 3.31 showed that the concentration transients of the free diffusion species through 250 and 500 μm microchannel A. The initially rate of diffusion of each channels

quickly increased until around 2.5 hours and then seemed to get a gentle slope when it was a stable diffusion. The effect of device included different size of microchannel was clearly visible; concentration increasing with time goes on.
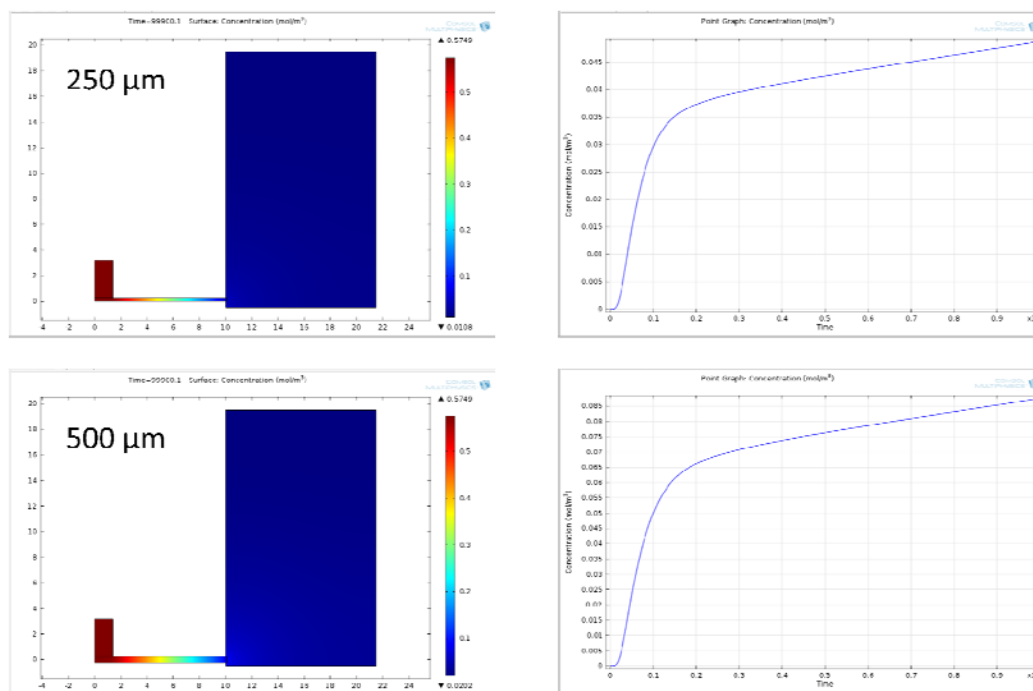


Figure 3. 26 Results of concentration changes at the ahead of outlet reservoir for 24 hours in microchannel A.

### 3.7.6    Effect of Device includes Microchannels using COMSOL

Figure 3.32 shows that the concentration of drug across the modeling domain through various geometries of microchannel in a device. The initially rate of diffusion of each channels quickly increased until around 2.0 hours and then seemed to get a gentle slope when it was a stable diffusion, which was similar behavior with simulation of

microchannel A. The effect of device includes different geometry of microchannel was clearly visible, concentration increasing with time goes on.
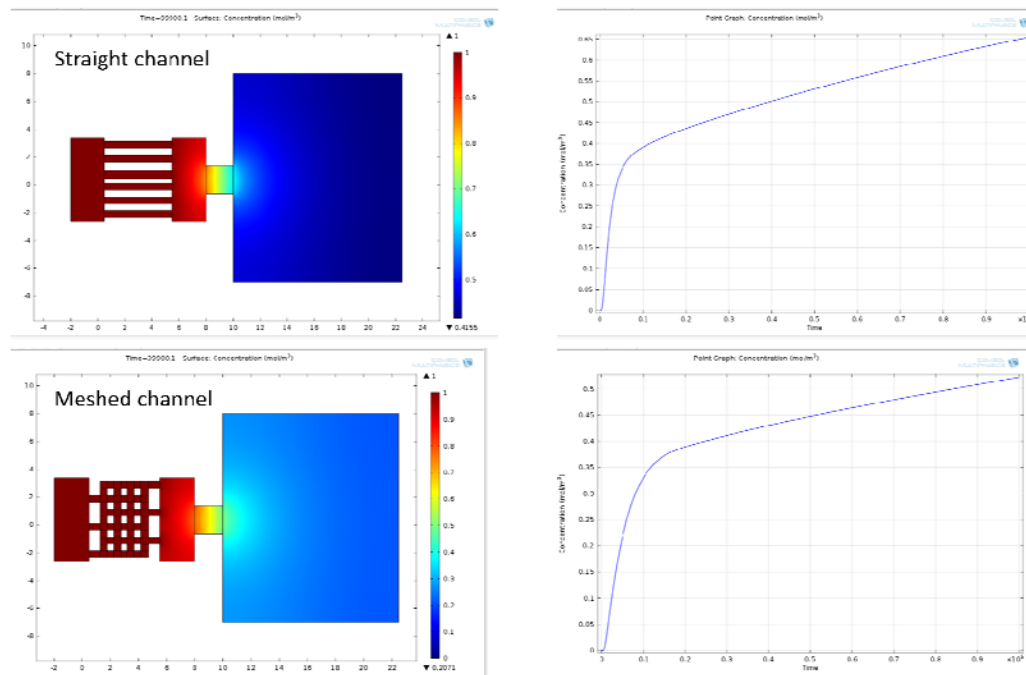


Figure 3. 27 Results of concentration changes at ahead of outlet reservoir for 24 hours in a device.

Figure 3.33 showed that the diffusion rate of each microchannel was calculated based on the concentration changes with respect to time (T1, T2) at the outlet reservoir. T1 and T2 were selected as a transition period between steepest slope and gentle slope.

| | Time (sec) | Straight | Mesh | Tournament | Osmotic |
|---|---|---|---|---|---|
| Diffusion rate (kmol/sec) | T1 | 3.72E-12 | 2.84E-12 | 2.4E-12 | 1.21E-12 |
| | T2 | 7.65E-13 | 3.46E-13 | 4.25E-13 | 1.54E-13 |
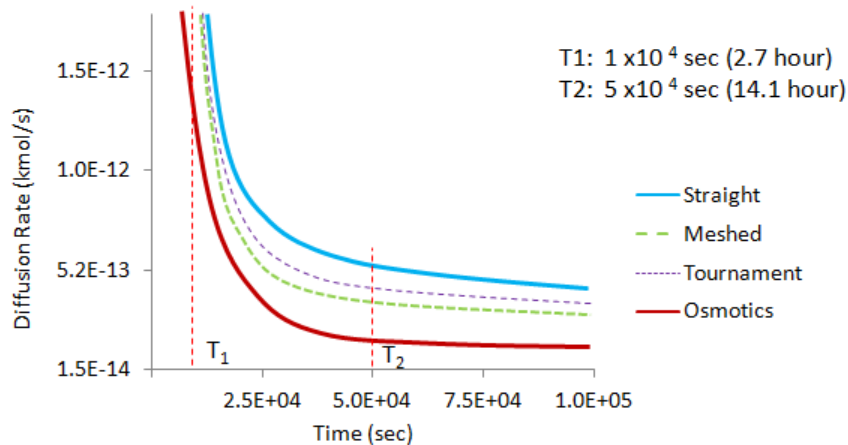


Figure 3. 28 Comparison of Diffusion rate at T1 and T2 with four microchannel configurations

3.7 Discussion

The effects of the microchannel A and B were investigated in correlation with diffusive velocity and pressure changes at each time step. Based on the results obtained through microchannel A, B, various microchannel configurations, the microchannel was suitable to control the diffusion rate for the developed ocular drug delivery device. In order to demonstrate the diffusion through the microchannel and entire device, an analysis was carried out using different size of microchannel and reservoirs. The results of diffusion rate at various times for all microchannels were investigated. Very slow diffusion occurred most likely at the narrow and small channel paths. This demonstrated

that the developed microdevice was capable of delivering the drug through the microchannel configuration. The results obtained from the simulations confirmed that the microchannels had the potential to be used as a drug delivery system depending on desired flow rates and drug concentrations. Since drug consumption occurred at the blood vessel of a vitreous body which could be approximated as zero, the amount of diffusion may vary with the concentration gradient; however, a constant drug release rate could be obtained. The proposed device could produce a constant delivery rate, which was favorable to the treatment of eye disease.

### 3.8 Summary

A microdevice concept for ocular drug delivery was proposed in this chapter. The design involved development of an implantable device with micro-/nanochannels with top and bottom covers.

Single straight microchannels were designed to achieve uniform flow distribution in order to eliminate significant factors of pressure and concentration changes from the geometric configurations, and to optimize diffusion efficiency. Straight microchannel A and B were performed the simulation to obtain the velocity magnitude and pressure changes. Diffusion rates were calculated based on the diffusion coefficient with respect to time for each microchannel. Four different channel configurations were developed and analyzed for their diffusion characteristics. Diffusion rates could be customized to obtain effective levels by varying height, width, and length of microchannels.

# CHAPTER 4 Fabrications and Testing

## 4.1 Introduction

In order to illustrate the proof of concept, straight and various microchannel configurations were etched on the silicon substrate using photolithography technology. To build a functional microfluidic device or a "lab-on-a-chip", one must effectively integrate components such as microchannels, valves, and reservoirs. This section described fabrication of functional microfluidic devices for applications in drug delivery. We focused on PDMS-based systems, for which substantial progress had been made on the integration of components, because they both allowed rapid prototyping and served as final functional devices. Microfluidic components had been integrated using other materials to build impressive devices for drug delivery [31].

## 4.2 Fabrication of PDMS

Master molds for both upper and bottom layers of the reservoir were made of Acura 50 plastic (3D system corp.) and constructed from 3D stereolithography process using 3D Viper SLA system (3D system corp.). PDMS [76, 77] was mixed silicone elastomeric base and a curing agent with a 10:1 ratio (SYLGARD 184, DOW CORNING) and poured into a mater mold. The resulting PDMS was peeled from the master mold. The second molding step was then performed by pouring a mixture of Sylgard PDMS and curing agent over the master mold. A mold release material, water base white peelable barrier coat (Berkley, Akron, PA, USA), was placed at the surface of

the master mold prior to pouring to allow simplistic separation between the PDMS and master mold.

The PDMS was degassed in a vacuum machine for 20 minutes (Durable medical equipment Inc., Richmond, VA). Using a vacuum chamber on the PDMS material allowed removing all of the air bubbles from the polymer to provide for a smooth, air bubble free volume. Removal of air from the PDMS was crucial to ensure there were not defects that would cause sealing issues while bonding and testing. The PDMS cured at room temperature for 24 hours or $80 \circ C$ for 2 hours. Semi-cured PDMS as the bonding technique was suitable for bonding the microfluidic devices. The bond strength was close to that of bulk PDMS.

The fabrication process for the PDMS (Figure 4.1) was a straight forward procedure, but there were some alternate steps depending on how much strength of the PDMS material to produce. After the PDMS had been poured the molds were placed into an oven. The oven temperatures could range to 75 degrees Celsius. The mold was baked for one-hour and then removed from the oven. During a twenty-four hour period it was left to cure at room temperature. Following removal from the oven, the PDMS could be removed from the master mold. Removing the PDMS from the master mold was simple, but care must be exercised because a polymer could rip and tear with ease. Once the fabricated PDMS covers had been removed from the molds, they could experience the bonding process.
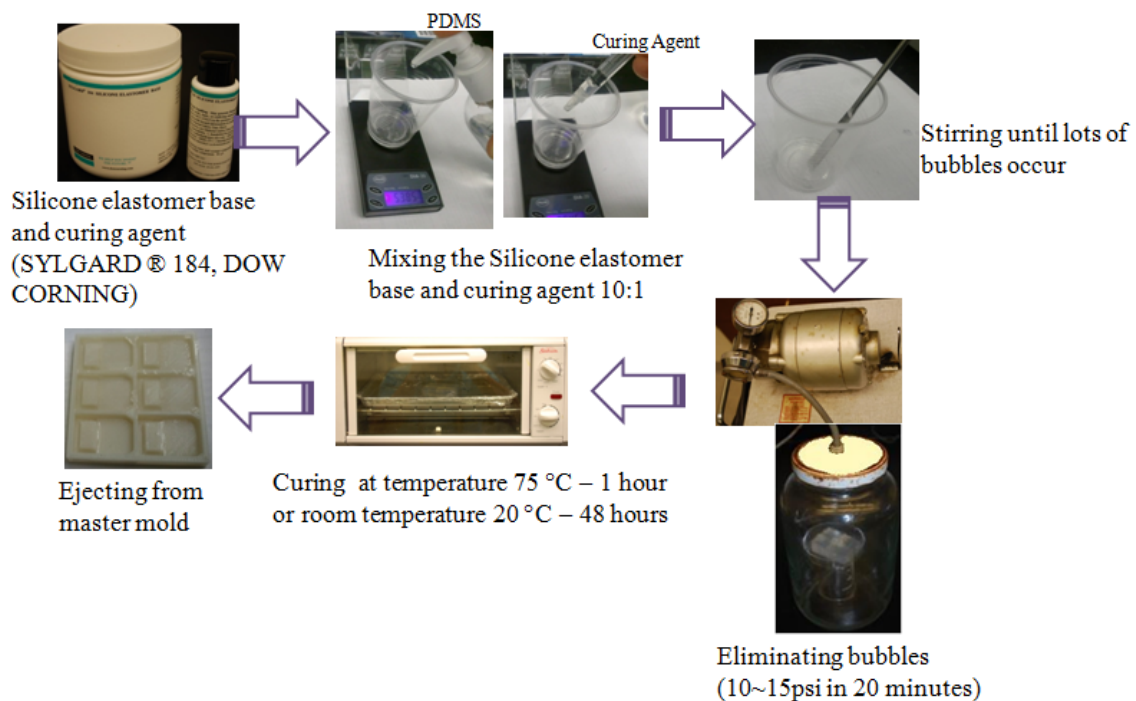
Figure 4.1 Fabrication process for PDMS.

4.3 Fabrication of Microchannels

The microchannel geometries were formed using soft lithography on the 4"
silicon wafers after baking at 1000∘C for at least 10 hours to get at least 1 μm thickness of
an oxides layer. The wafers were vapor coated with hexamethyldisilazane (HMDS)
adhesion promoter. After the mask was completed, photoresist (AZ ECI #3012, AZ
Electronic Materials, Branchburg, NJ, USA) was poured on the wafer around 2.5mL and
spin coated at 4000 rpm for 30 s (expected thickness less than 0.8 μm layer), and then the
wafer was baked at 90∘C for 1 minute. After exposure, native oxide was removed with a
20% KOH solution dip at 80∘C for 2 hours and 5 hours so that 100 and 250 μm etch

depths for the microchannels would be achieved. The final step of the wafer fabrication was to remove the oxide by using a BOE etch. The following microchannel fabrication process was shown in Figure 4.2.
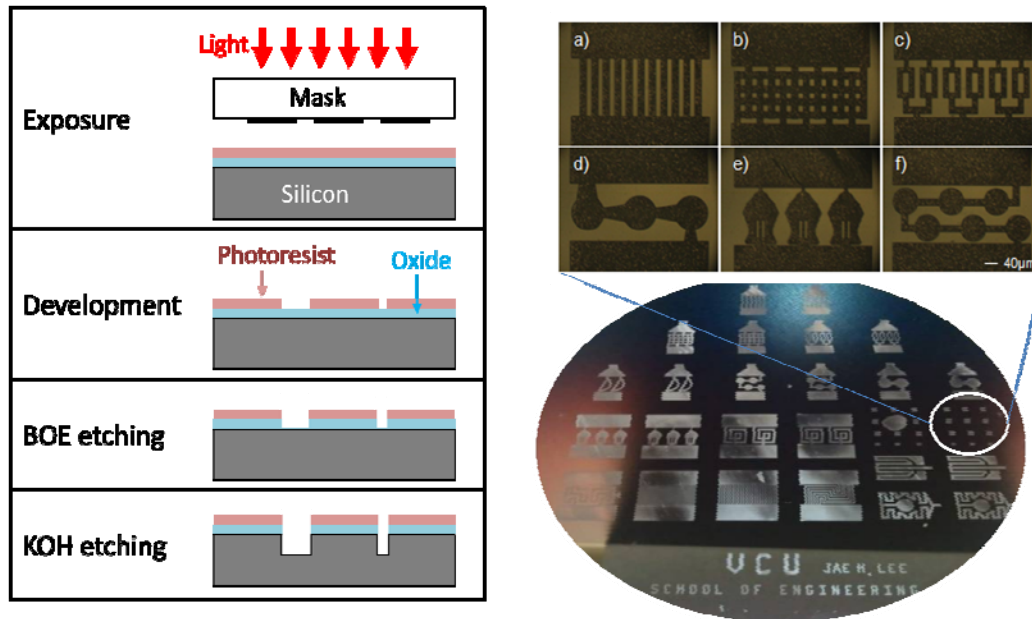


Figure 4. 2 Fabrication process for Silicon substrate.
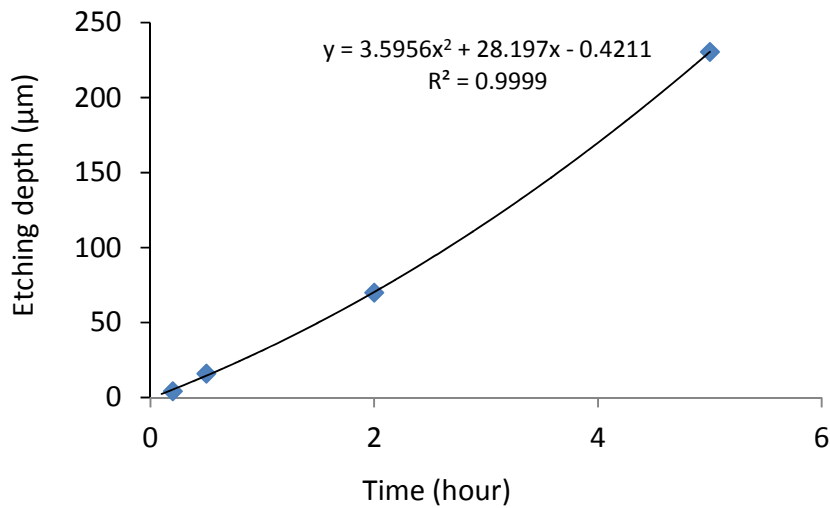
Figure 4. 3 KOH etching rate of 100 Si at 70 ˚C.
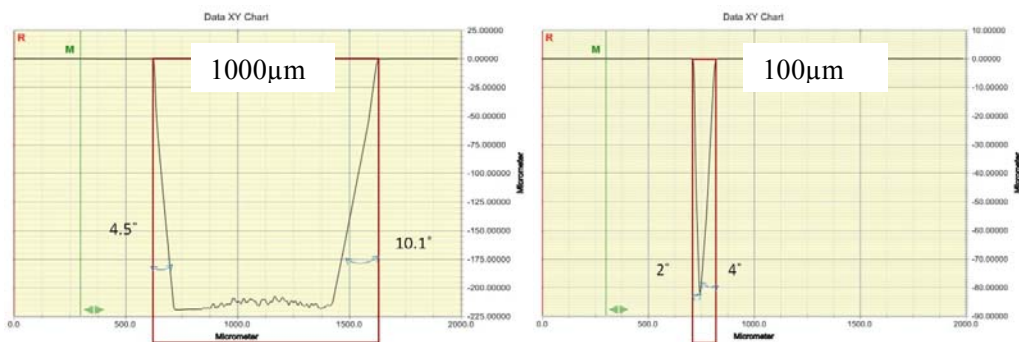


Figure 4. 4 Microchannel depth profiles of width of 100µm and 1000 µm after KOH etching for 5 hours.

    When the microchannel was completed on the silicon substrate, the etching rate of KOH was obtained through the Dektak 150 surface profiler (Figure 4.3 and 4.4). It can be seen in Figure 4.4 that the microchannel had not formed exactly a rectangular shape and

easily break with over 100μm depth or over 3hours of KOH etching. Majority of microchannels had very rough surface on the bottom of channel; around 12 μm roughnesses. The widths of 100 μm microchannel could not achieve a full depth. It suggested that a width of microchannel should be greater than 100 μm with over 12 μm depth.

### 4.4 Oxygen Plasma Bonding

Oxygen plasma technology was inclusive of many different purposes for surface treatment such as cleaning, coating, printing, painting, and adhesive bonding. Plasma technology had become to encompass so many different applications that it was now one of the top methods in surface treatment, especially in microelectronics and packaging industries. Since plasma treatment added another step to the bonding process, there was a tendency to reduce or even eliminate it all together. However, in general, the level of plasma treatment used should be the minimum amount that gave a reproducible bonded part having the desired level of performance. The pretreatment process consisted of three segments: cleaning, activation, and surface bonding. These steps were an extremely important part of plasma treatment because it directly affected the quality of the surface in which adhesive would later be applied. Cleaning the substrate surface could be done using a plasma system to remove even the finest particles of dust. The plasma actually consumed many of the particles through the surface reaction and completely removed them from the substrates.

Tang et al [57] studied how the bonded area varied under different plasma power and pressure. The passivation type, pressure and power, the peel test were performed. They suggested that reducing the plasma pressure from 500 to 30 mTorr helped to improve the bond quality through the peel test for PDMS bonding. They also observed that silicon to PDMS bonding area through peel test increased from 0 to 80 % when the plasma power was fixed at 80 W and the exposure time decreased from 40 to 10 s. The oven treatment temperature (100 ˚C vs. 150 ˚C) did not affect the bonding quality. The high power effect had been tentatively attributed to the damage of the PDMS backbone at 120 mTorr. Besides higher plasma power, an over-exposure to plasma was detrimental to the adhesiveness of PDMS to all the passivation materials [76, 77]. After the surface modification such as oxygen plasma, the channels may provide various diffusion rates in conjunction with the drug diffusion coefficient.

PDMS in microfluidics, its bonding properties to other substrates including Si containing and non-Si containing materials had been examined while using various methods such as plasma oxidization, thermal, pressure, and chemical bonding approaches [78]. The assorted microchannel was assembled to the PDMS reservoir and sealed using the O2 plasma etching processes in accordance with 600mTorr pressure and 20Wpower for 35 s.
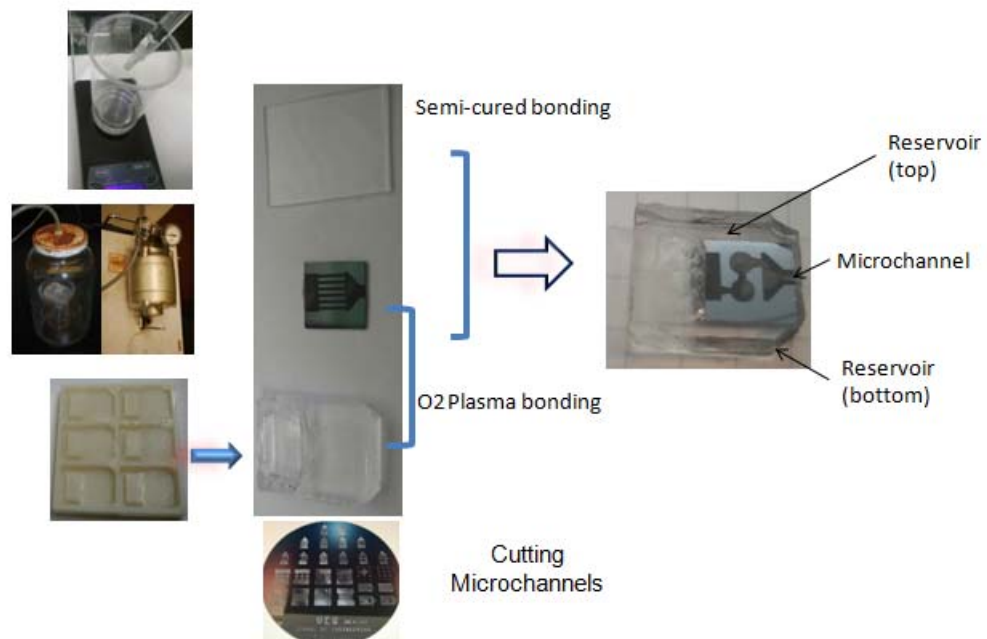
Figure 4. 5 Device assembly process.

The overall fabricated device was shown in Figure 4.5. The PDMS upper cover for the microchannel A and B were prepared by casting PDMS on a 20 by 14 cm rectangular Petri dish and then inspected under a microscope to identify any molding defects. The covers were cut into individual device and fitted with a microchannel substrate. Finally, the functionality of the device was being explored.

4.5 Experimental Procedure

4.5.1     <u>Contact Angle</u>

The contact angle was tested on the surface of PDMS and Silicon wafer with both water and Rhodamine B, which was used as a tracer dye to visualize the flow rate and direction of flow. A contact (or wetting) angle test was commonly used to assess plasma surface treatment.  Figure 4.6 below showed how most angles typically vary between 100 and 110 degrees prior to treatment which were drastically reduced to around half of initial contact angles after processing an oxygen plasma surface treatment.
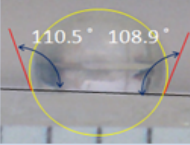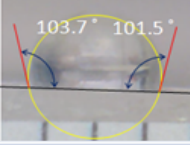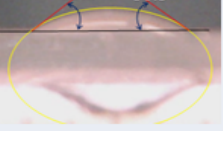


| Material / time | | Water | Rhodamine B |
|---|---|---|---|
| PDMS | t= 1 sec. | 110.5° 108.9° | 107.5° 107° |
| | t = 10 min. | 103.7° 101.5° | 103° 100.3° |
| PDMS with O2 plasma treatment | t= 1 sec. | 64.2° 64.1° | 63.1° 61.9° |
| | t= 10 min. | 52.9° 53° | 39.2° 38.3° |

Figure 4. 6 Measuring results of contact angle on the PDMS surface with water and Rhodamine B, and before and after oxygen plasma treatment.

It can be seen in Figure 4.7 that the contact angle changed along the time increasing and the contact angle was dependant of time. The water on the PDMS

substrate had generally constant contact angle in relatively short time and these substrates for which contact angle diminished rapidly. We found that PDMS substrates without $O_2$ surface treatment had highest contact angle.
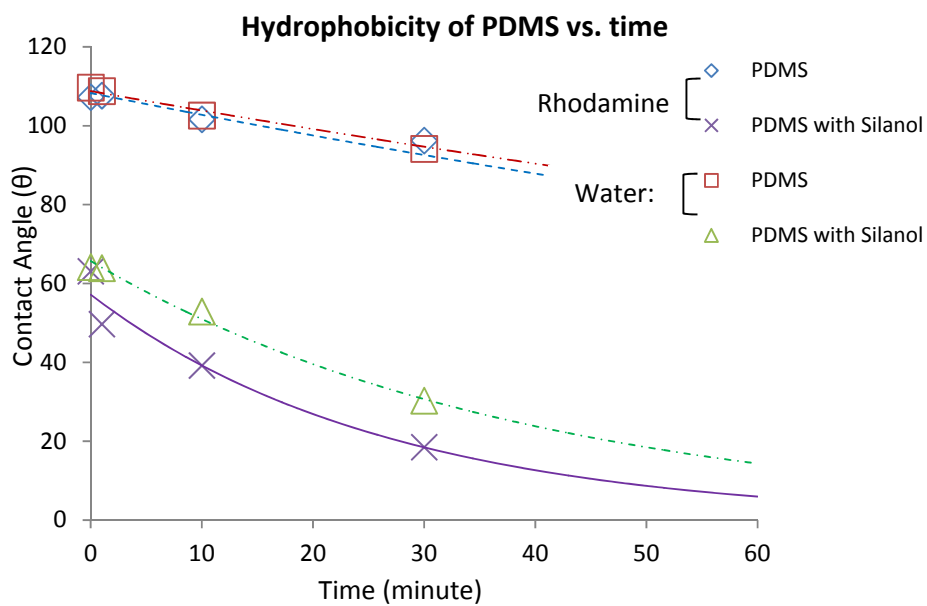


Figure 4. 7 Measuring results of contact angle as a function of time on the PDMS surface with water and Rhodamine B, and before and after oxygen plasma treatment.
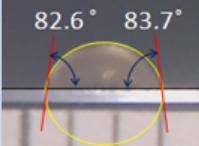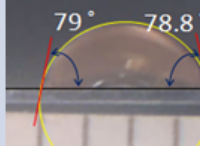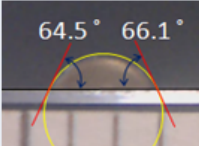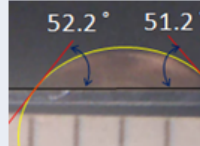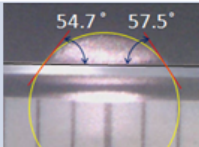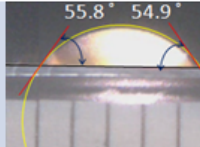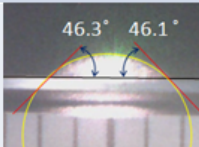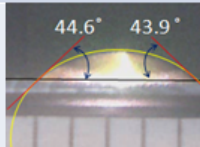
| Material / time | | Water | Rhodamine B |
|---|---|---|---|
| Silicon | t= 1 sec. | 82.6° 83.7° | 79° 78.8° |
| | t = 10 min. | 64.5° 66.1° | 52.2° 51.2° |
| Silicon with O2 plasma treatment | t= 1 sec. | 54.7° 57.5° | 55.8° 54.9° |
| | t= 10 min. | 46.3° 46.1° | 44.6° 43.9° |

Figure 4. 8 Measuring results of contact angle on the Silicon surface with water and Rhodamine B, and before and after oxygen plasma treatment.

Figure 4.8 above showed that measuring results of contact angle on the silicon surface with water and Rhodamine B, and before and after oxygen plasma treatment. It could be explained that most contact angles typically varied between 78 and 83 degrees prior to treatment which were increased to around one thirds of initial contact angles after processing an oxygen plasma surface treatment
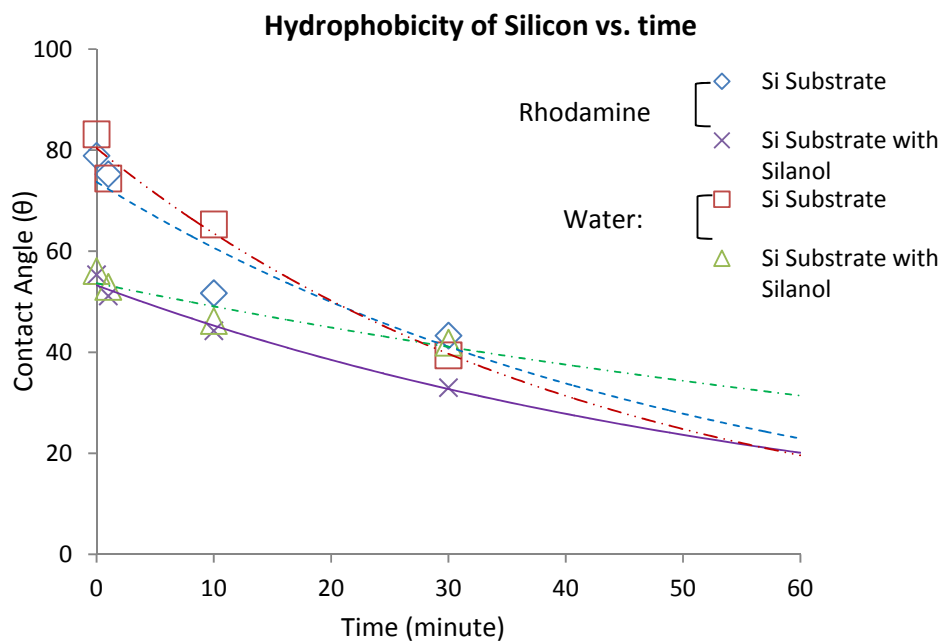
Figure 4. 9 Measuring results of contact angle as a function of time on the Silicon surface with water and Rhodamine B, and before and after oxygen plasma treatment.

In Figure 4.9, the contact angle decreased along the time increasing. The water on the silicon substrate had generally constant contact angle in relatively short time and these substrates for which contact angle diminished rapidly. We found that silicon substrates without $O_2$ surface treatment had highest contact angle at the beginning. The contact angle on the silicon surface without treatment diminished much faster than no-treatment. The $O_2$ surface treatment could generate hydrophilic surface to obtain better initial flow through microchannels.

### 4.5.2    Experimental Apparatus

The main purpose of these tests was to verify the simulation results to obtain the optimized drug delivery device based on the desired amount of drug should be delivered

for a long phase. As a first step, we needed to understand that one substance diffused in one direction through microchannel and how the size of microchannel and length affect diffusion rate. The diffusion could be generated with the relative concentration of both reservoirs depending on the microchannel along the time changes. It can be seen in Figure 4.10 that experimental was set up of both microchannel A and B. Since the microchannel A had an inlet reservoir using a tube, the end of the tube which inserted into PDMS before curing was flattened up with sand paper. The tube was reinserted into the hole and glue was then quickly smeared around the tubing and hole. Epoxy glue could also be used to bond PDMS to tube. This allowed the creation of thick mounting blocks on thin PDMS providing a more durable fit.
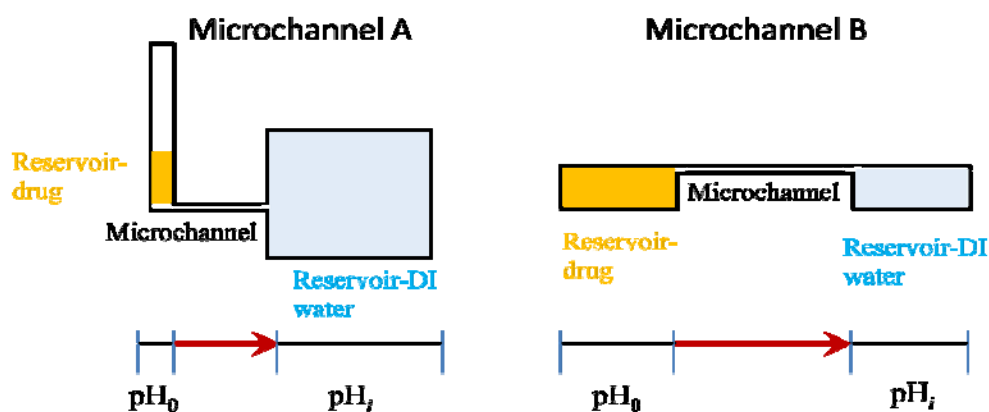


Figure 4. 10 Comparison of experimental set up between microchannel A and B.

Single straight microchannel A was set up into a beaker (10ml volume), which contains DI water as an unbiased solution. The pH measurement is potentiometric that explains the relationship between the electrode potential and the solution. The pH meter truthfully responds to the potential, it indirectly and mathematically converts the potential

to the pH scale according to the questionable linear Nernst slope. It does not correct the nonlinear deviations in the strong acid and neutral regions. In general, the accuracy of pH measurements relied on precision calibration of pH glass electrodes, reference electrodes and buffers. Although it would seem that the pH meter could make an accurate measurement of the change of pH value with need for the calibration, the electrode had robustness to the pH meter to display a pH value changing pattern. A pH meter was a method of characterizing solution concentration by measuring pH as the activity of the hydrogen cations or the amount of acidity that was diffused through a device. In a microchannel, like a test tube of water, all of the citric acid within the drugs would be diffused.

The pH/conductivity meter (Accumet® AR20, Fisher Scientific, Beverly, MA) with microelectrode (Ag/AgCl reference) was used to measure a rate of pH changes with respect to time for the entire test. The pH data were transferred and saved to computer through hyper network at a randomly selected time. The amount of mixed drug solution that contained in a reservoir was 5µℓ. DI water of 8.58 mℓ (same amount of human eye vitreous fluid) was used for measuring pH at a beaker. All experiments were performed 2-3 times, each microchannel and device with essentially similar protocols, at room temperature (20-22°C). Single straight microchannel B was set up same as microchannel A except the amount of drugs and DI water. The same amount of drugs and DI water of 0.33ml were used for both reservoirs in microchannel B.
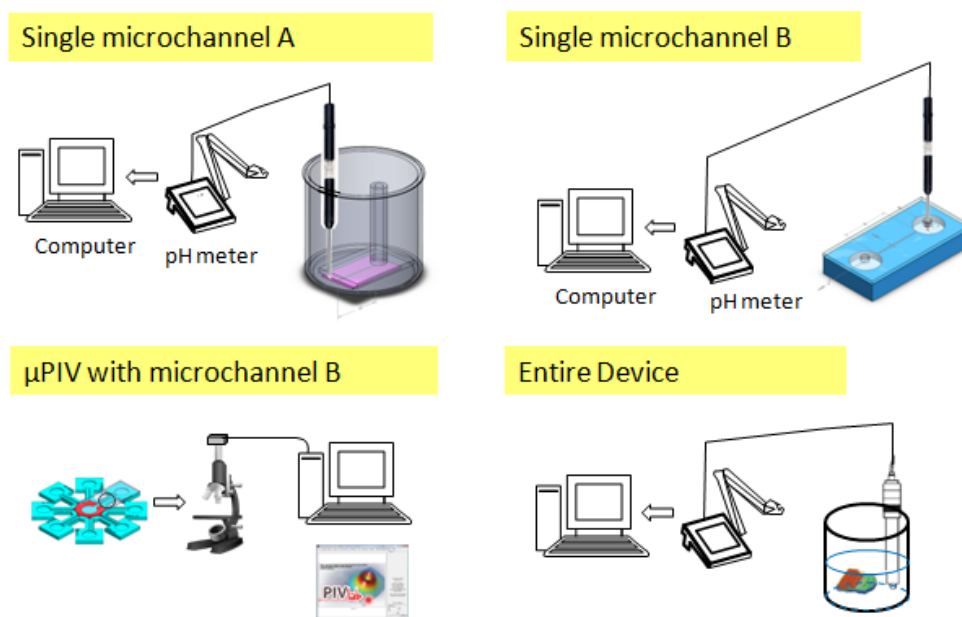
Figure 4. 11 Schematic of experimental equipments and pH electrode with each microchannel and device.

50 % of citric acid in a drug of eye multi- purpose solution (10g of citric acid was dissolved in 20ml of drug until all anhydrous crystalline was invisible) was used to measure the pH value which diffused through microchannel forward DI water at opposite site. The velocity of acid production in the outlet reservoir was calculated from the slope of the measured $H^+$ activity (concentration) over time and taking into account the buffering capacity.

### 4.5.3    UV-Visible Spectrophotometers

UV-Visible Spectrophotometers was used to quantify the amount of an absorbing drug of the Brimonidine. The drug solution made by dissolving 0.405g of Brimonidine ($C_{11}H_{10}BrN_5$) in enough DI water to make 5ml of solution.

Test condition;

Room temperature (~21 °C)

UV spectrum – 248nm

Absorbance - μV
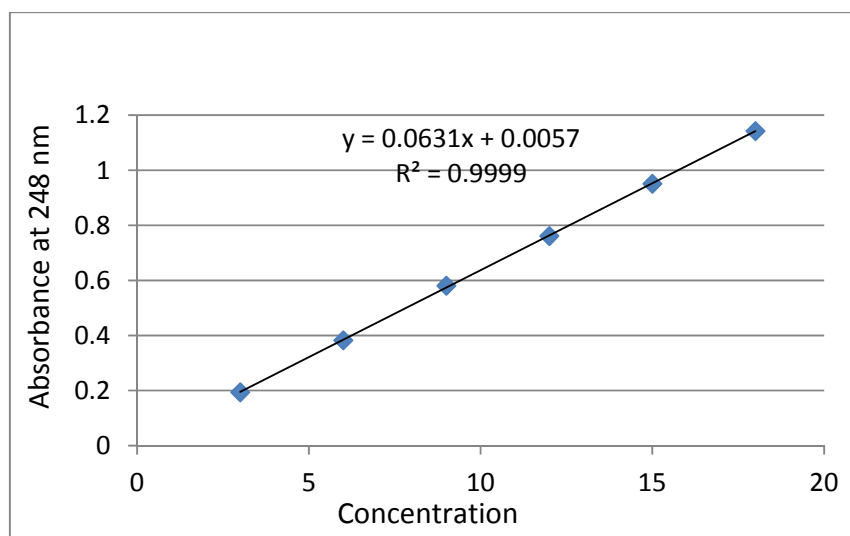


Figure 4. 12 Calibration data for the estimation of the Brimonidine, researched by Bhagav P et al (2010) and C.A. Holden et al (2012) [79, 80].

In Figure 4.12, the graph showed that Bhagav P et al [79] estimated the calibration data for concentration of the Brimonidine while measuring the absorbance of UV-Vis. at 248nm. It was depicted that the increasing drug concentration was linearly proportional to the absorbance. These estimations were implemented into our experiment results after obtained observance (Y= μV) while using the UV-Visible Spectrophotometers.

### 4.5.4    Diffusion Test with Microchannel A

Like for all potentiometric methods, the output signal was linear with the logarithm of concentration, i.e. at two different pH values the same change in pH value corresponds to different changes in concentration. To convert slopes of pH to metabolic fluxes of acidification, the pH values must therefore be converted to actual concentrations. We found an equilibrium concentration when drug solution was fully diffused out through all volume. It can be seen in Figure 4.13 that normalized pH values were continuously reduced to equilibrium concentration with respect to time. We were not quite sure that 250 μm microchannel performed somewhat differently compare to others. However we assumed that a leakage occurred at the gluing interface while measuring pH acidity. Experimental data of microchannel A for cumulative drug release versus time was shown in Figure 4.14.
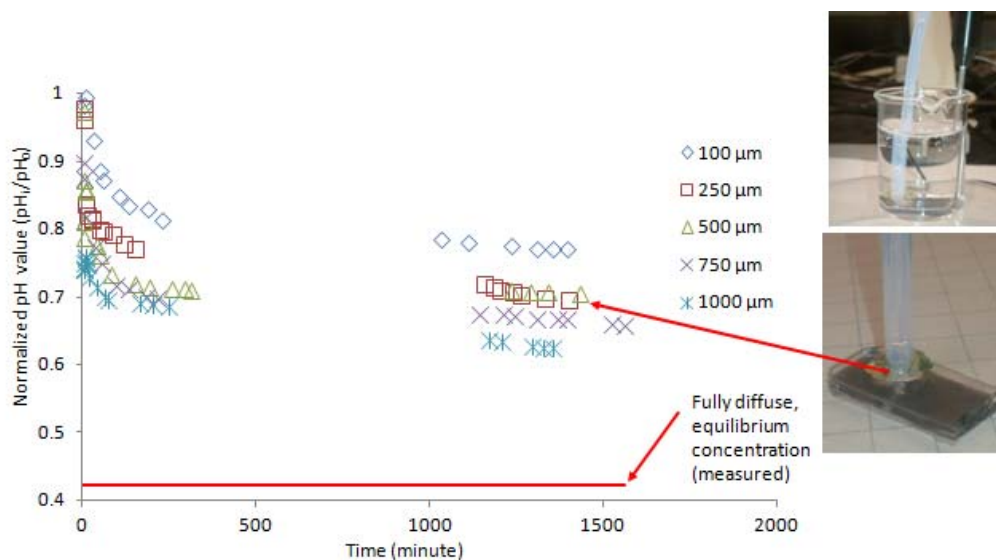


Figure 4. 13 Experimental data of microchannel A for normalized pH value versus time, pHi is pH value at each time increase, pH0 is pH value at the initial condition.
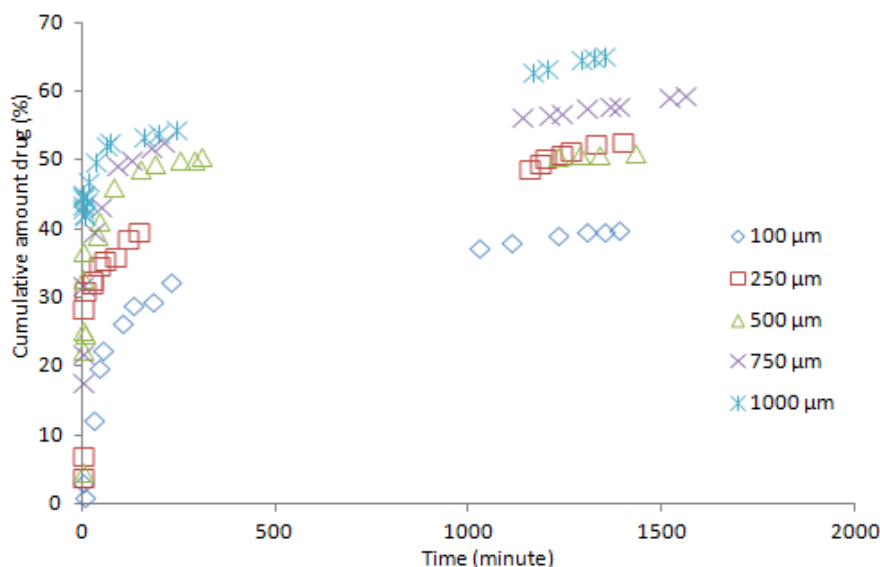
Figure 4. 14 Experimental data of microchannel A for cumulative drug release versus time.

### 4.5.5        Diffusion Test with Microchannel B

The rest of the measuring parameter and converting pH value to normalized number were identical with microchannel A. We also found an equilibrium concentration when drug solution was fully diffused out through all volume for experimental microchannel B. It can be seen in Figure 4.15 that normalized pH values were continuously reduced to equilibrium concentration with respect to time. The entire microchannel performed well as we expected that diffusion occurred dependently with microchannel size and concentration gradients. Experimental data of microchannel B for cumulative drug release versus time was shown in Figure 4.16.
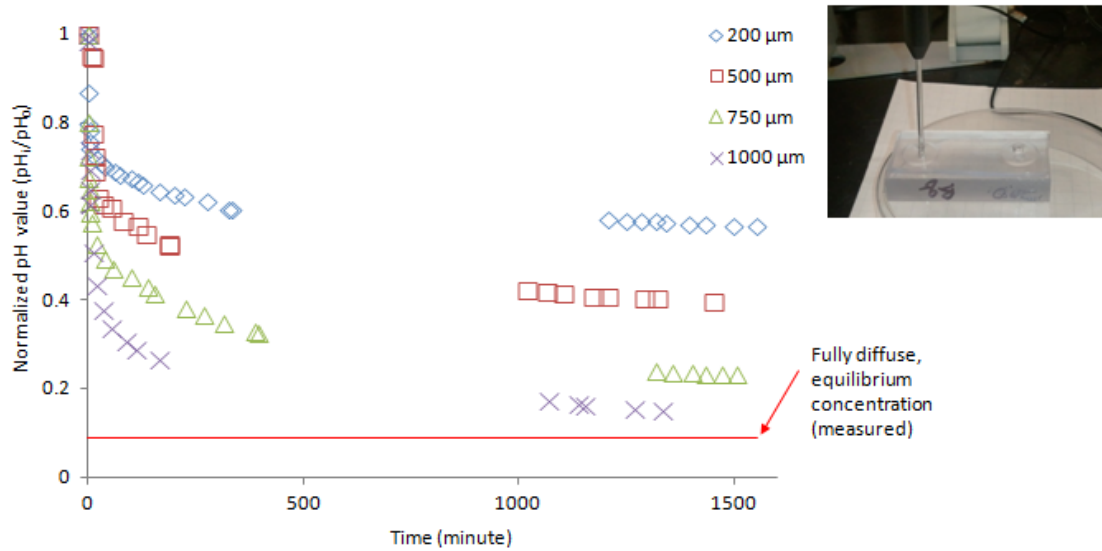
Figure 4. 15 Experimental data of microchannel B for normalized pH value versus time, pHi is pH value at each time increase, pH0 is pH value at the initial condition.
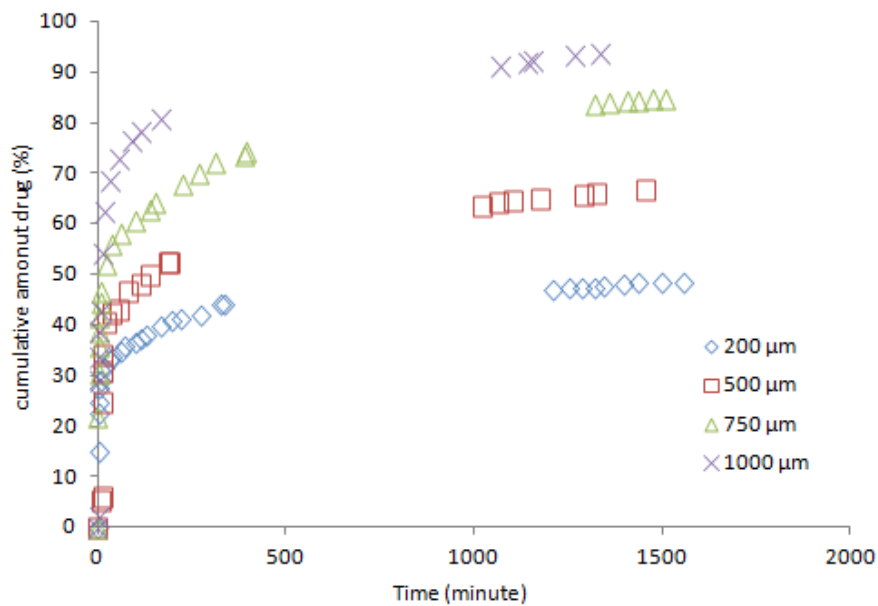


Figure 4. 16 Experimental data of microchannel B for cumulative drug release versus time.

### 4.5.6 Diffusion Test with Entire Device

The experimental data of entire device was shown in Figure 4.17. As we expected, the normalized diffusion data was in identical directions. Also noted that at the extreme end of each curves was not exceeded the calibrated pH scale and equilibrium concentration after 10 days. The obtained pH data were normalized by dividing each data point by the initial value for each test of microchannel. We generated a graph the normalized data versus time for each measurement and then fitted a logarithmic trend line to each curve.
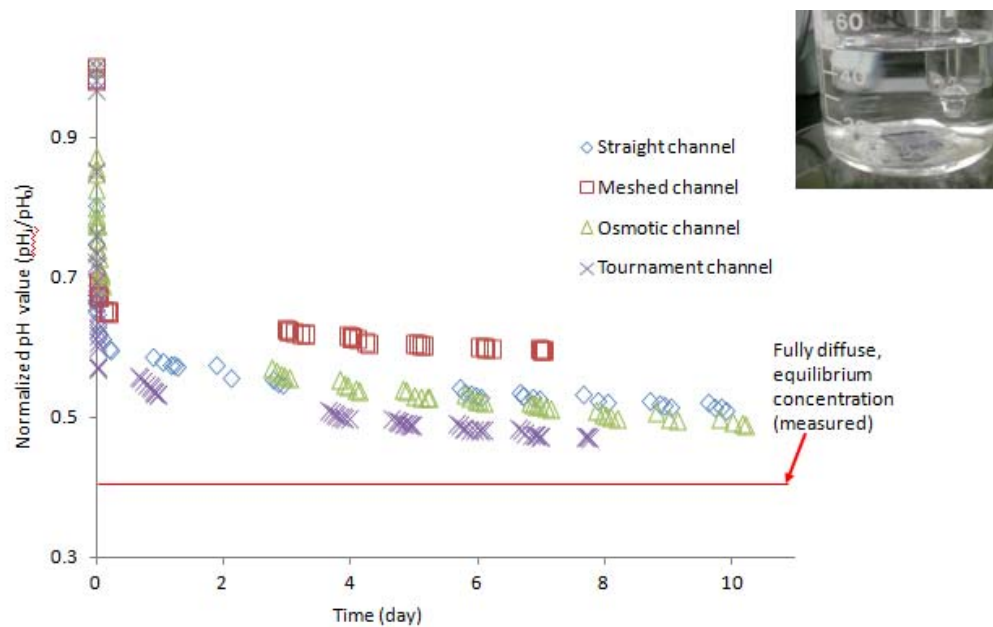


Figure 4. 17 Experimental data of entire device for normalized pH value versus time, pHi is pH value at each time increase, $pH_0$ is pH value at the initial condition.
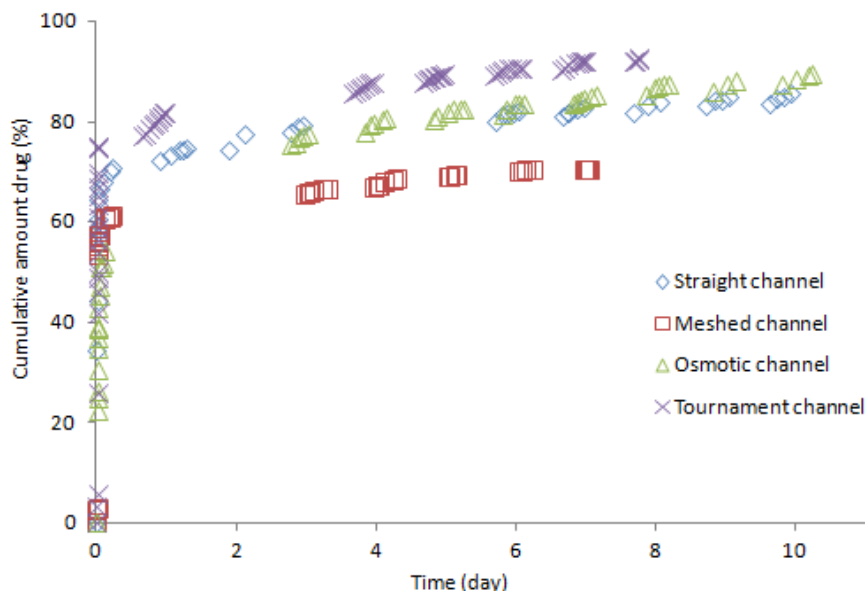
Figure 4. 18 Experimental data of entire device for cumulative drug release versus time.

### 4.5.7       Micro-Particle Image Velocimetry (μPIV)

The combination of Matlab μPIV functions and images were a powerful instrument for exploring other dynamic aspects of diffusion. A typical problem was to find out the rate of influx of particles to a certain fraction of objective space and in many interesting instances. For instance, how long it would take a particle that started at some position to reach some region. Since diffusion was not a deterministic process, the result would be a distribution of travel times for a given set of identical particles all following the same boundary and initial conditions. In some instances that distribution was agreeable to calculating a mean rate or median rate of arrival. In Figure 4.19, the images were obtained the diffusion of particles at the inlet microchannel at each time step. The

following a defining specific region and vector plot under calibration of actual distance were very important process to achieve constant evaluations.
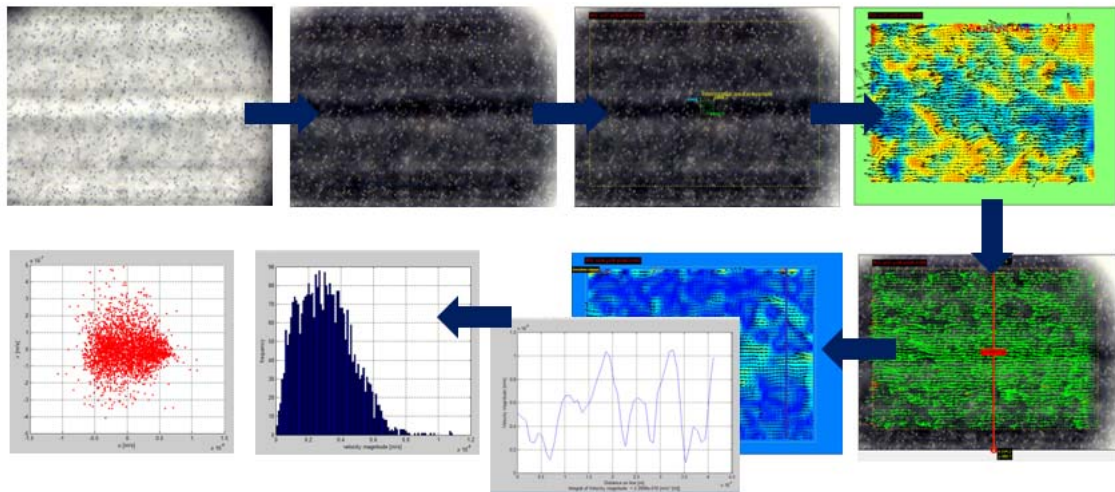


Figure 4. 19 Data mining process after obtaining images at each times using PIV methods in MATLAB.

The results of velocity magnitude of microchannel were shown in Figure 4.20. Images were captured at different time steps for each microchannel. Due to high mass density of polystyrene particles (3μm diameter), the velocity magnitude of the particles are relatively slow in comparison with citric acids. The difference of the velocity magnitude among the cross section of microchannel was not significant after diffusing for 5 minutes.
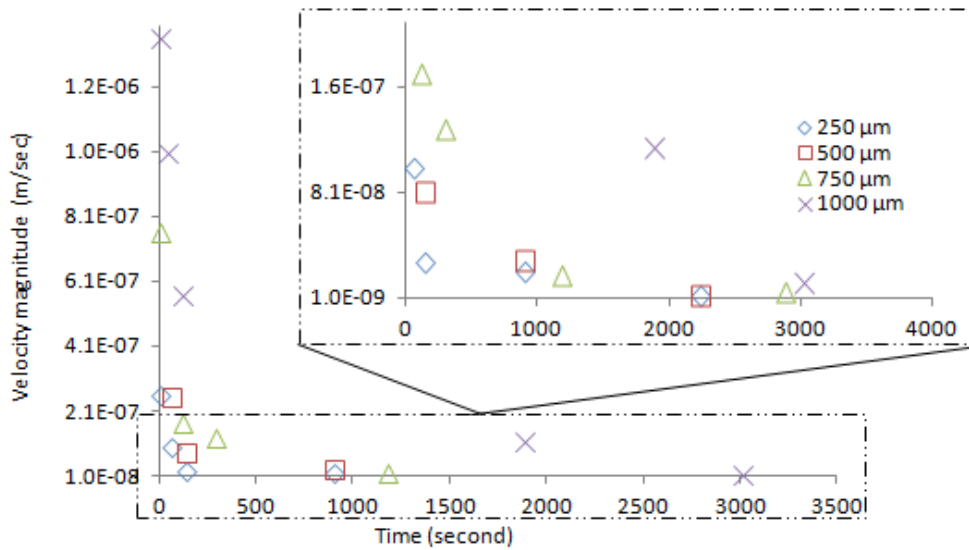
Figure 4. 20 Results of velocity magnitude of microchannel B, images were captured at different time steps for each microchannel.

We considered a one-dimensional particle which diffuses freely in the presence of a microchannel at x = 0. The diffusion equation could be solved with initial condition and boundary condition at x = l. Assumed that the microchannel, i.e., which transferred every particle diffusing on it, was located at x = 0, this situation was governed by the Einstein diffusion equation in one dimension.

$$\partial c(x;\, t|x_0,\, t_0) \,/\, \partial t = D\, \partial^2 c(x;\, t|x_0,\, t_0) \,/\partial x^2 \tag{32}$$

Once we converted the actual concentration c to the normalized concentration M with a percentage of particles in liquid volume, the normalized particle flux can be expressed by [81]

Normalized particle flux $\dfrac{M(x_i, t_i)}{M(x_0, t_0)}$

$$= \left( \frac{1}{\sqrt{4\pi D(t - t_0)}} \exp\left[-\frac{(x - x_0)^2}{4D(t - t_0)}\right] + \frac{1}{\sqrt{4\pi D(t - t_0)}} \exp\left[-\frac{(x + x_0)^2}{4D(t - t_0)}\right] \right) / M_0$$

$\times \ 0.125\%$ of Polystyrene microsphere in water $\times A$ (cross section), $x \geq 0, t \geq 27$

$$(33)$$

Although there were some variations between each microchannel, the result of velocity magnitude of microchannel B was apparently agreed with an analytical solution of 500μm channel in Figure 4.21.
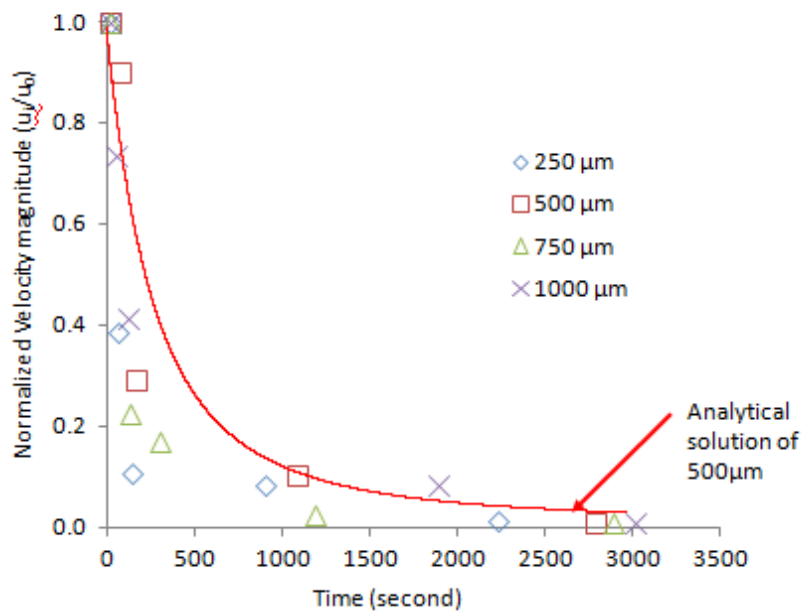


Figure 4. 21 Results of velocity magnitude of microchannel B with an analytical solution of 500μm channel.

4.6 Comparison of Simulation and Tests

4.6.1　　　Microchannel A and B

For each microchannel as function of time shown in Figure 4.13 and 4.15, diffusion constant was derived by fitting the error function to the measurement values. For the shortest diffusion time of 30 min a diffusion constant of D = 1.42 x $10^{-7}$ $m^2$/s was obtained. For the longer diffusion times an average diffusion constant was much less than initial diffusion constant. However, the experimental values of 250μm channel were so fast that did not fit of the theoretical curve. This fact suggested that device itself may have any critical leakage problems as shown in Figure 4.22. As these data points were not considered to be calibrated, they would be discarded.
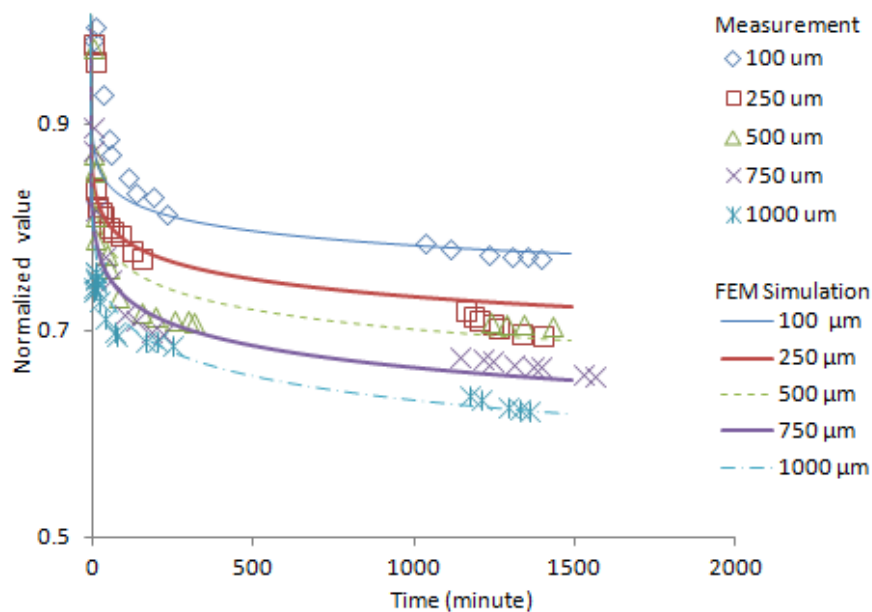


Figure 4. 22 Comparison of normalized value of microchannel A between simulation and tests.

Finally noted that there were positions where the motion of the diffusion performed rapidly. We assumed another reason that this was due to temperature drops in the laboratory during the night and had little impact on the analysis of the data.
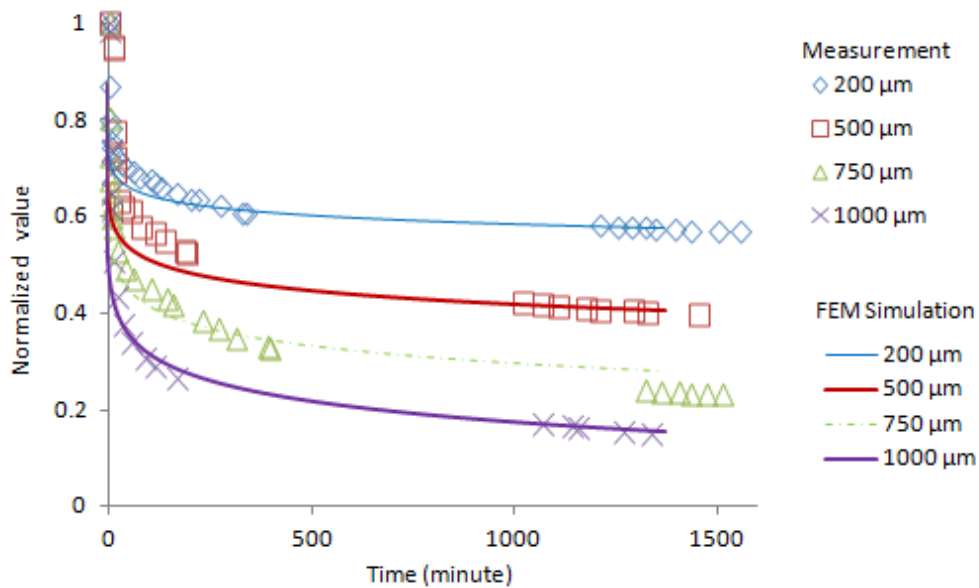


Figure 4. 23 Comparison of normalized value of microchannel B between simulation and tests.

For device samples with different geometry microchannels, the effective diffusion coefficient which minimized differences between simulation and experimental values was agreed. The diffusion coefficient value was verified performing another experiment. As a realistic solution for the diffusion coefficient, an error function was considered to generate the nonlinear logarithmic curves as function of time. This equation including error function was the solution in the case of a constant source of concentration with the diffusion coefficient and the time. The boundary condition of a constant source was not

fully satisfied in our experiment as can be seen in Figure 4.23 since the concentration in the reservoir decreased over time.

### 4.6.2 Entire Device
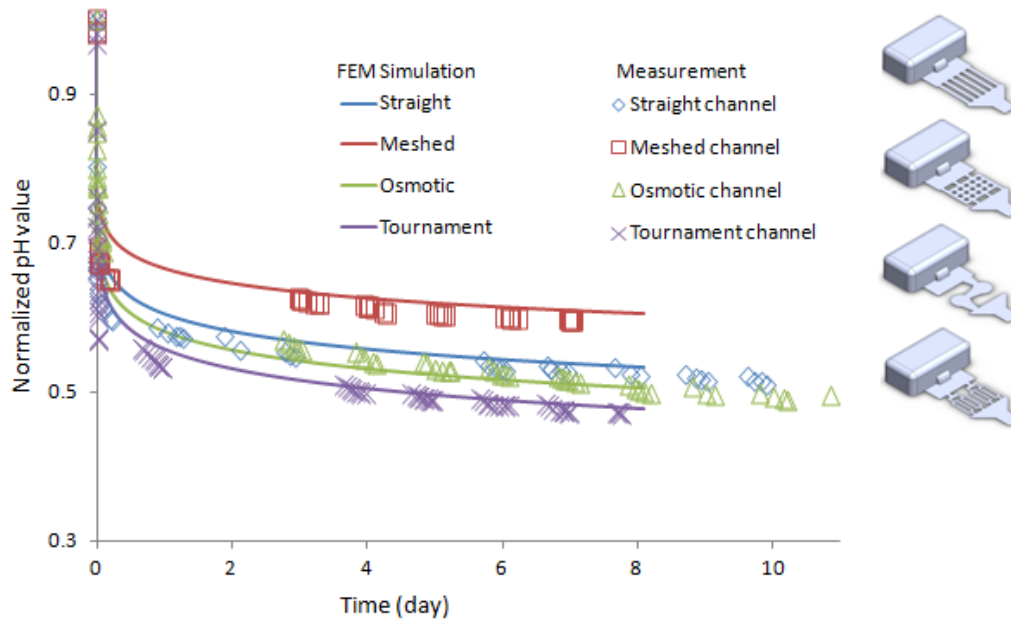


Figure 4. 24 Comparison of normalized value of entire device between simulation and tests.

The simulation showed agreement with the experiments. It can be seen in Figure 4.24 that after 8 days, each type of micrchannel geometry generated a different diffusion rate. The diffusion rate of tournament microchannel was bit higher than the others.

### 4.6.3 Simulation Results of Drug Release between Microchannel A and B

In the graph (Figure 4.24), drug release rate as a function of time for the microchannel A and B was calculated using a diffusion coefficient and error function

method. Our graph exhibited the same trend line as that obtained in the simulation results. This graph ignored the effects of peak value at the small cross section of microchannel. The coefficient of this logarithmic curve was well fitted with those that simulations were done.
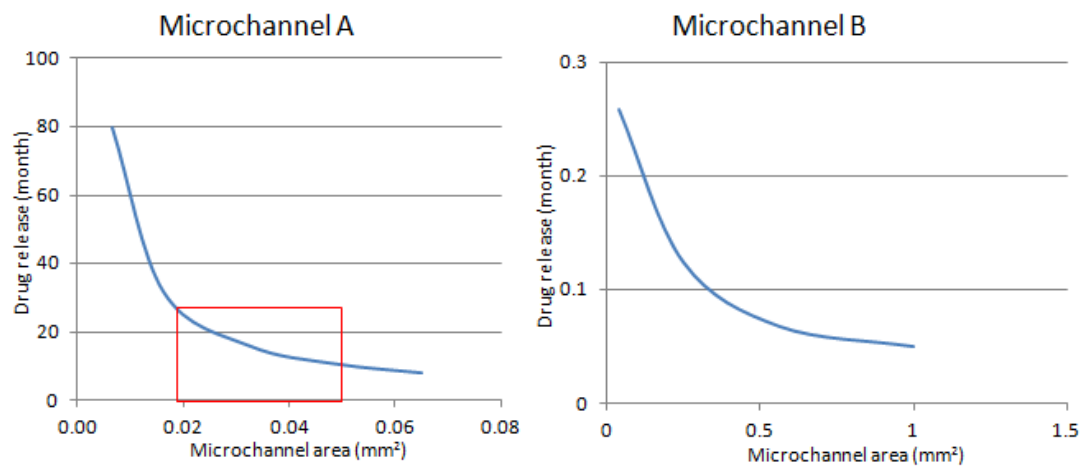


Figure 4. 25 Comparison of simulation results of drug release time between microchannel A and B.

It can be denoted that the range of 0.02~0.05 mm$^2$ may satisfy the drug release for 12 - 36 months. It can be predicted that the microchannel size of square of 210.8, 173.4, and 142.8 µm may satisfy the drug delivery term such as 12, 24, and 36 months, respectively (Table 5).

Table 5 Optimized Microchannel size based on simulation results.

| | Drug Release Time | | |
|---|---|---|---|
| | 12 months | 24 months | 36 months |

| Square channel | 210.8 x 210.8μm | 173.4x 173.4μm | 142.8 x 142.8μm |
|---|---|---|---|
| Rectangular channel | 200 x 222.2 μm | 200 x 150.5 μm | 200 x 102.0 μm |

Table 4.1 values were used in an attempt to model diffusion and consequently calculated the effective diffusion coefficient and release rate in period of month.

### 4.6.4 Experimental Results of Drug release between Microchannel A and B

Drug release rate as a function of time for the microchannel A and B was calculated in the graph (Figure 4.25) using a measured pH value that converted to normalized value. Our graph exhibited the same trend line as that obtained in the experimental results. This graph also ignored the effects of peak value at the small cross section of microchannel.
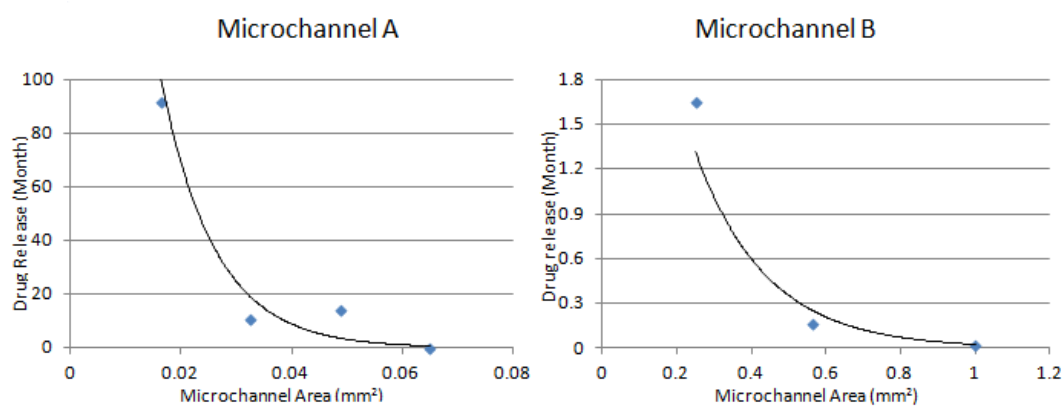


Figure 4. 26 Comparison of experimental results of drug release time between microchannel A and B.

Although the drug release rate of microchannel size between 0.03 and 0.05 μm were not expectable, it can be denoted that the range of 0.02~0.05 mm$^2$ may satisfy the drug release for 12 - 36 months. It also can be predicted that the microchannel size of square of 192.3, 174.1, and 162.3 μm may satisfy the drug delivery term such as 12, 24, and 36 months, respectively (Table 6).

Table 6 Optimized Microchannel size based on experimental results.

|  | Drug Release | | |
|---|---|---|---|
|  | 12 months | 24 months | 36 months |
| Square channel | 192.3 x 192.3μm | 174.1 x 174.1μm | 162.32 x 162.32 μm |
|  | 200 x 185 μm | 200 x 151.5 μm | 200 x 131.7 μm |
|  | 250 x 148μm | 250 x 121.2μm | 250 x 105.4 μm |
| Rectangular channel | 500 x 74μm | 500 x 60.6μm | 500 x 52.7 μm |

### 4.6.5    t test Two Sample Assuming Equal Variances

We performed the t-test, which assumes that the two samples had equal ariances. For simple evaluation, the average difference between the simulation and tests were 7.6%, which was little higher than we expected, however it may have acceptable range for this investigation.

Table 7 Comparison of microchannel size between simulation and experimental results.

| | | Drug release | | |
|---|---|---|---|---|
| | | 12 months | 24 months | 36 months |
| Microchannel (square of) | Simulation | 210.8 µm | 173.4 µm | 142.8 µm |
| | Experiment | 192.3 µm | 174.1 µm | 162.3 µm |
| % of difference | | 8.78% | 0.40% | 13.67% |
| | | | Average | 7.62% |

Since the t statistic of -0.026 in one-tail was smaller than the critical value of 2.13 and probability of 0.98 in two-tail also was smaller than the critical value of 2.77; failed to reject the null hypothesis. The null hypothesis was that these means of simulation and experiment were equal (Significance level $p>0.05$).

Table 8 t test Two Sample Assuming Equal Variances.

| | Mean | Variance | t Stat | $P(T<=t)$ one-tail | t Critical one-tail | $P(T<=t)$ two-tail | t Critical two-tail |
|---|---|---|---|---|---|---|---|
| Simulation | 175.667 | 1159.85 | -0.0263 | 0.49012 | 2.13185 | 0.98025 | 2.77645 |
| Experiment | 176.233 | 228.413 | | | | | |

### 4.6.6 Diffusion Results of the Bimonidine
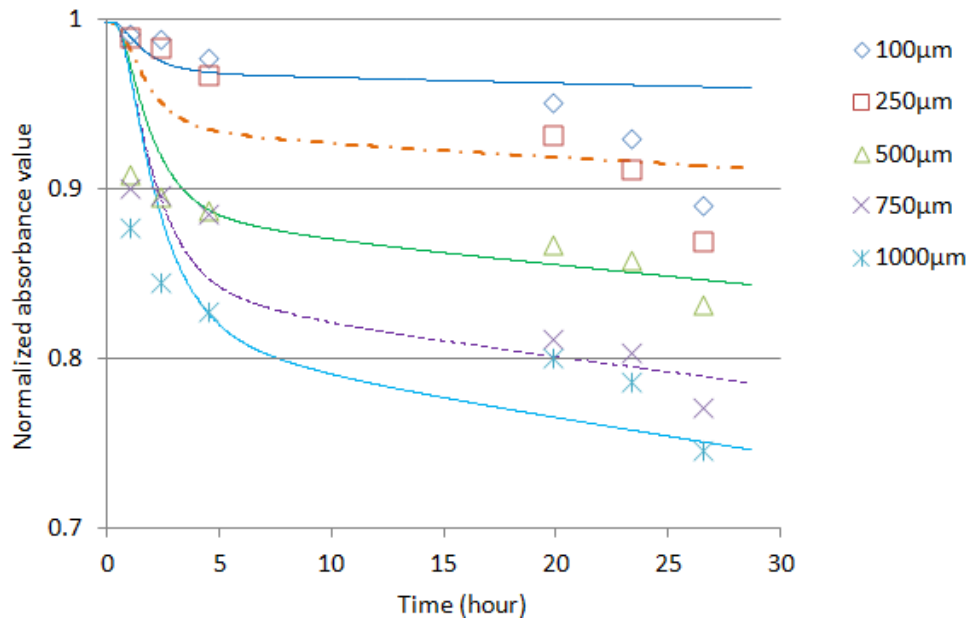


Figure 4. 27 Comparison of simulation (COMSOL) and experiments (UV-Vis) with microchannel A
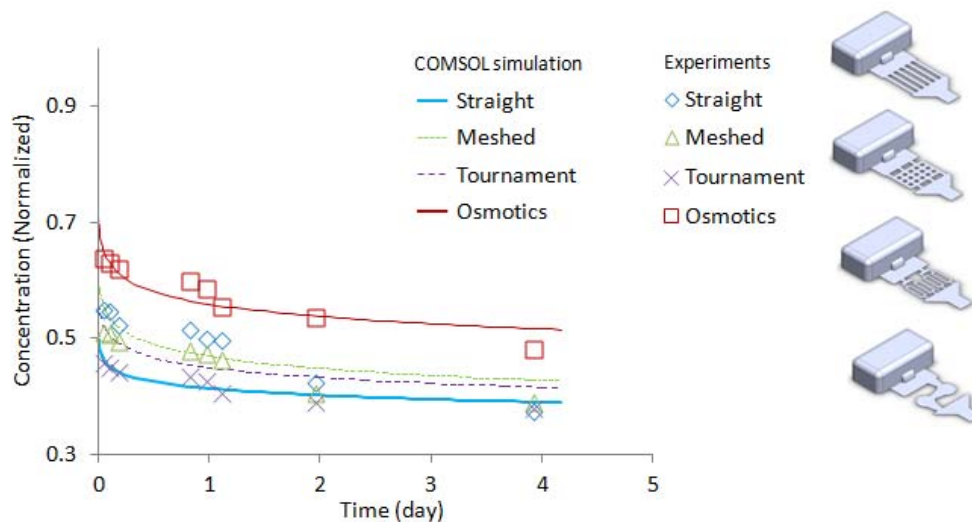
Figure 4. 28 Comparison of simulation (COMSOL) and experiments (UV-Vis) with device

In Figure 4.27, results showed that after 24 hours, Brimonidine ($C_{11}H_{10}BrN_5$), with a molecular weight of 292 g/mole, obtained the biggest section of microchannel obtained the faster diffusion rate than the other small sections. Y-axis is a normalized data, which derived from an observance at 248nm (1- $\mu V_i$ / $\mu V_{peak}$) with respect to time.

The simulation showed agreement with the experiments. It can be seen in Figure 4.48 that after 4 days, each type of microchannel geometry generated a different diffusion rate. The diffusion rate of tournament microchannel was bit higher than the others, which was similar to result with citric acid experiments.

Table 9 Drug concentration after 24 hours was determined by the regression equation

| Amount of drug | Microchannel A | | | | |
|---|---|---|---|---|---|
| | 100 µm | 250 µm | 500 µm | 750 µm | 1000 µm |
| Concentration (µg/ml) / day | 0.6455 | 0.7883 | 1.037 | 1.4338 | 1.6031 |
| | Microchannel | | | |
| | Straight | Meshed | Tournament | Osmotic |
| Absorbance (µV) | 0.404 | 0.446 | 0.494 | 0.369 |
| Concentration (µg/ml) / day | 6.3333 | 7 | 7.7619 | 5.7778 |
| Drug Release (0.59mg/ml) | 93 days | 84 days | 76 days | 102 days |

Based on the research papers written by Bhagav P et al [79] and C.A. Holden et al [80], the regression equation, $C = (Y \text{ (absorbance)} - 0.005)/0.063$ could be used to estimate the drug concentration after 24 hours diffusion. In this experiment, the diffusion rate of the Brimonidine was approximately 16% faster than Citric acids that diffused through a 100µm channel after 24 hours. The drug release with 0.59mg/ml drugs could diffuse freely through a microchannel for over 102 days with a device including an osmotic channel as shown in table 9.

4.7 Discussion

The top and bottom covers were fabricated from PDMS through replica-molding techniques. The microchannels along with top and bottom covers were all integrated into the device. The experiment was designed to maintain a constant distance between the drug delivery device and the electrode, which was preferable for two reasons. First, by maintaining a constant distance from the outlet of the drug delivery device, the diffusion of the citric acid needed not to be adjusted to the output of the pH measurement. As long as the electrode distance remained constant, the output of the pH meter was all that was needed to determine the size of the microchannels.

The microchannel and device were being tested for its functionality and diffusion characteristics. However, there were significant challenges related to achieving reliable and sustainable micro scale geometry on a silicon, bonding, diffusion of the drug into channels, and controllability. The test evaluation was performed measuring the change in pH of a neutral solution using a strong citric acid; it could be diffused out through the device. The final pH test of the theoretical calculations was to apply the nonlinear logarithmic curve to correct a set of measurements and compare them to a reference measurement. The form of the nonlinear residue curves was quite comparable, showing the same nonlinear trends and the increase in nonlinearity as the area of microchannel was decreased. In terms of absolute value, a comparison of these showed those in all cases the theoretical curves were actually slightly larger than the experimental curves. It was hypothesized that one possible reason for this inconsistency may be the presence of

additional factors in the entire device that leak small amounts of acid to the outlet and place the distance of the measuring probe. It is well known that indeed the diffusion rate between the Brimonidine and Citric acid were significantly different because the lighter the particle was going to move the faster.

The simulations showed different behavior for thermal and for mass, which was due to the different values of the Lewis number, diffusivity. The heat and mass transport were both diffusion dominated and the differences were determined by the highly unequal diffusivities. The presence of an additional factors term may raise the magnitude of the velocity, but further work would be required to prove this. Since the t statistic for both simulation and experiment was smaller than the critical value, these two variables were equal. The drug release rate with specific size of microchannel was satisfied to diffuse for 1-3 years. These challenges were being addressed and were presented.

### 4.8 Summary

This chapter described an experimentally verified diffusion scheme between a PDMS reservoir and various size of microchannel. A PDMS reservoir was chosen because of its biocompatible and typically no reaction with drug substance. The entire drug delivery system except silicon microchannel could therefore be modeled completely in the simple structure. To quantify the release of the drug molecules from the reservoir we used pH meter. The value of pH meter observed could be correlated to the concentration of the drug.

As results of microchannel diffusion measurement in light intensity, we could clearly understand that the distance from the inlet reservoir to microchannel or microchannel to outlet reservoir was significantly effects for the diffuion rate as a function of time. When the pH probe on the right was positioned above a device, the resulting data revealed the differences between the outlet measurement and the vertical measurement. We could consider this outlet measurement as the actual distance. Comparing the diffusion rate between the end of microchannel and middle of outlet reservoir were consequently different as shown in Figure 4.29. Therefore keeping the consistent measuring position was one of the important procedures to obtain reliable data.
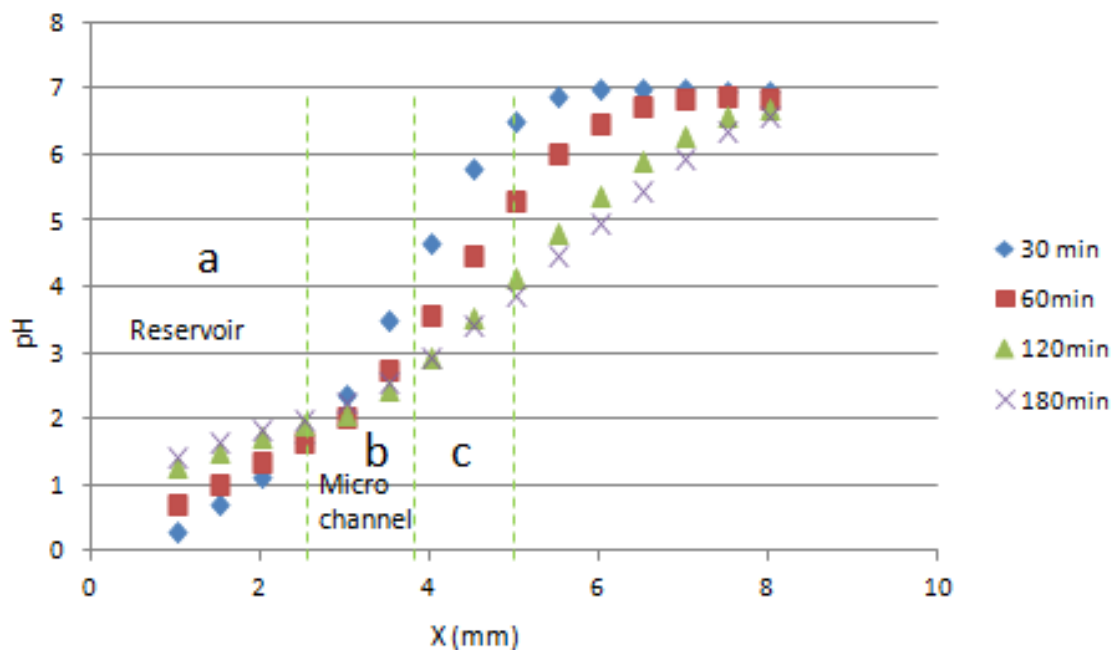


Figure 4. 29 Results of microchannel diffusion with a width of 1000μm and a height of 500 μm, Light intensity measurements modified from Heeren A. et al [72].

The main reason for maintaining a constant distance had been illustrated in Figure 4.29. Specifically, for different microchannel size of both the nominal distance and the increase were affected. By positioning the exact fixture at the nominal distance, the variation factor was removed from consideration.

# CHAPTER 5 Conclusions and Recommendations

## 5.1 Conclusions

Microchannels were significant components of miniaturized passive diffusion fluid systems. They were used for example to direct the diffusion flow from inlet to outlet in miniaturized PDMS device.

Variations of drug diffusion rate of all models from single microchannel to entire device were carried out through simulations and experiments. The analytical simulations and experiments for microchannels and device were conducted to verify the diffusion rate. Based on the proposed single channel dimension, the geometry and size of channels could be modified to satisfy the specification of diffusion rates for ocular drug delivery device. Moreover a surface of device should be manipulated in order to keep an optimized implant angle and to avoid a patient's inconvenience. Various approaches had been tested experimentally to increase the efficiency of ocular drug delivery device. These drug delivery devices were designed to provide relatively constant drug delivery over long periods of time, making it easier for patients to remain adherent to treatment and possibly reducing the risk of side effects.

### 5.1.1 Hydrophobic to Hydrophilic

Obtaining a good seal between microchannel substrate and PDMS reservoir was important in preventing leakage after the drugs were filled. The plasma treated PDMS and microchannels provided a more reliable seal than any other bonding methods for microchannel. Moreover, the surface of PDMS and microchannel showed that the

hydrophobicity switched to hydrophilic after processing oxygen plasma that both PDMS and microchannel were ready to make a free diffusion easy.

### 5.1.2 Comparison of Simulation and Test

The diffusion characteristic of a microchannel was the result of two effects. First, the diffusion coefficient of the drug in a solution led to a concentration dependent gap. If the shape of the gap was known, the microscopic flow through the gap could be calculated. From the theoretical point of view this can be done either by finite-element analysis or by approximate formulae. From the experimental point of view, the diffusion characteristic of microchannel could be recorded by pH and UV-Vis measurements. Typical diffusion characteristic curves of passive microchannel, made by microfabrication of silicon, were depicted in Figure 4.2. In many cases a very non-linear behavior can be seen in forward direction. So it was impossible to define a constant diffusion flow coefficient.

Variations of drug diffusion rate of all models from single microchannel to entire device were carried out through simulations and experiments. The analytical simulations and experiments for microchannels and device were conducted to verify the diffusion rate.

A thorough analysis of both the simulation and experimental data had shown the importance of diffusion coefficient whenever the microchannel was applied to a medium.

Otherwise the accuracy of the experimental data, in terms of absolute distance, linearity, and consistency, was called into question.

Use of the values of the diffusion coefficients and normalized constant obtained from our device measurements, both lower than those used by simulation of microchannel A and B, and entire device implantation in eye. It still led to the prediction of substantial effects. These should affect the reduced coefficient in the way predicted in the simulation. The results were consistent with the prediction, suggesting a microchannel sensitive to the present device.

Eventually it may be possible to develop a set of general, nondimensionalized equations or curves that represented the changes in slope as a function of diffusion coefficient with microchannels. Practical measurements such as an experiment of a particular microfluidic device can be used as a guide for selection of microchannel geometry and cross section. For comparison with the results of microchannel A and B, measurements were made in the pH meter a citric acid concentration of 0.5 g/ml. The results were converted to normalized value which initial pH value was divided by measured pH value at each time for hundred hours and plotted in Figure 4-12, 4-13. It was clear that there was a marked effect of citric acid concentration with size of microchannel. It appeared to be significant deviations occurring from nonlinearity of diffusion against size of microchannel.

Some factors may have affected the rate of diffusion of the substances in the experiment which may have led to inaccurate results. Such factors may include but were

not limited to inconsistent temperatures and concentrations, the type of medium used, or handling and execution of the experiment.

### 5.1.3    Drug Delivery Device Models

Based on the proposed single channel dimension, the geometry and size of channels can be modified to satisfy the requirement of diffusion rate for ocular drug delivery device. Since all these experimental results exhibited non-linearity, this fact would tend to make the variations seen in Figure 4-15, which was greater or less than they would be if assumed at constant velocity gradient. However, it can be assumed that the measuring position of ph electrode in a beaker made variations as we had known from research paper by Heeren et al [70].

### 5.1.4    Determination of Drug Release Time

The results of test represent the straight single channel of square 192, 174, and 162 μm can get diffusion rates that release drugs for over 1, 2, and 3 years respectively. Although the simulation results of drug release rate were around 7% different, the rate of microchannel size was fairly agreed with the experimental results.

A variation against the simulation results, our experiment showed some sort of inconsistency with our early mentioned hypothesis on the first experiment of microchannel A. The rate of diffusion of a substance was affected by its molecular weight. As the molecular weight increased, the rate of diffusion was generally low. This

was because the larger the size of a particle, a greater amount of force, in this case, thermal energy was required to move the particle [84].

### 5.2 Scientific Contributions

Although these results showed a complex relationship of diffusivity to size of microchannel, concentration changes and diffusion rate, two interesting conclusions could be drawn from them; (i) The diffusivity was strongly dependent on size of microchannel under all conditions. (ii) There was a remarkable dependence of microchannel geometry on diffusion coefficient with relatively high concentration at the inlet.

This study provided beneficial results to determine the diffusivity of drugs or any other micro/nano particles flow through the microchannel. We developed a novel channel design and further simulate, optimize, fabricate, and test to obtain the state of art drug delivery devices. The present device could be applicable other applications with the multi-scale model, e.g., drug delivery for targeted tissues and cancer disease.

The detailed drug diffusion description in this model allowed for the investigation of many design parameters relevant to biomedical engineering. This case presented the effect of microchannel on drug release as a function of time and geometry. Furthermore, it was straightforward to study the influence of the drug similarity by varying the rate constants, or the influence of drug loading by varying the drug density. The ability to examine alternative microchannel geometries and simple membrane structure of PDMS could give even more design flexibility.

## 5.3 Recommendations

Therapeutic drug levels could be achieved in the vitreous body of eye with a smaller implanted device dose if the molecular size of the drug was reduced. The smaller device decreased the systemic drug load however possibly reduced the incidence of serious systemic side effects [84, 85].

Since microchannels provided a nonlinear diffusion rate after the drugs reach the outlet of device, a careful operation was necessary to fully fill out drugs into the microchannels. Various geometries of microchannel may prevent a back diffusion flow of drugs from the vitreous humor. The drug reservoir should be considered to be a semi-sphere or cylindrical to minimize the residual drugs while operating for a long period of time as shown in Figure 5.1.
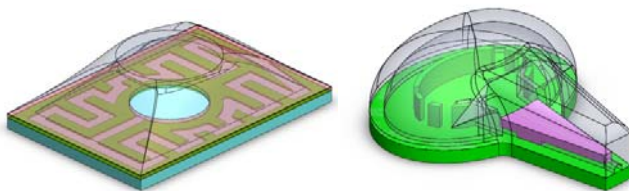


Figure 5. 1 Schematic of new design concept with sphere dome reservoir for reducing residual drugs.
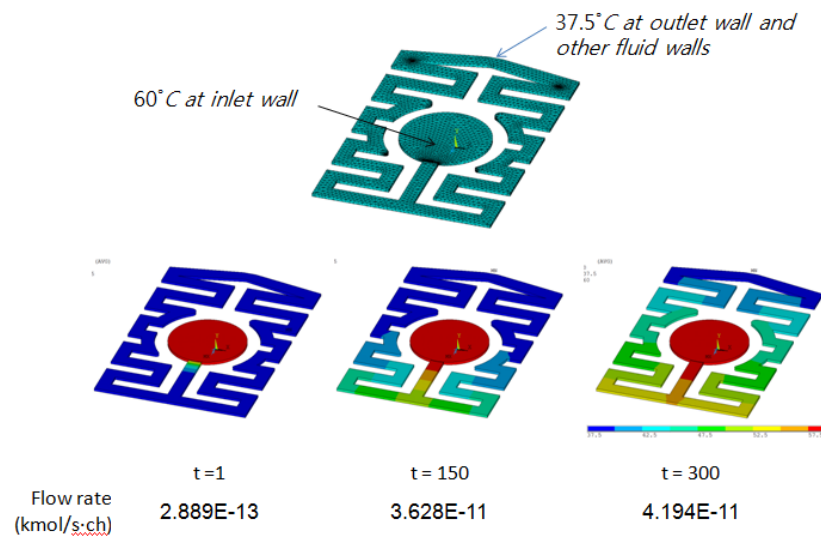
Figure 5. 2 Contour plot of molecular flow rate with new microchannel.

## 5.4 Future Works

Although large variability was common in ocular pharmacokinetic studies, an additional cause of variability in the present studies may effect that the drugs were administered as diffusion from the implanted device that did not immediately dissolve within the vitreous cavity. To ensure as small as possible the residuals drugs remained in the device, new design concept model was necessary and to be optimized.

Developing around less than 100 μm of microchannels on a PDMS substrate may be a big challenge to make a biocompatible and biodegradable device. Hydrogels could stimulate the fluid flow as a pressure driven resource while shrinking or swelling with pH response. A hydrogels-based microvalve could be another way to control the drug release. Having an array of orifices or mesh-like holes with an internal structure designed to anchor the hydrogels while allowing it to gate the flow across the membrane. The

hydrogels could completely occupy the empty space of the orifice, completely blocking pressure-driven fluid flow [73].
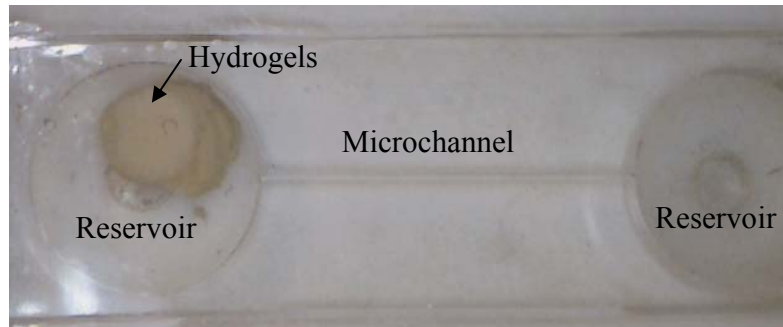


Figure 5. 3 Experiment of 200μm microchannel flow with pH responsive hydrogels (pH 4 to 8) while swelling.

An electrochemically actuated bilayer diaphragm as a low cost and low power micropump concept that was composed of a PDMS membrane was investigated by Kim [86]. In Figure 5.4, an isometric view and structure of concept design is illustrated, which is similar to piezo- actuation mechanisms. New micropump models were considered to optimize micro-flow efficiency and filtering micro-particles. These micropump models consisted of microchannels, connecting one pump chamber and an inlet/outlet ports and piezo-actuator on the top of chamber operated by a two-phase input power. All components except the piezo-actuator were fabricated with PDMS elastomer. The diameter and thickness of the actuator diaphragm were 5mm and 500μm, respectively.
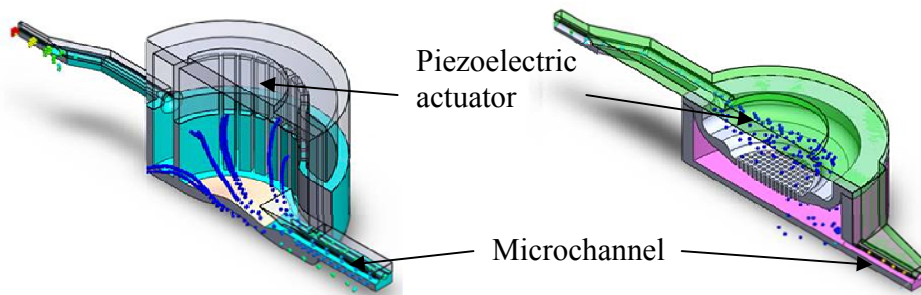
Figure 5. 4 Schematic of new micropump for experimental application.

The length, width and the depth of the microchannel were 250, 100 and 50μm, respectively. If the two-phase electrical power is applied to the piezo-actuator, the pressure in the sealed actuator chamber was varied by the size of microchannel and total movement of membrane in the actuator chamber. The magnitude of the electric power could be determined by the pressure change amount. If the two-phase input power signal was applied to the piezo-actuator of the micropump, the two-phase motions of the actuator diaphragms conveyed the fluid in the pump chamber. We assumed that the working fluid should be sucked into the inlet chamber and pushed out from outlet chamber. Based on these fluid release kinetics and transport mechanisms of biodegradable polymeric actuation system, it could be considered in the future works.

The schematic of a check valve integrated into microfluidic drug delivery devices was shown in Figure 5.5. The polystyrene ball can be acted as a value to close or open the fluid flow while maintaining consistent diffusion flow. The coupled structure simulation is required to predict the behavior of the check valve for further discussion.
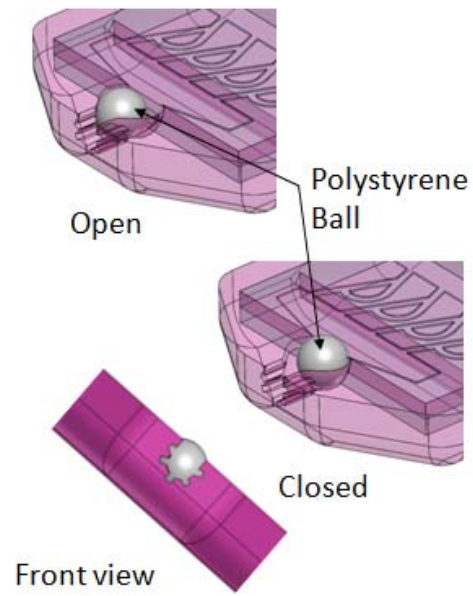
Figure 5. 5 Schematic of a check valve integrated into microfluidic drug delivery devices

# List of references

# References

[1]     Eye Conditions and Eye Diseases, http://www.allaboutvision.com/conditions/

[2]     J.C. Lang, Ocular drug delivery conventional ocular formulations. Adv Drug Delivery Rev., 16 (1995) 39–43.

[3]     L. Jiahorng, J.R. Robinson, The Effect of polyethylene glycol molecular weight on corneal transport and the related influence of penetration enhancers. Int J Pharm 88, (1992) 125–140.

[4]     K.G. Janoria, S. Hariharan, C.R. Dasari, A.K. Mitra, Recent patents and advances in ophthalmic drug delivery. Recent Pat Drug Deliv Formul 1, (2007) 161–170.

[5]     K. Jarvinen, T. Jarvinen, A. Urtti, Ocular absorption following topical delivery. Adv Drug Del Rev 1, (1995) 3–19.

[6]     D. H. Geroski, H. F. Edelhauser, Drug delivery for posterior segment eye disease, Investigative Ophthalmology and Visual Science, vol. 41, no. 5, (2000) 961–964.

[7]     R. Gaudana, J. Jwala, S. H. S. Boddu, A. K.Mitra, Recent perspectives in ocular drug delivery, Pharmaceutical Research, vol. 26, no. 5, (2009) 1197–1216.

[8]     R. Lo, P.T. Li, S. Saati, R.N. Agrawal, M.S. Humayun, E. Meng, A passive MEMS drug delivery pump for treatment of ocular diseases, Biomed Microdevices Volume 11, (2009) 959-970.

[9]     M. Staples, K. Daniel, M. J. Cima, R. Langer, Application of micro- and nano-electromechanical devices to drug delivery, Pharmaceutical Research, vol. 23, no. 5, (2006) 847–863.

[10]    V.H.L. Lee, Precorneal, cornea, and postcorneal factors. In: A.K. Mitra (Ed.), Ophthalmic Drug Delivery, Marcel Dekker, New York 59 (1993).

[11]    C.X. Zhao, A.P.J. Middelberg, Two-phase microfluidic flows. Chem. Eng. Sci., 66, (2011) 1394-1411.

[12]    V. Kumar, M. Paraschivoiu, K.D.P. Nigam, Single-phase fluid flow and mixing in microchannels. Chem. Eng. Sci., 66, (2011) 1329-1373.

[13]    T.M. Squires, S.R. Quake, Microfluidics; Fluid physics at the nanoliter scale. Rev. Mod. Phys., 77, (2005) 977-1026.

[14]    R. D. Jager, W. F. Mieler, J. W. Miller, Age-related macular degeneration, The New England Journal of Medicine, vol. 358, no. 24, (2008) 2606–2617.

[15]    H. R. Coleman, C. C. Chan, F. L. Ferris, E. Y. Chew, Age related macular degeneration, The Lancet, vol. 372, no. 9652, (2008) 1835–1845.

[16]    I. Ahmed, T.F. Patton, Importance of the noncorneal absorption route in topical ophthalmic drug delivery. Invest Ophthalmol Vis Sci. 26, (1985) 584–587. IOVS, April 2000, Vol. 41, No. 5 Posterior Segment Eye Disease 963.

[17]    I. Ahmed, R.D. Gokhale, M.V. Shah, T.F. Patton, Physico-chemical determinants of drug diffusion across the conjunctiva, sclera, and cornea. J Pharm Sci. 76, (1987) 583–586.

[18]    G.E. Sanborn, R. Anand, R.E. Torti, Sustained-release ganciclovir therapy for treatment of cytomegalovirus retinitis. Arch Ophthalmol. 110, (1992) 188–195.

[19]    N. K. Basavaraj, F.V. Manvi, A.S. Manjappa, In situ-forming hydrogels for sustained ophthalmic drug delivery. Journal of Controlled Release, 122, (2007) 119–134.

[20]    K.S. Sahoo, S.A.D. Fahima, K. Kumar, Nanotechnology in ocular drug delivery, Drug delivery today, 13, (2008) 144-151.

[21]    J. Weidener, Mucoadhesive ocular inserts as an improved delivery vehicle for ophthalmic indications. Drug Discovery Today, 8, (2003) 906– 907.

[22]    J.C. Lang, R.T.E. Roehrs, R. Jani, Ophthalmic preparations, Lippincott Williams and Wilkins, Edition 21, (2005) vol-1.

[23]    G.P. Andrews, T.P. Laverty, D.S. Jones, Mucoadhesive polymeric platforms for controlled drug delivery Review article. European Journal of Pharmaceutics and Biopharmaceutics, 71, (2009) 505–518.

[24]    R.G. Alany, T. Rades, J. Nicoll, I.G. Tucker, N.M. Davies,W/O microemulsions for ocular delivery: Evaluation of ocular irritation and precorneal retention. Journal of Controlled Release, 111, (2006) 145-152.

[25]    Y. Tsutomu, O. Yuichiro, K. Hideya, S. Eiji, T. Yasuhiko, Drug delivery from Ocular Implants, Expert Opin. Drug Deliv. 3(2), (2006) 261-273.

[26]    Tsai J C, Denniston A K O, Murray P I, Huang J J and Aldad T S, Oxford American Handbook of Ophthalmology, Oxford University Press, (2011) 262-268.

[27]   M.J. Meziani, P. Pathak, Y.P. Sun, Supercritical fluid technology for nanotechnology. Nanotechnology in Drug Delivery. New York, NY: Springer (2009) 69–104.

[28]   E. Reverchon, R. Adami, G. Caputo, I. De Marco, Spherical microparticles production by supercritical antisolvent precipitation: interpretation of results. J Supercrit Fluids. 47, (2008) 70–84.

[29]   U.B. Kompella, K. Koushik, Preparation of drug delivery systems using supercritical fluid technology. Crit Rev Ther Drug Carrier System. 18 (2), (2001) 173–199.

[30]   X. Tongwen, H. Binglin, Mechanism of sustained drug release in diffusion-controlled polymer matrix-application of percolation theory, International Journal of Pharmaceutics, 170, (1998) 139–149.

[31]   H. Leuenberger, J.D. Bonny, M. Kolb, Percolation effects in matrix-type controlled drug-release system. Int. J. Pharm. 115, (1995) 217.

[32]   A. Adrover, M. Giona, M. Grassi, Analysis of controlled release in disordered structures: a percolation model. J. Membrane Science. (1996) 113, 21.

[33]   L. Simon, P. Bolisetty, M.N. Erazo, Dynamics of dissolution and diffusion-controlled drug release systems, Current Drug Delivery. 8 (2), (2011) 144-151.

[34]   J.B. Dressman, C. Reppas, In oral drug absorption: Prediction and assessment; Permeability measurement, (2000) 168-205.

[35]   P.P. Bhatt, Osmotic drug delivery system for poorly soluble drug, Pharma venture ltd. (2004), Patent Publication Number: 2368556.

[36]   M.A. Ramdan, R. Tawashi, The effect of hydrodynamic conditions and delivery orifice size on the rate of drug release from elementary osmotic pump system, Drug Dev. Ind. Pharm. 13(2), (1987) 235-248.

[37]   R. Langer, N.A. Peppas, Advances in biomaterials, drug delivery, and bionanotechnology. AIChE Journal, 49(12), (2003) 2990–3006.

[38]   Q. Wang, G. Wang, Z. Cheng, Oscillatory Swelling Behavior of Hydrogels Incorporated with Ion-Exchange Nanoparticles, Drug Delivery Letters, 1, (2001) 58-61

[39]  E. Meng, T. Hoang, MEMS-enabled implantable drug infusion pumps for laboratory animal research, preclinical, and clinical applications, Advanced Drug Delivery Reviews, (2012) in review.

[40]  R. Lo, K. Kuwahara, P.Y. Li, R. Agrawal, M. S. Humayun, E. Meng, A Passive Refillable Intraocular MEMS Drug Delivery Device, Proceedings of 2006 International Conference on Microtechnologies in Medicine and Biology Okinawa, Japan (2006).

[41]  S. Saati, R. Lo, P.Y. Li, E. Meng, R. Varma, M.S. Humayun, Mini drug pump for ophthalmic use. Curr Eye Res. 35, (2010) 192-201.

[42]  R. Gonzalez-Soto, R.A. Brant-Fernades, M.S. Humayn, R. Vama, M. Journey, S. Caffey,  Intravitreal infusion of ranibizumab with an infusion pump in rabbits. Presented at the Associattion for Research in Vision and Ophthalmology Annual Meeting, Fort Lauderdale, FL (2011).

[43]  J. Flanigan, Biotech tries to shrug off setbacks. The New York Times (2009).

[44]  Genentech. Genentech announces first milestone payment to device-maker ForSight VISION4, Inc. in development of sustained delivery Lucentis. Available at: http://www.gene.com/gene/news/press-releases/display.do?method =detail&id=13808.

[45]  ClinicalTrials.gov. Safety and preliminary efficacy study of PDS-1.0 in patients with neovascular AMD. Available at: http://clinicaltrials.gov/ct2/show/NCT01177644?term=forsight+PDS&rank=1.

[46]  A. Ohtori, K. Tojo, In vivo / in vitro correlation of intravitreal delivery of drugs with the help of computer simulation, Biol. Pharm. Bull. 17, (1994) 283–290.

[47]  K. Uno, K. Nakagawa, A. Ohtori, K. Tojo, Drug targeting to the vitreous body and its peripheral tissues, Drug Deliv. Syst. 11, (1996) 133–137.

[48]  S. Friedrich, Y-L. Cheng, B. Saville, Finite element modeling of drug distribution in the vitreous humor of the rabbit eye, Ann. Biomed. Eng. 25. (1997) 303–314.

[49]  J. Park, P. M. Bungay, R.J. Lutz, J.J. Augsburger, R. W. Millard, A. S. Roy, R. K. Banerjee, Evaluation of coupled convective–diffusive transport of drugs administered by intravitreal injection and controlled release implant, Journal of Controlled Release 105, (2005) 279–295.

[50]  K. Tojo, A pharmacokinetic model for ocular drug delivery, Chemical and Pharmaceutical Bulletin, vol. 52, no. 11, (2004) 1290–1294.

[51] J. C. Keister, P. S. Heidmann, and P. J. Missel, Transient analysis of ocular drug delivery: zero-volume effect, Journal of Pharmaceutical Sciences, vol. 86, no. 9, (1997) 1040–1045.

[52] T. R. Thrimawithana, S. Young, C. R. Bunt, C. Green, and R. G. Alany, Drug delivery to the posterior segment of the eye, Drug Discovery Today, vol. 16, no. 5-6, (2011) 270–277.

[53] S. D. Swanson, Selective MRI and MRS of PEGylated compounds, in Proceedings of the 14th Scientific Meeting International Society for Magnetic Resonance in Medicine, The University of Michigan, Ann Arbor, Michigan, USA (2006).

[54] S. A. Molokhia, H. Sant, J. Simonis, The capsule drug device: novel approach for drug delivery to the eye, Vision Research, vol. 50, no. 7, (2010) 680–685.

[55] T. Li, D. O. Kildsig, K. Park, Computer simulation of molecular diffusion in amorphous polymers, Journal of Controlled Release, vol. 48, no. 1, (1997) 57–66.

[56] G. J. Jaffe, C. H. Yang, H. Guo, J. P. Denny, C. Lima, P. Ashton, Safety and pharmacokinetics of an intraocular fluocinolone acetonide sustained delivery device, Investigative Ophthalmology and Visual Science, vol. 41, no. 11, (2000) 3569– 3575.

[57] K.C. Tang, E. Liao, W.L. Ong, J.D.S. Wong, A. Agarwal, R. Nagarajan, L. Yobas, Evaluation of bonding between oxygen plasma treated polydimethyl siloxane and passivated silicon, Journal of Physics: Conference Series, 34, (2006) 155–161.

[58] F. Yang, C.M. James Li, New Fick's law for self-diffusion in liquids, J. Appl. Phys. 80, (1966) 6188-6191.

[59] G. Nellis, S. Klien, Heat Transfer: Chapter 9 Mass Transfer (2008), available at http://www.cambridge.org/us/engineering/author/nellisandklein/ downloads/ extended/ chapter%209.pdf.

[60] J.L. Nickerson, A. Paradijeff, H.I.S. Feinhandler, A study of the effects of externally applied sinusoidal forces on the eye, Aerospace Medical Research Laboratory (AMRL)-TR-63-120 (1963).

[61] W.P. Eaton, F. Bitsie, J.H. Smith, D. W. Plummer, A New Analytical Solution for Diaphragm Deflection and its Application to a Surface-Micromachined Pressure Sensor, Sandia National Laboratories, Albuquerque, NM, (1999) 640-643.

[62]    J.H. Lee, R.M. Pidaparti, G.M. Atkinson, R.S. Moorthy, Design of an Implantable Device for Ocular Drug Delivery, Journal of Drug Delivery, Volume 2012, (2012) 8 pages.

[63]    J.H. Lee, R.M. Pidaparti, Drug Transport Microdevice Mimicking an Idealized Nanoscale Bio-molecular Motor, Journal of Bionic Engineering, Volume 8, (2011) 445-463.

[64]    D.A. Chang-Yen, D.G. Myszka, B.K. Gale, A Novel PDMS Microfluidic Spotter for Fabrication of Protein Chips and Microarrays, J. of Microelectromechanical systems, vol. 15, (2006) 1145-1151.

[65]    J.C. Eloy, Technologies and market trends for polymer MEMS in microfluidics and lab-on-chip, Proc. SPIE, vol. 5718, (2005) 60–64.

[66]    M.O. Reese, R.M. van Dam, A. Scherer, S.R. Quake, Microfabricated fountain pens for high-density DNA arrays, Genome Res., vol. 13, (2003) 2348-2352.

[67]    O. Yogi, T. Kawakami, M. Yamauchi, J.-Y. Ye, M. Ishikawa, Ondemand droplet spotter for preparing pico- to femtoliter droplets on surfaces, Anal. Chem., vol. 73, (2001) 1896.1902.

[68]    N. Rupcich, A. Goldstein, J.D. Brennan, Optimization of sol-gel formulations and surface treatments for the development of pin-printed protein microarrays, Chem. Mater., vol. 15, (2003) 1803.1811.

[69]    S.A. Lange, V. Benes, D.P. Kern, J.K.H. Horber, A. Bernard, Microcontact printing of DNA molecules, Anal. Chem., vol. 76, (2004) 1641.1647.

[70]    E.L. Cussler, Diffusion, Mass Transfer in Fluid Systems. Cambridge, Cambridge University Press (1984).

[71]    R. Zengerle, M. Richter, Simulation of microfluid systems. Journal of Micromechanics and Microengineering 4(4), (1994) 192-204.

[72]    A. Heeren, C.P. Luo, G. Roth, A. Ganser, R. Brock, K.H. Wiesmueller, W. Henschel, D.P. Kern, Diffusion along microfluidic channels, Microelectronic Engineering 83, (2006) 1669–1672.

[73]    P.S. Williams, S. Levin, T. Lenczycki and J. C. Giddings, Continuous SPLITT Fractionation Based on a Diffusion Mechanism. Industrial and engineering chemistry research 31, (1992) 2172-2181.

[74] D. Mark, S. Haeberle, G. Roth, F. von Stetten, R. Zengerle, Microfluidic lab-on-a-chip platforms: requirements, characteristics and applications. Chem. Soc. Rev. 39, (2010) 1153-1182.

[75] M.L. Sin, J. Gao, J.C. Liao, P.K. Wong, System Integration - A Major Step toward Lab on a Chip. J. Biol. Eng. 5, (2011) 6.

[76] B.H. Jo, L.M. van Lerberghe, K.M. Motsegood, D.J. Beebe, Three-dimensional microchannel fabrication in polymethylsiloxane (PDMS) elastomer, J. Microelectromech. Syst. 9, (2000) 76–81.

[77] S. Bhattacharya, A. Datta, J.M. Berg, S. Gangopadhyay, Studies on surface wettability of poly(dimethyl)siloxane (PDMS) and glass under oxygen-plasma treatment and correlation with bond strength J. Microelectromech. Syst. 14, (2005) 590–7.

[78] P. Rezai, P.R. Selvaganapathy, G. RWohl, Plasma enhanced bonding of polydimethylsiloxane with parylene and its optimization, J. Micromech. Microeng. Vol 21, 065024 (2011) 13.

[79] P. Bhagav, P. Deshpande, S. Pandey, S. Chandran, Development and Validation of Stability Indicating UV Spectrophotometric Method for the Estimation of Brimonidine Tartrate in Pure Form, Formulations and Preformulation Studies, Der Pharmacia Lettre, 2(3), (2010) 106-122.

[80] C. A. Holden, P. Tyagi, A. Thakur, R. Kadam, G. Jadhav, U.B. Kompella, H. Yang, Polyamidoamine dendrimer hydrogel for enhanced delivery of antiglaucoma drugs, Nanomedicine: Nanotechnology, Biology and Medicine, Volume 8, Issue 5, (2012) 776–783.

[81] R. Chang, Chemistry, McGraw-Hill Science/Engineering/Math; 10 edition (2009).

[82] S. Maiti, S. Pauk, R. Mondol, S. Ray, B. Sa, Nanovesicular Formulation of Brimonidine Tartrate for the Management of Glaucoma: In Vitro and In Vivo Evaluation, AAPS PharmSciTech, Vol. 12, No. 2, (2011) 755-763.

[83] M.H. Aburahma, A.A. Mahmoud, Biodegradable Ocular Inserts for Sustained Delivery of Brimonidine Tartarate: Preparation and In Vitro/In Vivo Evaluation, AAPS PharmSciTech, Vol. 12, No. 4, (2011) 1335-1347.

[84] J. Ambati, C.S. Canakis, J.W. Miller, E.S. Gragoudas, A. Edwards, D.J. Weisgold, I. Kim, F.C. Delori, A.P. Adamis, Diffusion of high molecular weight compounds through sclera, Invest. Ophthalmol. Vis. Sci., 41, (2000) 1181–1185.

[85]    S. Kakkar, I.P. Kaur, Spanlastics—A novel nanovesicular carrier system for ocular delivery, International Journal of Pharmaceutics, Volume 413, Issues 1–2, (2011) 202–210.

[86]    J.H. Kim, K.T. Lau, R. Shepherd, Y. Wu, G, Wallace, D. Diamond, Performance characteristics of a polypyrrole modified polydimethylsiloxane (PDMS) membrane based microfluidic pump Sensors and Actuators A 148, (2006) 239–244.

# VITA

## PERSONAL INFORMATION

Date of Birth:          January 23, 1966

Birthplace:             KeongKi, South Korea

Nationality:            South Korea

## EDUCATION

2009–Present    **Virginia Commonwealth University**, Richmond, VA
Ph.D. in Engineering
Field of study: Mechanical Engineering
Current GPA: 3.57/4.00
Dissertation topic: "Design and Development of Microfluidic Device for Drug delivery"
Expected graduation: May 2013

2006–2008       **Virginia Commonwealth University**, Richmond, VA
Master of Business Administration
Field of study: Decision Science
GPA: 3.26/4.00

2004–2005       **Chung Nam National University**, Dae-Jeon, Korea
Industrial Graduate School (Master, Incomplete)
Field of study: Mechanical Engineering
GPA: 3.92/4.50

1984–1988       **Myong-Ji University**, Seoul, Korea
Bachelor of Engineering
Field of study: Mechanical Engineering
Specialty: Solid Mechanics and Fluid Mechanics
GPA: 3.2/4.50

## HONORS AND AWARDS

- VCU School of Engineering Teaching Assistantship
- Design and development of MEMS microfluidic devices funded by NSF (National Science Foundation) ECCS-1058067.

## TEACHING EXPERIENCE

| | |
|---|---|
| Fall 2010 | Department of Mechanical Engineering, Virginia Commonwealth University <br> Teaching Assistant for EGRM565- Design Optimization class |
| Spring 2011 | Department of Mechanical Engineering, Virginia Commonwealth University <br> Teaching Assistant for EGRM510- Advanced Solid Mechanics and Materials class |
| Fall 2011 | Department of Mechanical Engineering, Virginia Commonwealth University <br> Teaching Assistant for EGRN650- Nuclear Radiation and Shielding class |
| Fall 2012 | Department of Mechanical Engineering, Virginia Commonwealth University <br> Teaching Assistant for ENGR102 - Engineering Statics class |

## RESEARCH EXPERIENCE

| | |
|---|---|
| 2009–Present | Department of Mechanical Engineering, Virginia Commonwealth University <br> Graduate Research Assistant for Prof. Ramana M. Pidaparti |

**WORK EXPERIENCE**

1991–2005    <u>Windshield Wiper System and Motor Development Team/ Dae-Jeon,</u>

<u>Korea</u>

Senior Design Engineer (1$^{st}$ Group leader)

Responsible for taking projects through from conceptual design to detailed drawings for manufacture.
Designed and developed test set-ups for the testing and evaluation of wiper motor and system.

Project Leader (03/01-07/05)

Development of windshield wiper motor for the HYUNDAI, KIA, GM, SAMSUNG, VW, and MAZDA
Development of new generation windshield wiper motor
Applied project methodology and enforce project standard procedure based on level of development (Platform, Variant, or Application)

QS 9000 Internal Auditor (09/99-09/05)

# Publications

Lee, J.H., Pidapart Ramana M., Atkinson Gary M.  Moorthy Ramana S.  "Design of an Implantable Device for Ocular Drug Delivery", *Journal of Drug Delivery*, Volume 2012, 8 pages.

Lee, J.H., Pidaparti, R.M. "Drug Transport Microdevice Mimicking an Idealized Nanoscale Bio-molecular Motor", Journal of *Bionic Engineering,* Volume 8, 2011, pp. 445-463

Pidaparti, R.M., Lee, J.H. "Structural Morphology Changes of the Nuclear Pore Complex at Nano-Scale Through Computational Vibration Model*", Advanced Science Letters,* Volume 6, 2012 , pp. 107-112

J.H. Lee, R. M. Pidaparti, "Geometry Optimization for Fluid Transport of a Bio-inspired Nano-fluidic System", Presentation and Proceeding of the 10th IEEE international conference on Nanotechnology 2010, August 17-20, 2010, KINTEX, Korea

# Presentations

Lee, J.H., Pidaparti, R.M., "Design and development of an implantable device for ocular drug delivery", Abstract and poster presentation at the Mid-Atlantic Micro/Nano Alliance 2012 Symposium, March 27, 2012, United States Naval Academy, MD

Lee, J.H., Pidaparti, R.M., "Geometry Optimization for Fluid Transport mimicking a Bio-inspired System", Abstract and presentation at the AIAA region 1-Young Professional, Student, and Education Conference 2010, October 29, 2010, Johns Hopkins University, MD

Lee, J.H., Pidaparti, R.M., "Geometry Optimization for Fluid Transport of a Bio-inspired Nano-fluidic System", Presentation and Proceeding of the 10th IEEE international conference on Nanotechnology 2010, August 17-20, 2010, KINTEX, Korea

Lee, J.H., Pidaparti, R.M., "Structural Optimization for a Nano-fluidic System mimicking the Transport through Nuclear Pore Complex", Abstract and presentation at the 88th Annual Meeting of the Academy, Virginia Academy of Science, May 20-22, 2010, James Madison University, VA

Lee J.H., Pidaparti, R.M., "Geometry Optimization for Fluid Transport of a Bio-inspired Nano-fluidic System", Abstract and poster at the13th Annual Graduate Student Symposium & Exhibit, April 20, 2010, Virginia Commonwealth University, VA